

AD-761 168

LASER INDUCED DAMAGE IN SOLIDS

David W. Fradlin

Harvard University

Prepared for:

Office of Naval Research

May 1973

DISTRIBUTED BY:

**NTIS**

National Technical Information Service  
U. S. DEPARTMENT OF COMMERCE  
5285 Port Royal Road, Springfield Va. 22151

AD 761168

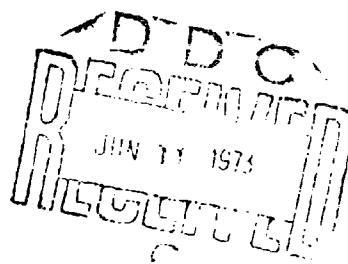
Office of Naval Research  
Contract N00014-67-A-0288-0006 MR-372-012

## LASER INDUCED DAMAGE IN SOLIDS



By

David W. Gradin



May 1973

Technical Report No. 643

This document has been approved for public release and sale; its distribution is unlimited. Reproduction in whole or in part is permitted by the U. S. Government.

Division of Engineering and Applied Physics  
Harvard University • Cambridge, Massachusetts

201

Office of Naval Research  
Contract N00014-67-A-0298-0006  
NR-372-012

LASER INDUCED DAMAGE IN SOLIDS

By

David W. Fradin

Technical Report No. 643

This document has been approved for public release and sale; its distribution is unlimited. Reproduction in whole or in part is permitted by the U. S. Government.

May, 1973

The research reported in this document was made possible through support extended the Division of Engineering and Applied Physics, Harvard University by the U. S. Army Research Office, the U. S. Air Force Office of Scientific Research and the U. S. Office of Naval Research under the Joint Services Electronics Program by Contracts N00014-67-A-0298-0006, 0005, and 0008.

Division of Engineering and Applied Physics  
Harvard University · Cambridge, Massachusetts

Unclassified

Security Classification

DOCUMENT CONTROL DATA - R & D

(Security classification of title, body of abstract and indexing annotation must be entered when the overall report is classified)

1. ORIGINATING ACTIVITY (Corporate author) Division of Engineering and Applied Physics Harvard University Cambridge, Massachusetts		2a. REPORT SECURITY CLASSIFICATION Unclassified	
3. REPORT TITLE  LASER INDUCED DAMAGE IN SOLIDS		2b. GROUP	
4. DESCRIPTIVE NOTES (Type of report and, inclusive dates) Interim technical report			
5. AUTHOR(S) (First name, middle initial, last name)  David W. Fradin			
6. REPORT DATE May 1973	7a. TOTAL NO. OF PAGES 24,207	7b. NO. OF REFS 100	
8a. CONTRACT OR GRANT NO. N00014-67-A-0298-0006	9a. ORIGINATOR'S REPORT NUMBER(S)  643		
b. PROJECT NO.	9b. OTHER REPORT NO(S) (Any other numbers that may be assigned this report)		
c.			
d.			
10. DISTRIBUTION STATEMENT This document has been approved for public release and sale, its distribution is unlimited. Reproduction in whole or in part is permitted by the U. S. Government.			
11. SUPPLEMENTARY NOTES Details of illustrations in this document may be better studied on microfiche.		12. SPONSORING MILITARY ACTIVITY Office of Naval Research	
13. ABSTRACT Processes that can produce optical damage in transparent insulators are studied in the present work. A general discussion is given of laser induced damage which distinguishes between breakdown from intrinsic processes and damage from absorbing contaminants called inclusions. In order to measure properties of intrinsic breakdown it is necessary to either avoid inclusion damage completely or to distinguish its presence when it occurs. New and previously published techniques for identifying damage from inclusions are discussed and applied. Because self-focusing can develop and confuse bulk damage measurements, a detailed summary of self-focusing theory is given which establishes the conditions for minimizing beam distortion from self-focusing effects. A series of controlled experiments are then described which represent the first unambiguous measurements of an intrinsic damage mechanism at near-infrared and visible frequencies. The intrinsic damage process in the alkali halides at 1.06 $\mu\text{m}$ is identified as an electron avalanche that is virtually indistinguishable from dc dielectric breakdown. Measurements are discussed which probe the frequency and time dependence of avalanche breakdown and from which details of the avalanche mechanism can be inferred. The effect of crystal disorder on damage fields is also considered. A statistical character is observed in the intrinsic breakdown process and compared to previously published results of surface damage. A study of the relationship between surface and bulk damage is shown to confirm a model by Bloembergen of field enhancement at structural defects. Finally, a summary of avalanche breakdown theories is presented, and the implications of the experimental data for avalanche theory are discussed.			

DD FORM 1473

(PAGE 1)

S/N 0101-897-6811

Unclassified

Security Classification

A-31404

Unclassified

Security Classification

14 KEY WORDS	LINK A		LINK B		LINK C	
	ROLE	WT	ROLE	WT	ROLE	WT
Lasers Nonlinear Optics Optical Damage Dielectric Breakdown						

1-8

Unclassified

Security Classification

# LASER INDUCED DAMAGE IN SOLIDS

By

David W. Fradin

Division of Engineering and Applied Physics  
Harvard University · Cambridge, Massachusetts

## ABSTRACT

Processes that can produce optical damage in transparent insulators are studied in the present work. A general discussion is given of laser induced damage which distinguishes between breakdown from intrinsic processes and damage from absorbing contaminants called inclusions. In order to measure properties of intrinsic breakdown, it is necessary to either avoid inclusion damage completely or to distinguish its presence when it occurs. New and previously published techniques for identifying damage from inclusions are discussed and applied. Because self-focusing can develop and confuse bulk damage measurements, a detailed summary of self-focusing theory is given which establishes the conditions for minimizing beam distortion from self-focusing effects. A series of controlled experiments are then described which represent the first unambiguous measurements of an intrinsic damage mechanism at near-infrared and visible frequencies. The intrinsic damage process in the alkali halides at  $1.06 \mu\text{m}$  is identified as an electron avalanche that is virtually indistinguishable from dc dielectric breakdown. Measurements are discussed which probe the frequency and time dependence of avalanche

breakdown and from which details of the avalanche mechanism can be inferred. The effect of crystal disorder on damage fields is also considered. A statistical character is observed in the intrinsic breakdown process and compared to previously published results of surface damage. A study of the relationship between surface and bulk damage is shown to confirm a model by Bloembergen of field enhancement at structural defects. Finally, a summary of avalanche breakdown theories is presented, and the implications of the experimental data for avalanche theory are discussed.

## ACKNOWLEDGEMENT

The work presented here was carried out with the advice, collaboration, and assistance of many individuals whose contributions have greatly improved the work's quality and scope. Dr. E. Yablonovitch is responsible for the author's original interest in optical damage and suggested the experiment in Chapter 4. Prof. N. Bloembergen provided critical and competent review of all aspects of this work. Extensive measurements of breakdown statistics were made on the suggestion of Dr. M. Bass who was also the first to recognize the importance of the attenuation of the transmitted light as an indicator of the source of laser damage. Mr. D. Bua gave invaluable assistance on many experimental problems. The experiment on laser damage with subnanosecond pulses was conducted with the able assistance of Mr. J. P. Letellier. The author has particularly benefited from technical discussions with Drs. Y. R. Shen, H. Barrett, L. Holway, and J. Marburger, and many problems and ideas were discussed with Dr. F. Horrigan, J. M. Khan, M. Levenson, P. Miles, J. McMahon, M. Adlerstein, E. S. Bliss, and H. Ehrenreich. Mr. S. Maurice prepared most of the crystals used in this study, and Mr. D. W. Howe freely donated his talents on x-ray analysis. Messr. J. Keith and A. Francosa applied their considerable skill to many machining problems encountered during the work.

Raytheon Research Division provided laboratory facilities for most of this study as well as technical assistance and a friendly and stimulating

environment for research. The subnanosecond studies were conducted on facilities owned by Naval Research Laboratories. Financial support for this work was provided by the Joint Services Electronics Program, by the National Aeronautics and Space Agency, and by the Advanced Research Projects Agency as monitored by the Air Force Cambridge Research Laboratories.

## TABLE OF CONTENTS

	<u>Page</u>
ABSTRACT .....	i
ACKNOWLEDGMENT .....	iii
LIST OF FIGURES .....	viii
LIST OF TABLES .....	x
INTRODUCTION .....	1
CHAPTER 1    LASER INDUCED DAMAGE IN SOLIDS	
A.    Generalized Damage Process .....	9
B.    Inclusion Damage .....	15
C.    Intrinsic Damage Processes .....	25
CHAPTER 2    SELF-FOCUSING AND ITS RELATIONSHIP TO OPTICAL DAMAGE	
A.    Introduction .....	31
B.    General Formalism for a Steady-State Nonlinearity .....	34
C.    Effects of Nonlinearity on Focused, Low-Power Laser Beams .....	39
D.    Transient Effects .....	44
E.    Applications of Self-Focusing Theory to Optical Damage .....	46
F.    The Measurement of Self-Focusing Parameters Using Intrinsic Optical Damage .....	48
CHAPTER 3    THE LASER SOURCES AND EXPERIMENTAL TECHNIQUES	
A.    Introduction .....	59
B.    The Q-Switched Lasers and Beam Handling Optics .....	59

	C. The Mode-Locked Laser .....	72
	D. The Distinction Between Intrinsic and Inclusion Induced Damage .....	76
CHAPTER 4	INTRINSIC OPTICAL DAMAGE IN THE ALKALI HALIDES INDUCED BY 1.06 $\mu\text{m}$ RADIATION	
	A. Introduction .....	87
	B. The Experiment .....	90
	C. Discussion of Results .....	101
CHAPTER 5	THE EFFECTS OF LASER FREQUENCY, PULSE DURATION AND CRYSTAL DISORDER ON INTRINSIC OPTICAL DAMAGE FIELDS	
	A. Introduction .....	107
	B. Avalanche Breakdown Induced by Ruby Laser Light .....	108
	C. The Pulse-Width Dependence of Optical Avalanche Breakdown .....	114
	D. Effects of Disorder on the Intrinsic Damage Field .....	122
CHAPTER 6	LASER DAMAGE STATISTICS	
	A. Introduction .....	127
	B. Experimental Measurement of Laser Damage Statistics .....	128
	C. Sources of Damage Statistics .....	144
CHAPTER 7	OPTICAL SURFACE DAMAGE	
	A. Introduction .....	153
	B. The Experiment .....	154
CHAPTER 8	THEORIES OF DC AND OPTICAL ELECTRIC BREAKDOWN	
	A. Introduction .....	165

B. Historical Review of Breakdown Theories .....	166
C. Implications of Experimental Results to Theory .....	179

CHAPTER 9 SUGGESTIONS FOR FUTURE WORK

APPENDIX

REFERENCES .....	199
PUBLICATIONS .....	205

## LIST OF FIGURES

<u>Figure</u>		<u>Page</u>
1	Inclusion Damage .....	17
2	A Schematic Comparison of the Damage Thresholds for Avalanche Breakdown and Multiphoton Ionization as a Function of Laser Wavelength .....	27
3	Catastrophic Self-focusing for Unfocused Laser Beams .....	32
4	The Effect of the Index Nonlinearity on the Minimum Diameter of a Focused Laser Beam When $P < P_{cr}$ .....	43
5	The Dependence of Damage Power for Sapphire on Beam Focal Diameter .....	55
6	Q-switched Lasers and Variable Attenuator Configuration for Damage Studies .....	60
7	Intensity Distribution of the YAG:Nd Laser as a Function of Radial Distance from the Beam Center at the Position of the Focusing Lens .....	63
8	Intensity Distribution of the Ruby Laser Taken with a Multiple Reflection Camera .....	65
9	Schematic Diagram of a Laser Cavity Showing Mode-Selecting Intracavity Resonator .....	67
10	Effect of Rod Alignment on Output Pulses for Q-switched YAG:Nd Laser .....	68
11	Effects of Rod Alignment on Output Pulses for Q-switched Ruby Laser .....	69
12	Mode-Locked Laser with Electro-Optic Shutter for Single Pulse Measurements .....	71
13	Intrinsic Damage in RbCl .....	79
14	Inclusion Damage in RbCl .....	80
15	Comparison of Measured $f_N$ with $p_1 (1-p_1)^{N-1}$ for Intrinsic Bulk Damage in Fused Quartz .....	82
16	Ruby Laser Pulses Transmitted Through NaF .....	83
17	YAG:Nd Laser Pulse Transmitted Through the Sample .....	97

18	Comparison of Breakdown Strengths for Various Alkali Halides Studied at dc, 10.6 $\mu\text{m}$ , and 1.06 $\mu\text{m}$ .....	99
19	Rms Electric Fields Necessary to Induce Damage in Nine Alkali Halides Normalized to the Damaging Field for NaCl .....	110
20	The Rate of Ionization in NaCl as a Function of Electric Field .....	118
21	The Surface Damage Probability $p_1$ as a Function of Laser Power .....	129
22	The Occurrence of Internal Damage in NaCl Due to Ruby Laser Irradiation .....	132
23	Intrinsic Bulk Damage Occurring in NaCl on the Second of Two Ruby Laser Pulses .....	133
24	Measured Distributions of Bulk Breakdown Starting Times for Fused Quartz Using YAG:Nd Laser Irradiation .....	135
25	Measured Distribution of Bulk and Surface Breakdown Starting Times for NaF Using Ruby Laser Irradiation .....	136
26	Measured Distribution of Bulk Breakdown Starting Times for Sapphire Using YAG:Nd Laser Irradiation .....	137
27	Measured and Calculated Distributions of Breakdown Starting Times for Bulk Damage in Fused Quartz Using a YAG:Nd Laser .....	142
28	Electron Micrographs of the Surfaces of Fused Quartz and BSC-2 Glass .....	157
29	Residual Surface Damage on Ion-Beam Polished Fused Quartz .....	158
30	The Energy Balance in Average-Electron Breakdown Theories .....	169
31	Schematic of the Electron-Phonon Collision Frequency as a Function of Energy for Both Polar and Nonpolar Interactions .....	176
32	Comparison of Subnanosecond Laser Data to Shockley Model .....	181
33	Spherical Aberrations Introduced by Focusing Light Through a Plane Surface .....	196

## LIST OF TABLES

<u>Table</u>		<u>Page</u>
I	Damage Power in Sapphire for Different Beam Sizes .....	53
II	Laser Parameters .....	62
III	Calculated Steady-State, Self-Focusing Parameters and Experimental Values of Pulse Widths and Peak Power .....	92
IV	Relative Breakdown Fields--Normalized to $E_{NaCl} \approx 2 \times 10^6$ V/cm .....	98
V	Absolute Breakdown Strength of NaCl .....	100
VI	Experimental Breakdown Fields and Calculated Self-Focusing Parameters in NaCl .....	117
VII	Parameters Used to Calculate $g(t)$ in Fig. 27, Materials Studied: Fused Quartz .....	143
VIII	Comparison of Bulk and Surface Damage Fields for Different Samples and Surface Finishes ...	156
IX	Measured Bulk Damage Fields at $1.06 \mu m$ .....	162

## INTRODUCTION

### A. The Problem and Its History

Intense laser light is known to damage initially transparent solids. Such damage may be a cumulative material deterioration<sup>1</sup> or it may appear as a sudden catastrophic material failure accompanied by a spark and permanent material damage.<sup>2</sup> This second type of optical damage, which is the subject of the present work, represents a serious limitation on the design and operation of high-power lasers. In addition, damage to laser components such as windows, rods, and Pockels cells requires replacement and realignment which can be both expensive and time-consuming.

A plethora of published experiments and theories have appeared since 1964 with the aim of elucidating the mechanisms of optical damage and determining damage fields for initially transparent solids.<sup>3</sup> The early experimental work in the area was confused by a number of problems: uncertainties in the laser mode structure,<sup>4</sup> the presence of small absorbing particles,<sup>5</sup> self-focusing in the bulk,<sup>6</sup> and, perhaps most important, the lack of a theoretical framework for designing and interpreting damage studies.

Despite these problems a number of useful conclusions were reached concerning optical damage. First, it was found that the most frequent cause of laser-induced damage was extrinsic, a dirt effect caused by the heating of small

absorbine inclusions with diameters between about  $0.01 \mu\text{m}$  and  $1 \mu\text{m}$ . Second, confirming the expectations of a number of scientists,<sup>7</sup> it was found that in damage experiments the collapse of high-power laser beams from the well-known self-focusing nonlinearity<sup>8</sup> was increasing the light intensities inside solids to values in excess of the incident intensities.<sup>9</sup> Damage developed after this intensification so that apparent damage thresholds in the bulk of materials were actually thresholds for catastrophic self-focusing. Because techniques had not yet been developed for avoiding inclusion damage and catastrophic self-focusing, experimental measurements prior to 1971 gave virtually no information on the nature of intrinsic damage processes. The seemingly unavoidable self-focusing problem compelled many damage experimenters to focus their attention and their laser beams on the surfaces of transparent solids where self-focusing could not develop.<sup>10</sup> Work commenced on thin film damage<sup>11</sup> where numerous materials problems added new complexities.

In 1971 two important experimental studies of intrinsic optical damage were reported. The first, by Bass and Barrett,<sup>12</sup> observed statistics at  $1.06 \mu\text{m}$  and, in a later work, at  $0.69 \mu\text{m}$ <sup>13</sup> in the optical strengths of surfaces for several materials. These statistics could not be explained by laser fluctuations, but they were explained by a simple model for electron avalanche breakdown.

The second set of measurements, performed by Yablonovitch at Harvard,<sup>14</sup> was the first unambiguous study of optical

intrinsic bulk damage. Yablonovitch measured the damage properties of ten alkali halides at  $10.6 \mu\text{m}$  and found that the damaging process appeared to be identical to dc dielectric breakdown. Self-focusing was avoided by making use of an observation already present in the literature,<sup>6</sup> namely that catastrophic self-focusing cannot occur below a material-dependent critical power. By confining the laser input powers to values which were orders of magnitude less than the critical power for self-focusing while strongly focusing the laser beam with external optics, Yablonovitch was able to achieve the high intensities necessary to damage his crystals without the confounding presence of self-focusing. In designing his experiment, he was aided by the fact that the self-focusing threshold increases with wavelength as  $\lambda^2$  and that typical Gaussian beam diameters for the  $\text{CO}_2$  laser are about an order of magnitude larger than the Gaussian beam diameters for YAG:Nd and ruby lasers. Inclusion damage was distinguished from intrinsic breakdown by examination of the damage morphology.

The year following this work, Bloembergen completed a simple but intriguing model<sup>15</sup> which predicted that the apparent optical strength of surfaces would normally be less than the optical strength of the bulk. He recognized that the dielectric discontinuity occurring at structural defects can enhance the electric field over its average value. Such defects are likely to be created at surfaces by abrasive polishing.<sup>16</sup> Crisp, et al., had shown earlier<sup>17</sup> that surface field enhancement, in this case from Fresnel reflection, could

explain the paradoxical difference between the damage resistance of exit and entrance surfaces on the same sample.

A number of important experimental questions remained: While the process for intrinsic damage at  $10.6 \mu\text{m}$  is apparently the same as at dc, namely avalanche ionization, what intrinsic damage process is operative in the near infrared and visible? What are the thresholds for this intrinsic process in various materials? Are, in fact, the thresholds well-defined? What are the frequency and time dependences to the intrinsic process? Is the damage resistance of a single crystal any different from that of a polycrystal or an amorphous form of the same material? Is Bloembergen's model correct, or does surface absorption play a role in surface damage? In short, when damaging contaminants are eliminated, what magnitudes of optical fields can initially transparent solids withstand?

## B. Organization

The present work addresses itself to these questions. Chaps. 1-3 contain a general description of the optical damage process, a detailed study of self-focusing, and descriptions of the experimental arrangements and techniques. The remaining chapters summarize the experimental results and theory relevant to optical electron avalanche breakdown.

In Chapt. 1, the results of a simplified model of inclusion damage are discussed. Of particular importance is a discussion of the pulse-width dependence to inclusion damage.

It is shown that although the intensity threshold for inclusion damage will always increase with decreasing laser pulse width, the magnitude of this increase depends on the inclusion size. The qualitative frequency dependences of the two important intrinsic damage processes, electron avalanche breakdown and multiphoton ionization, are also described in Chapt. 1. Although multiphoton ionization has not been observed in the present work, a brief discussion of the multiphoton process is given.

Self-focusing is described in Chapt. 2 within the context of the paraxial ray approximation. In addition to clarifying the conditions under which catastrophic self-focusing can be avoided, the discussion also includes a novel technique for measuring self-focusing parameters using intrinsic optical damage.

Chapt. 3 summarizes the experimental arrangements for the measurements of intrinsic optical damage. A new technique for longitudinal mode selection of Q-switched lasers is described, and the various measurements characterizing the two types of lasers used in the present work are reported. A summary is given of new and previously published techniques for avoiding and identifying inclusion damage.

A series of controlled experiments on intrinsic optical damage at  $1.06 \mu\text{m}$  and  $0.69 \mu\text{m}$  are described in Chaps. 4-7. The first experiment, conducted at  $1.06 \mu\text{m}$  with a Q-switched laser, extends Yablonovitch's infrared measurements on the alkali halides to shorter wavelengths. It is found, contrary

to published predictions, that electron avalanche breakdown at  $3 \times 10^{14}$  herz is virtually indistinguishable from dc breakdown and intrinsic laser breakdown at  $10.6 \mu\text{m}$ . This observation has important implications relating to the electron-phonon interaction in high fields. A series of time related observations give additional evidence that an electron avalanche is responsible for intrinsic damage.

Damage measurements at visible frequency ( $0.69 \mu\text{m}$ ) are described in Chapt. 5 where evidence of frequency dispersion in the threshold fields for avalanche breakdown is presented. The dependence of the damage field on laser pulse duration, which gives information on the temporal development of the electron avalanche, has been studied in NaCl at  $1.06 \mu\text{m}$  using a mode-locked laser. It was found that the rms optical damage field increased by almost an order of magnitude to over  $10^7$  volts/cm as the laser pulse width was decreased from 10 ns to 15 ps. The laser data is used to calculate a field-dependent ionization rate that is found to agree at least qualitatively with estimates of the dc ionization rate as determined by Yablonovitch and Bloembergen.<sup>18</sup> Chapt. 5 concludes with an experiment and discussion of the effects of crystal disorder on the damage field.

Laser damage statistics is the subject of Chapt. 6. It is found that the bulk damage process in a number of materials, including NaF, has a statistical character. Measurements of the distribution of avalanche starting times is compared to the experiments of Bass and Barrett<sup>12</sup> on surface damage and

found to be consistent with those experiments. A direct comparison between surface and bulk damage on the same sample of fused quartz shows virtually identical statistics. A few speculative ideas are presented concerning the source of the statistics.

Chapt. 7 summarizes a short experiment which confirms Bloembergen's model of surface field enhancement.<sup>15</sup> Three surface finishing techniques are evaluated in terms of their ability to produce damage resistant surfaces.

Chapt. 8 summarizes the uncertain state of avalanche breakdown theory. The implications of our experimental results for avalanche theory are discussed. Some suggestions for future work in optical damage are made in Chapt. 9.

## CHAPTER 1

### LASER INDUCED DAMAGE IN SOLIDS

#### A. Generalized Damage Process

Optical damage in solids occurs when an intense laser beam causes an irreversible alteration of the medium. This alteration can be a thermally-induced fracture without a phase change, or more commonly, it is a phase change which may or may not be accompanied by thermally induced fractures.

The damage process can be conceptually divided into two steps. In the first step heat is deposited by some absorption process which may be extrinsic in origin or which may be a property of the pure crystal. In the second step, this heat deposition leads to a temperature elevation and a material irreversibility. Damage is normally only detected by the material irreversibility so that the observer is always a step removed from the physics of the heat deposition. A complete description of optical damage, therefore, must in principle include more than an analysis of how the material gains energy. It must also include a modeling of the thermal problem of how that heat produced a material irreversibility. Conditions under which this second step can be ignored in analyzing damage are discussed below.

In order to establish approximate minimum requirements for the heat deposition process, the details of the second step are replaced with an explicit model. It is assumed that heat is deposited adiabatically and that damage occurs when the solid is melted. The amount of heat necessary to incude damage can then be approximated in a simple manner.

According to the law of Dulong and Pettit, the specific

Preceding page blank

heat of a solid at room temperature is of the order of 1 joule/cm<sup>3</sup>-°K. In order to raise the temperature of a typical transparent insulator to its melting point of about 1000° K, about 10<sup>3</sup> joules/cm<sup>3</sup> must therefore be supplied. Melting of the lattice is equivalent, typically, to heating by another 1000° K so that a phase change in an insulator requires on the order of 10<sup>3</sup> to 10<sup>4</sup> joules/cm<sup>3</sup>. If this heat deposition is accomplished by the absorption of 1 μm light, approximately 10<sup>22</sup> photons must be absorbed per cm<sup>3</sup> in order for damage to be produced.

This energy density requirement can also be expressed in terms of an absorption coefficient if uniform bulk absorption is assumed. Because the laser intensity varies with propagation distance  $z$  as  $I_0 \exp(-az)$ , it is easy to show that for a typical damage intensity of 10<sup>10</sup> watts/cm<sup>2</sup> (see Chapt. 4) and for a laser pulse width of 10 ns, damage can occur only when  $a = 10 \text{ cm}^{-1}$ . Such a large absorption, if present for weak light signals, makes the solid opaque.

On the basis of this simple calculation, we can reach a useful conclusion concerning the relationship of absorption by atomic impurities to optical damage. The number of impurity states in a high-purity insulator is normally less than 10<sup>17</sup> /cm<sup>3</sup>. If each impurity absorbs one photon, the amount of energy per unit volume removed from the laser beam is less than 0.01% of the energy density necessary for damage. If absorption is occurring because of impurity excitation into a bound state, therefore, each impurity must be excited and

must subsequently relax nonradiatively a total of at least  $10^5$  times during the transit of the laser pulse if damage is to occur. Although systems can perhaps be found where this requirement can be met, it seems safe to conclude that impurity excitation into a bound state cannot normally produce optical damage in initially transparent solids.

As an application of this observation, consider the rare earth dysprosium in the crystalline host yttrium aluminum garnet (YAG). Dysprosium is known to strongly absorb  $1.06 \mu\text{m}$  radiation through an electronic excitation into a bound state having a lifetime longer than  $1 \text{ ns}$ .<sup>19</sup> An interesting experiment might appear to be a measurement of the damage threshold of YAG at  $1.06 \mu\text{m}$  as a function of dysprosium concentration. On the basis of the present discussion, however, we can predict that the dysprosium concentration will have very little effect on the breakdown strength of YAG. Under the intense irradiation necessary for damage, the dysprosium absorption will simply bleach.

An absorption process must be found which can produce an  $\alpha \approx 10 \text{ cm}^{-1}$  with reasonable electron densities. Joule heating of quasi-free electrons is such a process. Relaxation-time models of the electron-phonon interaction predict that the rate of energy deposition per unit volume is given by

$$\frac{dW}{dt} = N e \mu E^2 / (1 + \omega^2 \tau^2) \quad (1-1)$$

where  $N$  is the conduction-band population density,  $e$  is the

electronic charge,  $\mu$  is the electron mobility in the presence of a field  $E$  with frequency  $\omega$ , and  $\tau$  is the electron-phonon collision time. Letting  $\omega^2 \tau^2 \ll 1$  and inserting the mobility value for NaCl ( $10 \text{ cm}^2/\text{volt-sec}$ ) and damage field value ( $10^6 \text{ volts/cm}$ ), we find that a 10 ns (nanosecond) laser pulse can deposit a damaging amount of heat when  $N \geq 10^{17} / \text{cm}^3$ . The excitation of this density of electrons will involve a negligible loss of energy to the laser beam.

Let us apply this description to intrinsic damage processes. Intrinsic breakdown in transparent solids can be caused in principle by one of two processes, either electron avalanche ionization or multiphoton absorption.<sup>20</sup> The fundamental difference between these processes is not in the manner in which heat is deposited. In both processes energy is transferred to the electron population through joule heating of conduction-band electrons, and the lattice is heated through the mechanism of electron-phonon collisions. The processes are fundamentally different only in the manner in which they produce a high density of conduction band electrons. Electron avalanche breakdown is a chain reaction generation of quasi-free electrons through impact ionization of hot electrons into the conduction band. Multiphoton ionization, on the other hand, is the direct excitation of electrons across the band-gap because of the simultaneous absorption of more than one photon. It is the limiting case of frequency dependent tunneling.

Having considered some general aspects of heat deposition,

we now return to a discussion of the second stage of optical damage that establishes the link between absorption and actual material damage.

As the conduction-band population of the lattice or of an absorbing inclusion is being heated by joule heating, energy is very rapidly transferred to the lattice. The resulting local temperature rise induces heat flow which is described by the geometry-dependent thermal diffusion equation. When the heated region is very small, thermal diffusion effects can be extremely important in describing the temperature rise because the thermal diffusion time scales with radius  $R$  of the heated region as  $1/R^2$ . Thermal loss in principle raises the damage threshold and alters the dependence of damage fields on laser pulse width.

The thermal aspects of intrinsic damage are difficult to consider because  $R$  becomes a complicated function of time for intrinsic processes. For a highly nonlinear intrinsic process such as avalanche breakdown, however, the thermal aspects of damage need not be calculated because they have little or no measurable effect on damage threshold. If the focusing condition (in laser damage) or electrode design (in dc damage) of one experiment make breakdown less likely by altering the processes leading to material damage thereby requiring a higher rate of energy deposition, this higher rate can be achieved by an immeasurably small change in the electric field strength. The damage fields for avalanche breakdown, therefore, will depend only on the parameters which

describe the time evolution of the conduction-band population  $N(t)$  (and therefore the heat deposition) and will have no measureable connection with the geometry of the field configuration or the morphology of the damage.

Inclusion damage, on the other hand, is not highly non-linear so that the details of the thermal process can be extremely important in determining the dependence of damage thresholds on laser pulse width. This dependence will be discussed in some detail in the next section.

Two- and three-photon ionization is another possible source of intrinsic damage. It is expected that the sensitivity of the damage threshold to laser pulse width will be intermediate between that of avalanche breakdown and inclusion damage. A precise calculation of thermal effects is difficult because the size of the heated region is time dependent unless the multiphoton ionization is occurring in a uniform manner inside a microscopic inclusion. Bliss<sup>21</sup> has presented the results of a calculation for the pulse-width dependence of  $N^{\text{th}}$ -order multiphoton breakdown which ignores these thermal effects. His results follow from Eq. (1-1) with a simple modeling of  $N(t)$  and should be regarded as approximate.

In summary, then, laser damage most likely occurs from the joule heating of conduction band electrons in a bulk solid or in an absorbing inclusion. This absorption produces a temperature rise and eventually a material irreversibility that actually defines the onset of damage. A proper description of the damage process, especially of its pulse-width

dependence, must in principle include a discussion of the manner in which the heat deposition produces the material irreversibility.

#### B. Inclusion Damage

Optical damage can be caused by absorbing microscopic contaminants called inclusions if the temperature of an inclusion can be elevated sufficiently to induce a material irreversibility before an intrinsic damage mechanism develops. As already noted, inclusion damage is geometry dependent because the total process is sensitive to the manner in which the heat deposition produces a temperature rise. We will eventually use a simplified model to study this damage process and to determine, in particular, its pulse-width dependence.

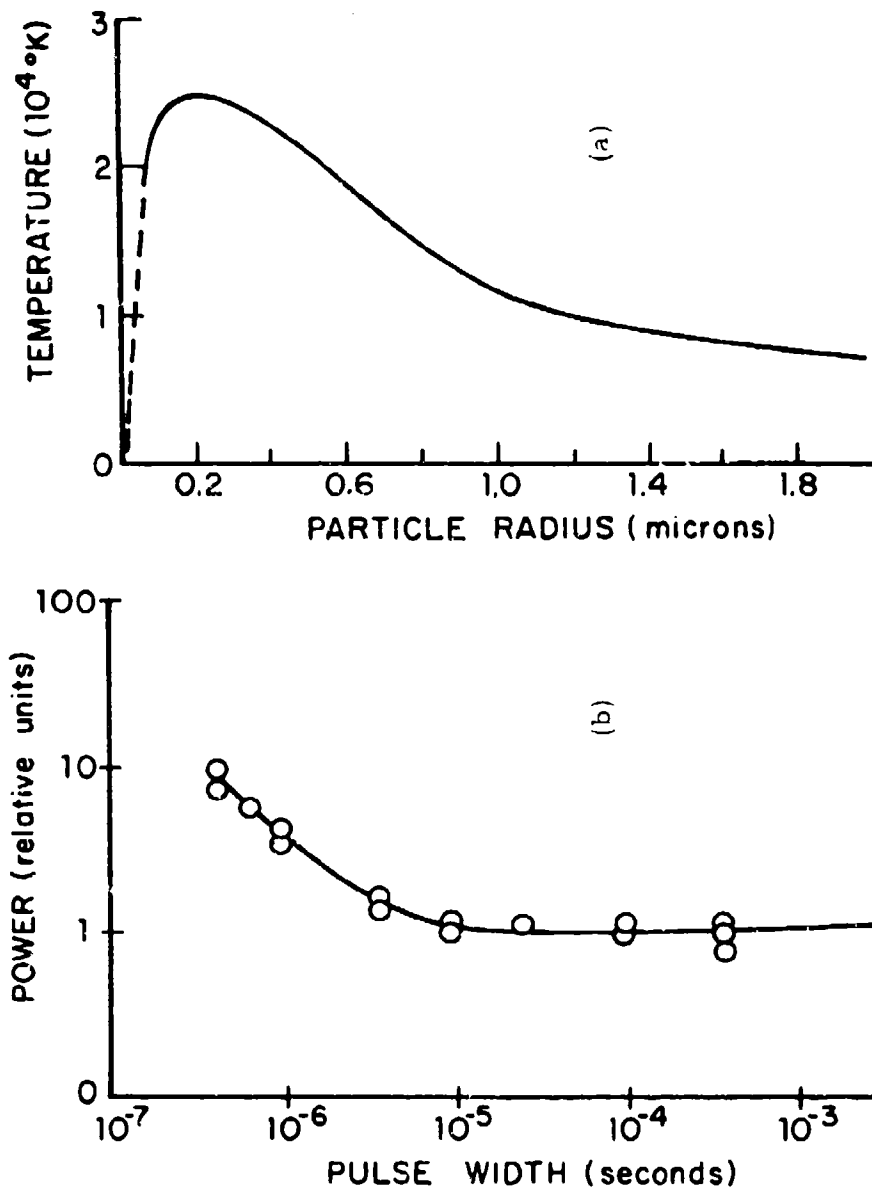
The temperature rise experienced by metallic spherical inclusions under Q-switched irradiation has been treated in detail by Hopper and Uhlman.<sup>5</sup> Damage was assumed to occur when a fracturing stress was thermally induced. Although this type of material irreversibility is not physically equivalent to a phase change, the energy deposition requirements are about the same. It was found that since the surface-to-volume ratio of spherical inclusions varies as  $1/R$ , the temperature rise induced by a fixed laser pulse incident onto an opaque inclusion will initially increase as the size of the particles is decreased. For very small particles, however, heat will begin to diffuse away from the inclusion during the transit of the laser pulse. Since the thermal diffusion

time is of the order of  $D/R^2$ , where  $D$  is the thermal diffusivity of the host (assumed to be much greater than the thermal diffusivity of the inclusion), the temperature rise as a function of  $R$  will be peaked when  $D/R^2$  is on the order of the laser pulse width  $t_p$ . This behavior is illustrated in Fig. 1a where it is seen that inclusions having diameters  $\leq 0.1 \mu\text{m}$  will probably not induce damage when irradiated by a Q-switched laser pulse having an energy density of 20 joules/cm<sup>2</sup> and a pulse duration of 30 ns.

For long pulses and fixed inclusion size the damage threshold should be dependent on the laser intensity or, equivalently, since the focusing conditions are fixed, on the laser power. When  $t_p$  is less than the thermal diffusion time, the threshold for damage will depend on the laser pulse energy so that the damage power will vary as  $t_p^{-1}$ . These simple predictions, which are also valid for semiconducting inclusions, explain the experimental data of Danileiko et al.<sup>10</sup> (see Fig. 1b) who irradiated the surfaces of sapphire samples with laser pulses of varying time duration.

We now consider a simplified model of inclusion damage that displays the qualitative features of Hopper and Uhlman's more accurate calculation for metallic inclusions. This model will be used to treat semiconducting inclusions and to account in an approximate manner for the finite wavelength of the incident laser light. Spherical inclusions are considered with the thermal diffusivity of the inclusions assumed to be much larger than that of the host. Damage is assumed to

Figure 1. INCLUSION DAMAGE



a) Calculated temperature of platinum particles in a glass host having thermal diffusivity  $3 \times 10^{-3} \text{ cm}^2/\text{sec}^{-1}$  and subject to a 20 joule/ $\text{cm}^2$ , 30-ns laser pulse. (Flopper and Uhlman, 1970).

b) Experimental dependence of the threshold power on the laser pulse duration for surface damage in sapphire. (Danileiko et al., 1970).

occur when the temperature of the surrounding host material reaches a critical value  $\Delta T_c$ . If the material damage is a phase change, then this critical temperature rise will be given by the difference between room temperature and the melting point with an appropriate addition to account for the heat of fusion.

In the absence of thermal dissipation, the temperature gain  $\Delta T$  of a metallic inclusion with radius  $R$  subject to a square laser pulse of intensity  $I$  is given by

$$C_v \Delta T = \epsilon_\lambda \frac{(\text{area})I}{(\text{volume})} t = \frac{3\epsilon_\lambda}{4} M \frac{It}{R} \quad (1-2)$$

where  $C_v$  is the specific heat,  $\epsilon_\lambda$  is the spectral emissivity, and  $M$  is a correction factor to account for the effects of the finite wavelength of the irradiating light on the absorption cross-section. For metallic particles,  $M$  is approximately given by<sup>31, 21</sup>

$$M = \begin{cases} 1 & \text{when } R \geq \lambda/20 \\ 20R/\lambda & \text{when } R < \lambda/20 \end{cases} \quad (1-3)$$

Exact calculations of  $M$  are very difficult, especially for absorbing semiconductors, and only a few special cases have been considered in detail. We will use the simplified form of Eq. (1-3) to describe the diffraction effects for both semiconducting and metallic inclusions.

After the laser pulse has passed, the inclusion will cool and  $\Delta T$  will decay approximately as

$$\Delta T = \Delta T_0 e^{-Dt/R^2} \quad (1-4)$$

where  $D$  is the thermal diffusivity of the host. Eqs. (1-2) and (1-4) together imply that the time-dependent temperature rise of a metallic inclusion during the transit of a square laser pulse is

$$\Delta T^{(m)} = \frac{3\epsilon_\lambda}{4C_v} \frac{IRM}{D} (1 - e^{-Dt/R^2}) \quad (1-5)$$

The damage intensity  $I_d$  is defined as the intensity of a laser pulse of duration  $t_p$  which induces a critical temperature rise  $\Delta T_c$ . From Eq. (1-5), we find

$$I_d^{(m)} = \left( \frac{4C_v D \Delta T_c}{3\epsilon_\lambda M} \right) \frac{1}{R} \left[ \frac{1}{1 - \exp(-Dt_p/R^2)} \right] \quad (1-6)$$

If the inclusions are made of a contaminated semiconductor, they can still absorb large amounts of light energy and cause optical damage. Residual inclusions in high purity optical crystals are normally less than a micron in diameter so that the absorption depth for a semiconducting inclusion will normally be greater than the particle diameter. For such inclusions  $\epsilon_\lambda$  in Eq. (1-2) is replaced by a term proportional to  $aR$  where  $a$  is the frequency-dependent absorption constant. The temperature rise and damage intensity then become

$$\Delta T^{(s)} \propto IR^2 M (1 - e^{-Dt/R^2}) \quad (1-7)$$

and

$$I_d^{(s)} \propto \frac{\Delta T_c}{MR^2} \left[ \frac{1}{1 - \exp(-Dt_p/R^2)} \right]. \quad (1-8)$$

Eq. (1-5) has the same qualitative form as the more accurate solution for metallic inclusions<sup>5</sup> as displayed in Fig. 1a. An optimum radius  $R_m$  exists for metallic particles in the sense that any other value of  $R$  will require a higher light intensity in order to produce the same temperature rise  $\Delta T$ .  $R_m$  can be shown to be

$$R_m = 0.9 (Dt_p)^{1/2} \quad (1-9)$$

when  $M = 1$  for the simple model we have considered. Heating of semiconducting inclusions produces a different behavior as seen by Eq. (1-7). When  $aR \ll 1$  as we have assumed, the temperature rise  $\Delta T^{(s)}$  increases monotonically with increasing radius so that an optimum radius for semiconducting inclusions does not exist.

Eqs. (1-6) and (1-8) have the same limiting behavior as the experimental data of Danileiko et al. as summarized in Fig. 1b. When  $Dt_p/R^2 \ll 1$ , the damage threshold is defined by the energy in the pulse reaching a critical value. I. e.,

$$I_d t_p \propto \begin{cases} R/M; & \text{metallic inclusions} \\ 1/M; & \text{semiconducting inclusions.} \end{cases} \quad (1-10)$$

For long pulse durations (or small particles) such that  $Dt_p/R^2 \gg 1$ , the damage threshold is independent of the laser

pulse duration. In particular,

$$I_d \propto \begin{cases} 1/MR; & \text{metallic inclusions} \\ 1/MR^2; & \text{semiconducting inclusions.} \end{cases} \quad (1-11)$$

Since the laser input power is proportional to the laser intensity, the pulse-width dependence to the damage power displayed in Fig. 1b is to be expected if damage is occurring from absorbing inclusions which all have the same radius  $R$ .

In an actual damage experiment inclusions present in the focal volume may be different sizes so that the experimental results of Danileiko et al. represent a special case. Let us consider the more general problem: An experiment is performed in which the threshold for damage is determined in a single sample for two different pulse durations. Using methods to be discussed in Chapt. 3, optical damage is shown to result from inclusion absorption. How does the damage intensity compare for the two pulse durations? It is assumed either that large focal volumes are irradiated so that each focal volume is effectively the same or that a large number of sites are probed and meaningful averages obtained.

The solution to this problem depends on the average distribution of inclusion sizes in the focal volume. We will study a few special cases.

Consider first a solid in which the probability of finding a metallic inclusion with  $R > \lambda/20 \approx 0.05 \mu\text{m}$  is unity for all  $R$ . If  $D = 3 \times 10^{-2} \text{ cm}^2/\text{sec}$  (appropriate for NaCl), then an optimum radius  $R_{\text{III}}$  can be found from Eq. (1-9)

whenever  $t_p \geq 1$  ns. By inserting Eq. (1-9) into (1-6), we can show that for such pulse durations the damage intensity  $I_d$  will scale with laser pulse duration as

$$I_d \propto (t_p)^{-1/2} \quad (1-12)$$

Eq. (1-12) predicts a behavior which is different from either Eq. (1-10) or (1-11).

When semiconducting inclusions are present in the focal volume with the same distribution of particle sizes and the same pulse-width range assumed for Eq. (1-12), the damage intensity is proportional to  $t_p^{-1}$  as in Eq. (1-10). This result assumes that  $Dt_p/R^2 \ll 1$ , a condition that is valid when the largest particle radius present is  $1 \mu\text{m}$  and  $t_p \ll 330$  ns. The reason that the pulse-width dependence is different for the two types of inclusions is that the damage intensity has a minimum as a function of  $R$  only for metallic inclusions. When semiconducting inclusions are present, the damage intensity will decrease with increasing  $R$  until  $aR \sim 1$ .

Consider now an experiment similar to that of Sect. C in Chapt. 5 in which damage is induced with laser pulses having durations of 15 ns and 15 ps (picoseconds). We wish to determine how the thresholds for inclusion damage compare for the two pulse durations. Assume first that all inclusion sizes with  $R < 1 \mu\text{m}$  are present. According to Eq. (1-8) the damage intensity for semiconducting particles will increase by a factor of  $10^3$  as the pulse width is decreased from 15 ns

to 15 ps. The situation is somewhat more complicated when metallic inclusions are present. If  $M = 1$ , an optimum radius  $R_m$  can be found as before and the relative damage fields calculated from Eqs. (1-6) and (1-9). When  $t_p \leq 1$  ns, however, Eq. (1-9) no longer applies. For such short pulse durations, diffraction effects as summarized by the parameter  $M$  in Eq. (1-3) introduce an additional factor of  $R$  in the expression for the damage field  $I_d^{(m)}$ . With this change,  $I_d^{(m)}$  has the same radius dependence as the damage field for large semi-conducting particles. The inclusion size which is most potentially damaging when  $t_p \leq 1$  ns, therefore, is  $R = \lambda/20$ . Using this fact, the damage field is found from Eqs. (1-6) and (1-9) to increase by a factor of about 150 when the laser pulse duration is decreased from 15 ns to 15 ps. This increase is almost an order of magnitude less than the corresponding increase for semiconducting inclusions.

When only particles with fixed radius are found in the focal diameter, the damage intensity for both types of inclusions scales with pulse duration as

$$\frac{I_d(t_2)}{I_d(t_1)} = \frac{1 - \exp(-Dt_1/R^2)}{1 - \exp(-Dt_2/R^2)} \quad (1-13)$$

If we let  $t_1 = 15$  ns and  $t_2 = 15$  ps, the calculated ratio of damage intensities for particles with  $R = 1 \mu\text{m}$  is  $10^3$ , and for particles with  $R = 0.01 \mu\text{m}$ , the ratio is 2.8.

It is thus seen that the change in damage intensity with decreasing pulse duration depends strongly on the distribution

of particle sizes in the focal volume. Under certain conditions, damage from semiconducting inclusions can have a different apparent pulse-width dependence than damage from metallic inclusions.

Particles as small as  $0.01 \mu\text{m}$  may not cause optical damage in an actual experiment with Q-switched laser pulses, because the damage intensity, especially for semiconducting inclusions, may exceed the intrinsic breakdown strength of the host.<sup>15</sup> The intrinsic breakdown field increases for subnanosecond laser pulses, however, as shown in Sect. C of Chapt. 5. As the laser pulse width is decreased from about 10 ns to 15 ps, the intrinsic damage intensity increases by a factor of about 35 in NaCl, and it may be possible to observe inclusion damage from small particles with a 15 ps mode-locked laser pulse when damage produced in the same sample by a Q-switched laser is observed to proceed by an intrinsic mechanism. Bliss and Milam,<sup>11</sup> in fact, have obtained evidence for this presumably rare situation in their studies of optical damage to thin film optics, and we have found during the subnanosecond damage study of Chapt. 5 that inclusion damage can occur more frequently compared to intrinsic damage when 15 ps light pulses are used to induce damage than when 5 ns light pulses are used. This situation is unusual, however. It is normally found that inclusion damage can be avoided by shortening the laser pulse duration.

The model of inclusion damage that we have applied in this section is phenomenological and should be considered

to be a qualitative description. It was presented largely to demonstrate the manner in which the second step of the damage process--the step that describes the sample's temperature elevation--affects the pulse-width dependence of inclusion damage. This dependence, which for spherical inclusions can be translated into an inclusion-size dependent damage intensity, can be treated accurately by using a thermal diffusion equation. Any prediction of the pulse-width dependence must include an assumption about the distribution of inclusion sizes.

The frequency dependence to inclusion absorption, which is determined by the details of the heat deposition (step 1), has been ignored to this point in the discussion. This dependence occurs because the absorption cross-section changes with frequency due to the frequency dependences of joule heating, impurity ionization, band-to-band absorption, optical scattering, etc. Even without attempting to quantify this frequency dependence, it is clear that normally inclusions will become more absorbing with increasing laser frequency in the visible and UV. This simple observation suggests that inclusion damage may become more of a practical problem as high-power lasers with shorter wavelengths become available.

### C. Intrinsic Damage Processes

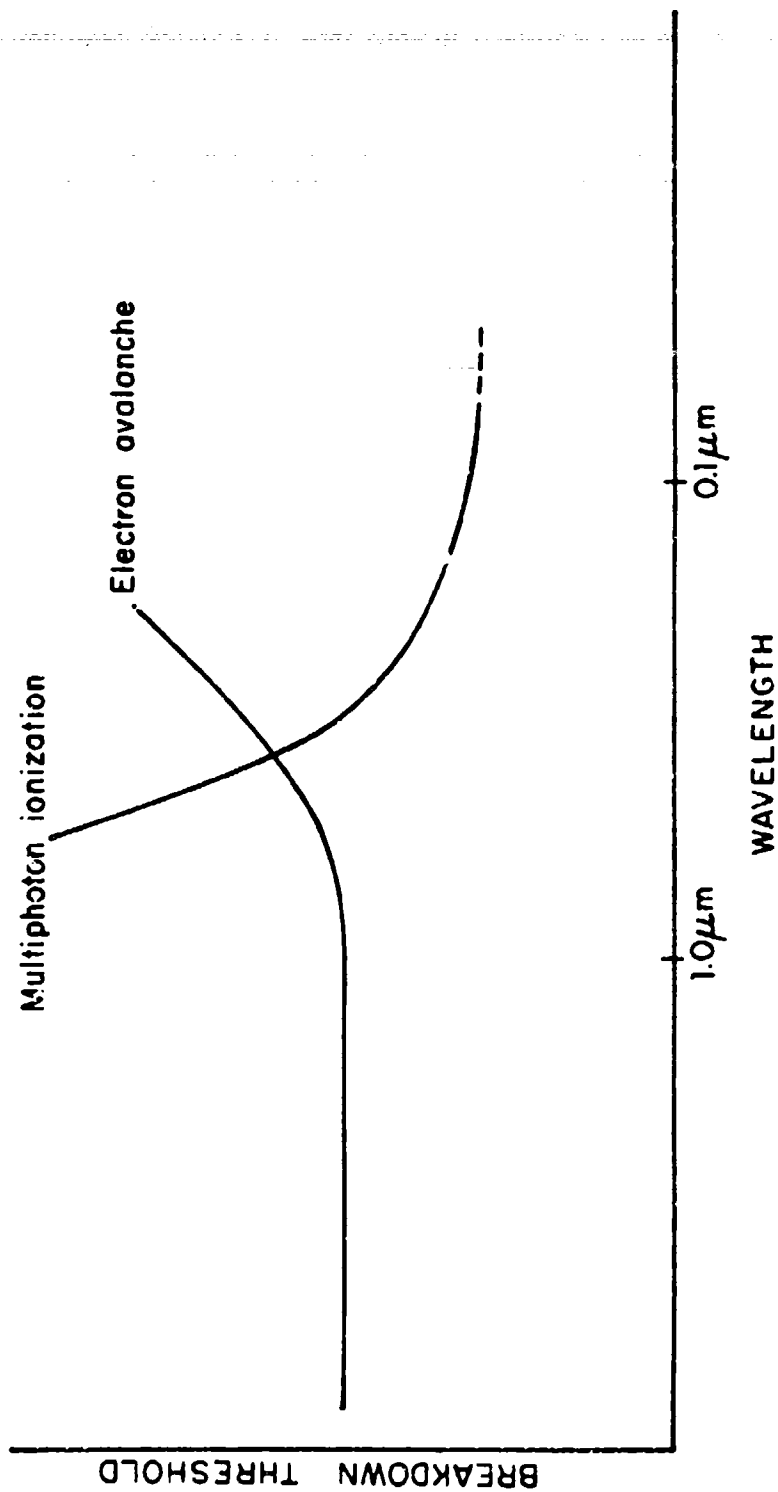
Avalanche breakdown and multiphoton ionization were introduced in Sect. A. In this section we will briefly reconsider these intrinsic breakdown mechanisms from the

viewpoint of their qualitative frequency dependences. This discussion will be extended somewhat in Chapt. 5 for avalanche breakdown. The laser pulse-width dependence of avalanche breakdown will also be considered in Chapt. 5.

Cross-sections for multiphoton ionization have been calculated from perturbation theory.<sup>22</sup> It is found that as the laser frequency increases, the cross-section for the ionization of valence-band electrons will increase in a complicated fashion. Successively lower-order multiphoton processes become possible as the frequency is raised until single-photon absorption or direct band-to-band excitation becomes possible. At low frequencies, where only high-order multiphoton processes can occur, the excitation process changes in a continuous manner into Zener tunneling as shown by Keldysh.<sup>20</sup> It is expected, then, that multiphoton absorption will have the behavior shown schematically in Fig. 2.

Quantitative calculations of multiphoton damage intensities cannot be accurately obtained from perturbation theory. Not only do the various matrix elements become large in typical damage fields of  $10^6$  volts/cm, but the electronic levels within a solid become distorted. When bound states are involved in the ionization process, say from impurities the distortion is particularly serious. This distortion develops because the state is life-time broadened due to the large probability of transitions into the conduction band or into other states<sup>23</sup> and because the Stark interaction mixes states and thereby increases the energy uncertainty.

Figure 2. A SCHEMATIC COMPARISON OF THE DAMAGE THRESHOLDS FOR AVALANCHE BREAKDOWN AND MULTIPHOTON IONIZATION AS A FUNCTION OF LASER WAVELENGTH



At low frequencies, avalanche breakdown normally has a lower threshold than multiphoton ionization and will thus be the cause of intrinsic electric damage. As the frequency is raised, however, breakdown from multiphoton ionization rapidly becomes more probable and eventually dominates avalanche breakdown.

Electron avalanche ionization involves an energy exchange between the electric field and the electrons described qualitatively by the joule heating formula of Eq. (1-1). In the absence of losses from electron diffusion and trapping, joule heating completely describes the energy input into the conduction band population. Eq. (1-1) shows that this energy input scales with frequency as  $E^2/(1+\omega^2\tau^2)$ , and because the details of the energy input should determine the electron distribution function and hence  $N(t)$ , the threshold for damage will scale in the same manner. More sophisticated calculations of breakdown<sup>24</sup> include an energy dependence in the collision time  $\tau$  and average Eq. (1-1) over the high-field electron distribution.

It is shown in Chapt. 4 and 5 that avalanche breakdown in the alkali halides appears to have an effective collision time on the order of  $10^{-16}$  sec.  $\omega^2\tau^2$  will be much less than 1, therefore, until frequencies near the visible spectrum. When the laser frequency becomes comparable to the collision frequency, the damage field should begin to increase as shown schematically in Fig. 2.

On the basis of this qualitative discussion, we can predict the relative importance of the two intrinsic damage mechanisms as a function of laser frequency. While it will be shown in Chapt. 4 and 5 that avalanche breakdown is the most likely cause of optical damage in transparent insulators near  $1 \mu\text{m}$ , breakdown from multiphoton ionization will become increasingly more important at high frequencies and should

eventually dominate avalanche breakdown as the frequency is raised. Fig. 2 summarizes the relative importance of these two processes as a function of laser wavelength. Unambiguous experimental confirmation has not yet been made of the competition of avalanche breakdown and multiphoton ionization so that future damage studies in the visible and UV are highly desirable.

## CHAPTER 2

### SELF-FOCUSING AND ITS RELATIONSHIP TO OPTICAL DAMAGE

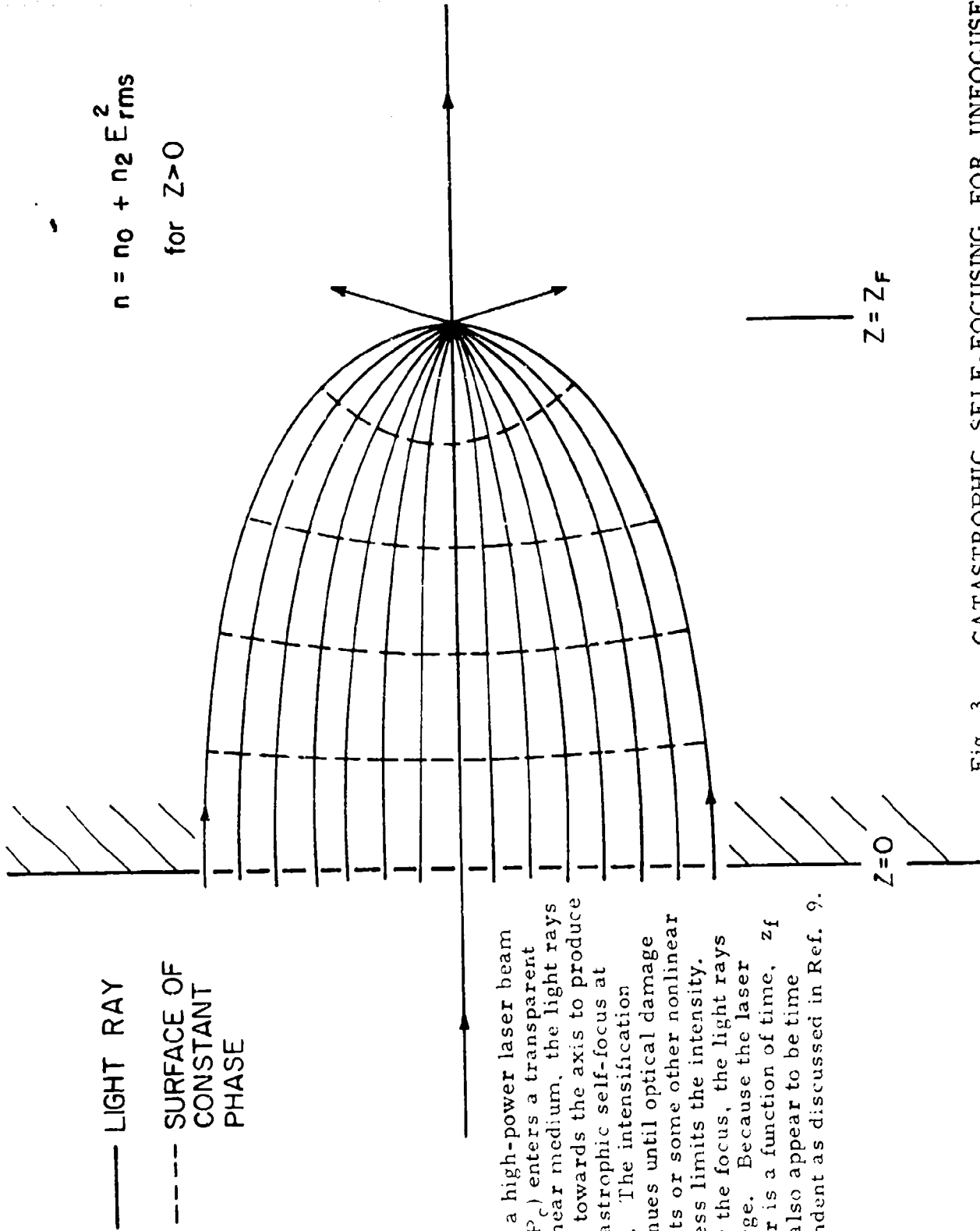
#### A. Introduction

A laser beam propagating in a transparent medium induces an increase in the index of refraction by an amount proportional to the laser intensity.<sup>6, 7</sup> At powers in excess of a critical power, this nonlinearity causes the intensity distribution to become unstable and a catastrophic beam collapse occurs in a finite distance  $z_f$ . In solids the nonlinearity normally results from electrostriction or from a nonlinear electronic polarizability.<sup>6</sup>

A physical description of this process is summarized in Fig. 3 where the propagation of a high-power laser beam having a Gaussian intensity distribution is followed. Diffraction effects are ignored. Along the beam axis the light intensity is highest so that the index of refraction is greater on axis than it is in the wings. Because the propagation velocity is given by  $c/n$ , where  $n$  is the total index of refraction including the nonlinear term (see Fig. 3), light in the wings of the beam will move faster than light along the axis, thereby causing initially plane phase fronts to become concave and the beam to focus. Beam collapse continues until some nonlinear process limits the intensification.<sup>18, 25</sup> The manner in which diffraction effects modify this description will be discussed in detail below.

Self-focusing is important to studies of optical damage, because unless great care is taken in the design of damage experiments, catastrophic self-focusing will occur and cause

**Preceding page blank**



— LIGHT RAY  
 --- SURFACE OF CONSTANT PHASE

When a high-power laser beam ( $P > P_c$ ) enters a transparent nonlinear medium, the light rays focus towards the axis to produce a catastrophic self-focus at  $z = z_f$ . The intensification continues until optical damage results or some other nonlinear process limits the intensity. After the focus, the light rays diverge. Because the laser power is a function of time,  $z_f$  will also appear to be time dependent as discussed in Ref. 9.

Fig. 3 CATASTROPHIC SELF-FOCUSING FOR UNFOCUSSED LASER BEAMS

the input laser beam to intensify.<sup>9</sup> The high intensity that results from self-focusing will then induce damage, but this high intensity may have no known relationship to the incident intensity. When catastrophic self-focusing is present, therefore, apparent damage thresholds will actually be thresholds for catastrophic self-focusing.

In this chapter the effects of the self-focusing non-linearity on the propagation of high power laser beams will be discussed within the framework of a paraxial ray approximation. This discussion provides the theoretical basis for the design of the bulk damage measurements. Some important results of this discussion are:

1. The tendency of light to diffract and the tendency to self-focus act in opposite directions in the sense that diffraction effects try to bend light rays away from the axis of propagation and cause initially plane phase fronts to become convex while self-focusing effects try to bend light rays towards the axis and cause initially plane phase fronts to become concave.
2. The relative balance between self-focusing and diffraction does not change as the beam propagates through the non-linear medium. As a result, if diffraction dominates at the entrance plane, it will dominate everywhere.
3. There exists a critical power  $P_c$  such that when the laser input power  $P$  is equal to  $P_c$ , the focusing effects from the nonlinear index approximately balance diffraction effects over the entire laser beam and an initially collimated

laser beam propagates with essentially no change in size. When  $P > P_C$ , the laser beam will collapse after propagating some finite distance inside the nonlinear medium. When  $P < P_C$ , catastrophic self-focusing is absent but beam distortion from the index nonlinearity is still present.

4. A second power,  $P_{CR}$ , is more useful in describing this beam distortion than is  $P_C$ .  $P_{CR}$  is defined as that value of input power for which diffraction and self-focusing effects balance on axis. For Gaussian beams its value is  $0.273 P_C$ .<sup>26</sup>
5. Transient effects make self-focusing more difficult.
6. When a laser beam with  $P < P_{CR}$  is focused inside a nonlinear medium, the focal diameter will be smaller than its diffraction limit even though catastrophic self-focusing is absent. Because the change in beam diameter can be calculated to high precision from the paraxial ray approximation when the index nonlinearity is in its steady state, self-focusing parameters can be calculated as demonstrated in Sect. F.

#### B. General Formalism for a Steady-State Nonlinearity

The effect of the nonlinear index of refraction on the propagation of light beams can in principle be determined exactly from Maxwell's equations. In practice, however, an analytical solution is impossible unless a number of simplifying assumptions are made. One such set of assumptions leads to a

paraxial ray approximation that describes the qualitative behavior of self-focusing at all power levels and, in addition, results in a good quantitative fit to numerical calculations at low laser powers where catastrophic self-focusing is absent.<sup>27</sup> Since we are primarily concerned with such low powers, we will use the paraxial ray approximation to describe self-focusing.

A paraxial ray equation for a nonlinear medium was first derived by Talanov<sup>28</sup> and was used in detail by Wang<sup>29</sup> and Wagner et al.<sup>30</sup> to describe catastrophic self-focusing. Zverev and Pashkov<sup>7</sup> applied this formalism to a focused, low-power laser beam. The applicability of the paraxial ray formalism is restricted to laser beams which have ray slopes much less than one and which have diameters  $2a$  much larger than a wavelength--conditions fulfilled in our damage experiments.

In order to describe the effects of the self-focusing nonlinearity on light propagation, we begin with Maxwell's equations. Wang<sup>29</sup> has shown that when the electric field vector  $E(r)$  is written as  $A(r) \exp i [k\phi(r) - \omega t]$ , where  $k_0 = \omega/c$  and the index of refraction is written as  $n_0 + n_2 A^2/2$ , Maxwell's equations reduce to the simplified form

$$[(n_0 + n_2 A^2/2)^2 - (\text{grad } \phi)^2] \vec{A} + \frac{1}{k_0^2} \nabla^2 \vec{A} = 0 .$$

Terms of order  $(n_2 A^2)^2$  have been ignored. When the scalar product of this equation is taken with  $A$ , a term containing the factor  $1/k_0^4$  dropped, and a cross term with  $n_2 A^2$  neglected, this result leads directly to an effective eikonal

equation

$$n_1^2 - (\text{grad } \phi)^2 = 0 \quad (2-1)$$

where

$$n_1 = n_0 + \frac{1}{2} n_2 A^2 + \frac{1}{2k_0^2 n_0} \frac{\nabla^2 A}{A} \quad (2-2)$$

In the limits of zero nonlinearity and infinitesimal wavelength,  $n_1 = n_0$  and Eq. (2-1) is just the basic equation of geometrical optics. Results derived from the usual eikonal equation can be used for the nonlinear problem if the index of refraction is replaced by Eq. (2-2). In particular, it can be shown<sup>31</sup> that the curvature  $d^2\vec{r}/d\rho^2$  for a pencil of rays with position vector  $\vec{r}$  and with  $\rho$  the coordinate along the ray path is given by

$$\frac{d^2\vec{r}}{d\rho^2} = \frac{1}{n_1} \left[ \text{grad } n_1 - \frac{dn_1}{d\rho} \frac{d\vec{r}}{d\rho} \right] \quad (2-3)$$

Eq. (2-3) can be simplified by applying several approximations. We restrict the treatment to cylindrically symmetric beams and assume that the maximum ray slope is small compared to unity. (In our experiments the maximum slope inside the sample and before the focus is less than 0.05.) Both the second term on the right in Eq. (2-3) and the longitudinal component of the Laplacian in Eq. (2-2) are negligible. The curvature is now expressed in a form first derived by Talanov.<sup>28</sup>

$$\frac{d^2\vec{r}}{d\rho^2} \approx \frac{d^2\vec{r}}{dz^2} = \frac{1}{n_1} \text{grad}_1 n_1 \quad (2-4)$$

This result is important to the study of self-focusing effects because the sign of  $d^2\vec{r}/dz^2$  indicates whether or not the beam is converging and its magnitude is a quantitative measure of that convergence or divergence. A positive curvature results in an increase in the slope of the ray path with respect to the propagation direction and thus represents a divergence from the axis. Diffraction alone will produce a positive curvature in an isotropic medium. A negative curvature, on the other hand, will cause convergence of the beam towards the axis and indicates the dominance of the self-focusing nonlinearity.

Eq. (2-4) can be written in a useful form by using a "constant shape approximation"<sup>26</sup> which we now describe.  $A^2(r,z)$  is proportional to the light intensity, and where the beam propagates with little or no change in shape, the intensity at  $r$  and  $z$  is equal to a function that describes the beam shape divided by the beam area  $\pi a^2(z)$ . The shape function also depends on  $r$  and  $z$ , but in a very simple manner. We denote it by  $p$ . This function may be Gaussian, for example, with  $p = \exp(-2r^2/a^2)$ . If only the beam radius changes with  $z$  and the beam shape does not change, then  $p$  is actually a function of a reduced radial coordinate and is independent of beam size. In particular, we can define the reduced coordinate  $x$  as  $x = r/a(z)$  and write  $A^2(r,z)$  in the simplified form

$$A^2(r,z) = p(x)/\pi a^2(z) . \quad (2-5)$$

The approximation of Eq. (2-5) is normally used in numerical calculations. Along with Eq. (2-4) it provides the basic relationship needed to calculate the critical power, the self-focusing length, and the quantitative influence of the index nonlinearity when diffraction dominates.

By expanding  $\nabla_{\perp}^2$  in cylindrical coordinates  $r$  and  $z$  it is easily seen that  $\nabla_{\perp}^2 A/A$  is also proportional to  $a^2$ . We can then write Eq. (2-2) as

$$n_1 = n_0 + \frac{1}{a^2(z)} f(x) \quad (2-6)$$

where  $f(x)$  is the sum of contributions from both diffraction and the index nonlinearity.  $\text{Grad}_{\perp}$  is just  $a(z)^{-1} \partial/\partial x$ , and  $n_1$  in the denominator of Eq. (2-4) can be replaced by  $n_0$ . Eq. (2-4) thus gives us the basic equation for light propagation within the paraxial ray approximation, namely

$$\frac{d^2 r}{dz^2} = \frac{1}{n_0} \frac{1}{a^3(z)} \frac{d}{dx} [f(x)] \quad (2-7)$$

The importance of neglected terms has been shown to be negligible<sup>29</sup> except near a catastrophic self-focus or under experimental condition where extreme external focusing is used.

We thus have our first important conclusion about self-focusing: the derivative of  $f(x)$ , which contains no dependence on  $z$ , determines the relative importance of diffraction and self-focusing. Once this relative importance is determined for one value of  $z$ , such as  $z = 0$  at the entrance plane, it

is determined for all  $z$ . The critical power  $P_c$  is in principle calculated from the requirement that the derivative  $f(x)$  vanish for all  $x$ , leading to a detailed balance of self-focusing and diffraction. Since  $f(x)$  contains no dependence on beam diameter, the critical power will not be dependent on beam diameter for a steady-state nonlinearity.

C. Effects of Nonlinearity on Focused, Low-Power Laser Beams

The index nonlinearity leads to intensity distortions even below the critical power for catastrophic self-focusing. Using Eq. (2-7), quantitative corrections from the nonlinearity can be derived.

The coordinate  $r$  can be replaced by  $x a(z)$  on the left side of Eq. (2-7) to obtain a differential equation for the beam radius  $a(z)$ , namely

$$\frac{d^2 a}{dz^2} = \frac{1}{a^3(z)} \left[ \frac{1}{n_0 x} \frac{d}{dx} f(x) \right] \quad (2-8)$$

Wagner et al.<sup>30</sup> have evaluated Eq. (2-8) for a Gaussian beam near  $x = 0$ . They obtain, to first order,

$$\frac{d^2 a}{dz^2} = [1/k^2 a^2(z)] (1 - P/P_{cr}) \quad (2-9)$$

where  $P$  is the total power in the beam,  $k = 2\pi/\lambda$ , and  $P_{cr}$  is given by

$$P_{cr} = \frac{c\lambda^2}{32\pi n_2} \quad (2-10)$$

When Eq. (2-9) is multiplied by  $z(da/dz)$ , it can be integrated subject to the boundary conditions that  $(da/dz)_z=0 = \dot{R}_0$  and  $a(0) = R_0$ . When the laser beam is focused sufficiently far inside the material,  $\dot{R}_0$  is the tangent of the far-field diffraction angle whose exact value will be given later. We find

$$\left(\frac{da}{dz}\right)^2 = -\frac{(1-P/P_{cr})}{k^2 a^2(z)} + \dot{R}_0^2 + \frac{(1-P/P_{cr})}{k^2 R_0^2} \quad (2-11)$$

The minimum beam radius  $a_1$  (i.e., the radius of the focal point) is found by setting  $da/dz = 0$  and solving the resulting equation for  $a_1$ . This procedure gives the focal radius  $a_1$  as a function of input power and self-focusing parameters. That is,

$$a_1 = (1-P/P_{cr})^{1/2} [k^2 [\dot{R}_0^2 + (1-P/P_{cr})/k^2 R_0^2]]^{-1/2} \quad (2-12)$$

For the power range of interest to our damage experiments ( $P < P_{cr}$ ), Eq. (2-12) can be considerably simplified because, as we now demonstrate, the power dependent term in the brackets can be neglected. We want to show that

$$\dot{R}_0^2 + 1/k^2 R_0^2 \gg \frac{P/P_{cr}}{k^2 R_0^2} \quad (2-13)$$

To simplify the demonstration that this equality is valid, the positive term  $1/k^2 R_0^2$  on the left of Eq. (2-13) is ignored and  $P/P_{cr}$ , which is less than unity in the region of interest, is replaced by 1. Eq. (2-13) thus reduces to

$$|R_0| \gg 1/k R_0 \quad (2-14)$$

The rate of change of the Gaussian beam radius at the entrance plane is given by

$$|\dot{R}_0| = \tan \epsilon \quad \begin{cases} = a_0 & \text{for small angles (weak focusing)} \\ > a_0 & \text{for large angles (strong focusing)}. \end{cases}$$

Assuming the worse and letting  $|\dot{R}_0| = \theta_0$  where

$$\theta_0 = \frac{2}{\pi} (\lambda/2a_0)$$

for a Gaussian beam, we find that the inequality of Eq. (2-13) becomes

$$(2/\pi) (\lambda/2a_0) \gg \lambda/2\pi R_0$$

or

$$2 R_0 \gg a_0$$

Since in our experiments the diffraction-limited Gaussian beam radius  $a_0$  is at least an order of magnitude smaller than the incident Gaussian radius  $R_0$ , this inequality is easily satisfied.

Because we can neglect the power dependent term in the bracket of Eq. (2-12), that equation takes the simple form

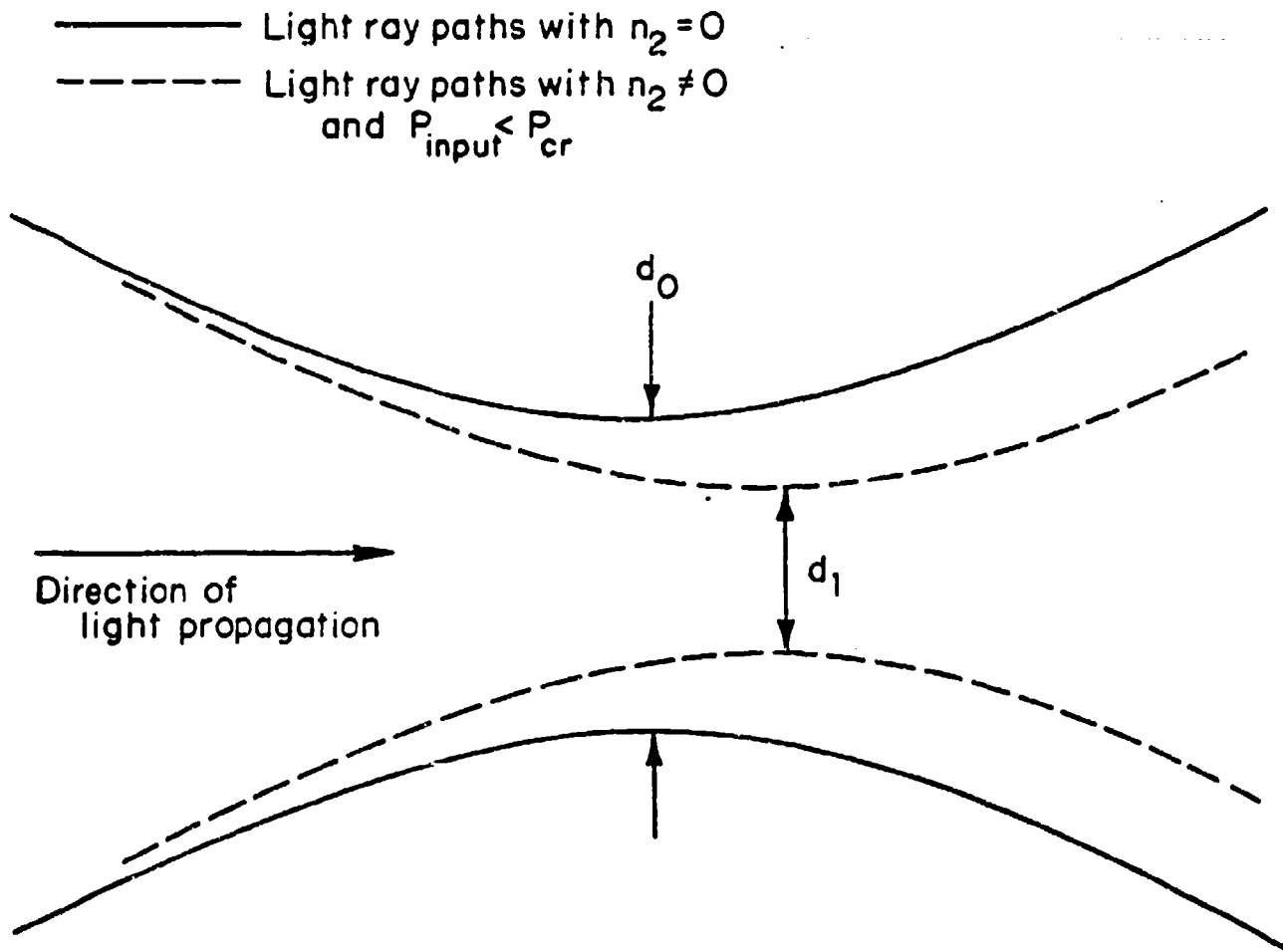
$$a_1 = (1 - P/P_{cr})^{1/2} a_0 \quad (2-15)$$

Eq. (2-15) summarizes the behavior of a laser beam with  $P < P_{cr}$  that is focused into a nonlinear medium. The radius of the focus is reduced below its diffraction limit  $a_0$  because of the self-focusing nonlinearity. This behavior is illustrated in Fig. 4. As the laser power  $P$  approaches  $P_{cr}$ , the focal radius decreases until it becomes so small that the approximations used to derive Eq. (2-15) are no longer valid. Eq. (2-15) appears to be a useful approximation for  $P \leq 0.9 P_{cr}$ . In any nonlinear medium, therefore, the laser intensity on-axis is increased above its diffraction limit by the factor  $(a_1/a_0)^2$  where  $a_0$ , the diffraction-limited focal radius, is the same for light focused in air or in a solid.

$P_{cr}$  can be shown to be the laser input power for which diffraction and self-focusing effects balance at the center of a Gaussian light beam. For input powers greater than  $P_{cr}$  but less than the critical power  $P_c$ , diffraction dominates everywhere except near the beam axis. Numerical calculations<sup>27</sup> show that a collimated beam will initially intensify at such powers until the diffraction of the wings forces the on-axis intensity to drop.  $P_{cr}$  differs from  $P_c$  because the latter is a quantity averaged over the entire beam while  $P_{cr}$  is determined by the behavior near the center. In fact,  $P_c$  is not a precisely defined quantity because it is not possible to exactly balance diffraction and self-focusing over the entire beam cross-section. At an input power of  $P_c$ , therefore, a propagating beam will not change its size measurably and so not experience a catastrophic self-focus, but its intensity

Fig. 4. THE EFFECT OF THE INDEX NONLINEARITY ON THE MINIMUM DIAMETER OF A FOCUSED LASER BEAM WHEN  $P < P_{cr}$

PBN-72-1287



The tendency to self-focus acts in opposition to diffraction. Whereas diffraction produces a positive ray curvature, self-focusing produces a negative ray curvature. The focal diameter  $d = 2a$  inside a nonlinear medium ( $n_2 \neq 0$ ) will be effectively reduced, therefore, from  $d_0$  -- its value with  $n_2 = 0$  -- to  $d_1$ , and the on-axis light intensity at the focus will be correspondingly increased. As shown by Wagner et al. (see Ref. 30), the presence of the index nonlinearity also causes the point of minimum beam radius to be displaced to the right toward the geometrical focus. This latter observation is not important to the discussion in the text.

distribution will be distorted.  $P_c$  has the same functional form as  $P_{cr}$  and differs by just a numerical factor as  $P_{cr} = 0.273 P_c$  for Gaussian beams.<sup>26</sup>

#### D. Transient Effects

The above analysis is correct only in the steady state. In solids the dominant nonlinearity is normally electrostriction,<sup>6</sup> and if the process is transient, it is no longer true that the relative balance between diffraction and self-focusing is independent of propagation distance and that the critical powers are independent of beam diameter. The changes occur because electrostriction becomes non-local in both a temporal and a spatial sense. Although a susceptibility approach such as used here is no longer strictly correct, it is nonetheless useful for establishing functional dependences for self-focusing parameters and approximate quantitative values.

Two results from a transient analysis are important.<sup>32</sup> The first is that transient effects decrease the effective nonlinear index  $n_2$  and thus make self-focusing more difficult. The second important result involves the dependence of the critical power on laser pulse width and on beam diameter. In the steady state, the nonlinear index  $n_2$  is given by<sup>6</sup>

$$n_2 = \frac{n_o (\rho \frac{\partial n}{\partial \rho})^2}{4\pi o v^2}$$

where  $n_0$  is the index of refraction in the absence of the nonlinearity,  $\rho$  is the material density, and  $v$  is the acoustical sound velocity. The quantity  $(\rho \partial n_0 / \partial \rho)$  for cubic materials such as the alkali-halides may be found approximately by differentiating the Clausius-Mosotti equation.<sup>33</sup> The remaining constants are tabulated in handbooks.

When the laser pulse width  $t_p$  is shorter than the electrostrictive response time  $t_R = a/v$ ,  $n_2$  is decreased in value, thereby increasing the critical power. For a triangular pulse, Kerr<sup>32</sup> has shown that

$$(n_2)_{\text{transient}} = (n_2)_{\text{steady-state}} \left[ 1 - \frac{a}{v\rho} D\left(\frac{v\rho}{a}\right) \right] \quad (2-16)$$

where  $D\left(\frac{v\rho}{a}\right)$  is Dawson's integral with

$$D(\xi) = \exp(-\xi) \int_0^\xi \exp \eta^2 d\eta$$

When  $t_p \leq t_R/2$ ,

$$(n_2)_{\text{transient}} \approx k(n_2)_{\text{steady-state}} \frac{v^2 t_p^2}{a^2}$$

This result is valid for more general and realistic pulse-shapes with the numerical constant  $k$  being of order unity and having a value dependent on the precise time-structure of the pulse. When this result is inserted into Eq. (2-10), the critical power becomes

$$(P_c)_{t_p/t_R \lesssim 1/2} = (P_c)_{\text{steady-state}} \frac{a^2}{k v^2 t_p^2} \quad (2-17)$$

For short laser pulses, therefore, when the process is transient, there exists more properly a critical intensity rather than a critical power, and fairly small changes in pulse-width will have a significant effect on the critical power.

#### E. Applications of Self-Focusing Theory to Optical Damage

When catastrophic self-focusing occurs in solids, the results are dramatic--an extended spark and local disruption of the crystal. Because such optical damage apparently always accompanies catastrophic self-focusing in crystals, it has become customary in the damage literature to associate damage with total collapse of the laser beam.<sup>34</sup> Results of the preceding sections show, however, that it is possible to induce optical damage without measurable beam distortion from self-focusing. This is possible because catastrophic self-focusing and beam distortion depend on the laser incident power whereas intrinsic optical damage depends on intensity for a fixed laser pulse width.

These observations form the basis for the design of our optical damage experiments. A laser beam with input power much less than  $P_{cr}$  is focused tightly with external optics in order to achieve the high intensities necessary to induce intrinsic damage. Great care is taken to avoid measurable aberrations in the focusing optics.

In order to apply this technique, estimates of  $P_{cr}$  are required. The nonlinear index from electrostriction can be

calculated in the manner discussed in the previous section, and the electronic self-focusing parameters can be calculated from the third-order electronic susceptibility.<sup>35</sup> In particular,

$$n_2 = \frac{\pi \chi^{(3)'}}{n_0} \quad (2-18)$$

where  $\chi^{(3)'}$  is the real part of the electronic nonlinear susceptibility  $\chi_{1111}^{(3)}$ .  $\chi^{(3)'}$  can be obtained from measurements of third-harmonic generation.<sup>36</sup> Typically,  $P_c$  from steady-state electrostriction at 1.06  $\mu\text{m}$  is on the order of 1 MW ( $10^6$  watts) while the electronic critical power is about an order of magnitude larger. Because of transient effects, electrostriction will weaken as the laser pulse width is lowered below about 5 ns for a 50  $\mu\text{m}$  beam diameter and will generally be unimportant for subnanosecond laser pulses.

Experimental checks are necessary to confirm the absence of significant beam distortion. Previous experimenters had connected the damage morphology with self-focusing,<sup>9, 37</sup> but morphology is not a reliable indicator of the presence of self-focusing. Intrinsic damage in the absence of self-focusing effects can have a morphology similar to that seen with optical damage preceded by catastrophic self-focusing. (See Chapt. 7.)

The simple test used in the present work to confirm the absence of self-focusing consists of measuring the damage field with lenses having different focal lengths. If the input power required to induce damage scales with the square of the

focal length, as expected for an intensity dependent process such as intrinsic breakdown, then catastrophic self-focusing from a steady-state nonlinearity is absent. In addition, using Eq. (2-15) we can show that significant beam distortion is also absent.

If, on the other hand, the laser pulse width is less than the electrostrictive response time ( $a/v$ ), Eqs. (2-15) and (2-17) predict just the results obtained. It may be desired to demonstrate the absence of transient electrostrictive self-focusing by changing the laser pulse width and comparing the input damage powers with those expected from Eq. (2-17). Because intrinsic breakdown is weakly pulse-width dependent as shown in Chapt. 5, care must be used in interpreting results.

#### F. The Measurement of Self-Focusing Parameters Using Intrinsic Optical Damage

Experimental values of  $n_2$  for various materials have been determined from measurements of induced birefringence,<sup>38</sup> by studies of the movement<sup>9</sup> or positions<sup>39</sup> of optical damage tracks in crystals, or by observing the changes in the intensity distribution of the transmitted laser beam as the input power is increased.<sup>40</sup>

A new technique for measuring self-focusing parameters was developed from the results of Sects. B-D. It consists of determining the powers necessary to induce intrinsic bulk

damage as lenses with different focal lengths are used to focus the radiation and then comparing these results to predictions based on Eq. (2-12). High input powers are not needed so that relatively small, stable lasers can be used. This technique is described in detail below, and as an illustration of its application, the self-focusing parameters for sapphire are determined. Some experimental results and ideas developed in later chapters will be briefly introduced.

Fig. 4 illustrates schematically the effect of the index nonlinearity on a  $TEM_{00}$  laser beam when  $P < P_{cr} < P_c$ . As shown by Eq. (2-15), the focused beam radius is decreased from its diffraction limit of  $a_0$  to a smaller value,  $a_1$ , because of the nonlinear index. As a result, the on-axis intensity is increased by the factor  $(a_0/a_1)^2$ . If  $I_0$  is the intensity when  $n_2 = 0$ , then from Eq. (2-15) we find that the intensity  $I_d$  in the presence of the nonlinear index is given by

$$I_d = I_0 / (1 - P/P_{cr}) \quad (2-19)$$

where  $P$  is the input power of the laser beam and  $P_{cr}$  in esu units is given by Eq. (2-10). As the input power is increased to a value within a few percent of  $P_{cr}$ , corrections to Eq. (2-19) due to diffraction of the wings of the laser beam may become important<sup>26</sup> and numerical calculations may be required to accurately establish the relationship between  $I_d$  and  $I_0$ .

Although we have considered only Gaussian beams, Eq. (2-19) is valid for any smoothly varying intensity distribution which has its most intense region along the axis and which is

quadratic in  $r$  near the axis. The precise value of  $P_{cr}$ , however, depends on the coefficient of the quadratic term. It was shown in Sect. C that corrections to Eq. (2-19) are unimportant when  $P < P_{cr}$  and the beam is focused sufficiently to induce intrinsic damage.

The steady-state analysis summarized by Eq. (2-19) is appropriate for tightly focused laser beams, because the electronic contribution to  $n_2$  is in its steady state for all attainable laser pulses<sup>38</sup> and electrostriction is in its steady state whenever the laser pulse width  $t_p$  is greater than a response time  $t_R$  given by the ratio of the radius of the focused laser beam and the radial compression wave velocity  $v$ .<sup>6</sup> (In sapphire, where  $v = 1.1 \times 10^6$  cm/sec for light propagation along the crystalline  $c$  axis,  $t_p/t_R = 1$  when  $t_p = 10^{-8}$  sec and the focused beam diameter is 220  $\mu$ m.) If electrostriction is slightly transient, Eq. (2-19) may still be used with  $P_{cr}$  corrected in the manner discussed in Sect. D.

Having thus determined the intensification produced by the index nonlinearity, we look for a process which is sensitive to a constant value of on-axis laser intensity. The powers necessary to reach this intensity will be recorded as lenses with different focal lengths are used. The basic requirements for this process are, first, that it be easily observable with a reasonably well-defined intensity threshold and, second, that its threshold can be reached with strong external focusing when  $P$  is constrained to values less than  $P_{cr}$ . Intrinsic optical damage from avalanche breakdown will be shown in later

chapters to meet these requirements.<sup>41</sup> Breakdown leads to a spark and local melting of the material and is therefore easily observed.

$P_{cr}$  is determined from measurements of the damage power  $P$  made with various lenses having different focal lengths. Because  $P$  must be less than  $P_{cr}$ , short focal lengths are required. Complications from aberrations in the focusing optics and inaccuracies in determining the input powers can be greatly reduced by the use of a reference crystal such as NaCl that can be damaged over a large range of input powers before self-focusing becomes important. (See Chaps. 4 and 5.) Approximate values of  $P_{cr}$ , which are useful for the initial selection of focusing optics, can be calculated as discussed in the previous section.

The focal lengths of the various lenses can be related to the focal spot size in air  $a_0$ . (The focal radius in air and the focal radius in the crystal are, neglecting aberrations and self-focusing, identical.) A measurement is thus made of the incident power necessary to induce damage as a function of the focal radius in air  $a_0$ . In Eq. (2-19),  $I_0$  is replaced by  $kP/a_0^2$  where  $k$  is a constant that depends on the index of refraction  $n_0$  and the intensity distribution of the laser pulse. If  $I(r) = I_0 \exp(-2r^2/a_0^2)$ ,  $k$  has a value of  $(2/\pi) n_0$ . Eq. (2-19) then becomes

$$\frac{1}{P} = \left( \frac{2n_0}{\pi I_d} \right) \frac{1}{a_0^2} + \frac{1}{P_{cr}} \quad (2-20)$$

The damage intensity  $I_d$  does not depend on  $a_0$  for avalanche breakdown. A plot of  $1/P$  as a function of  $1/a_0^2$  yields a straight line with  $1/P_{cr}$  as the intercept and  $2/\pi I_d$  as the slope.

Two precautions should be taken when using this measurement technique. The first is to avoid damage from absorbing inclusions, and the second is to account for any dependence of avalanche breakdown on the laser pulse width. Methods for distinguishing between inclusion and intrinsic damage are discussed in detail in Chapt. 3. Inclusion damage can often be completely avoided, because the use of strong external focusing which is needed for the present technique results in the sampling of volumes that are so small that damaging inclusions are normally avoided. The laser pulse width dependence to the damage field will be shown in Chapt. 4 to be small for Q-switched laser pulses. Measurements conducted with mode-locked lasers, however, cannot be directly compared to those made with Q-switched lasers.

As an illustration of the use of this technique, we consider data accumulated in two different experiments on optical damage in sapphire. In the first experiment<sup>34</sup> a Q-switched TEM<sub>00</sub> ruby laser was used by Giuliano et al. to damage sapphire with three different lenses. In the second, reported in Chapt. 7, a measurement was made with two different lenses and a Q-switched TEM<sub>00</sub> YAG:Nd laser. The pulse widths were 20 ns and 5 ns, respectively.<sup>42</sup> Table I summarizes the relevant results of these studies.

TABLE I

Damage Power in Sapphire  
for Different Beam Sizes

<u>Wavelength</u>	<u><math>a_0(\mu\text{m})^*</math></u>	<u>P (MW)</u>
0.6943 $\mu\text{m}$	20	0.51 $\pm$ .04
(ref. 34)	53	0.74 $\pm$ .07
	140	1.23 $\pm$ .10
1.064 $\mu\text{m}$	9.0	0.24 $\pm$ .05
(Chart. 4)	4.1	0.05 $\pm$ .02

\*The beam radius is defined to be the  $1/e^2$  radius for the intensity. In both experiments Gaussian laser beams were used.

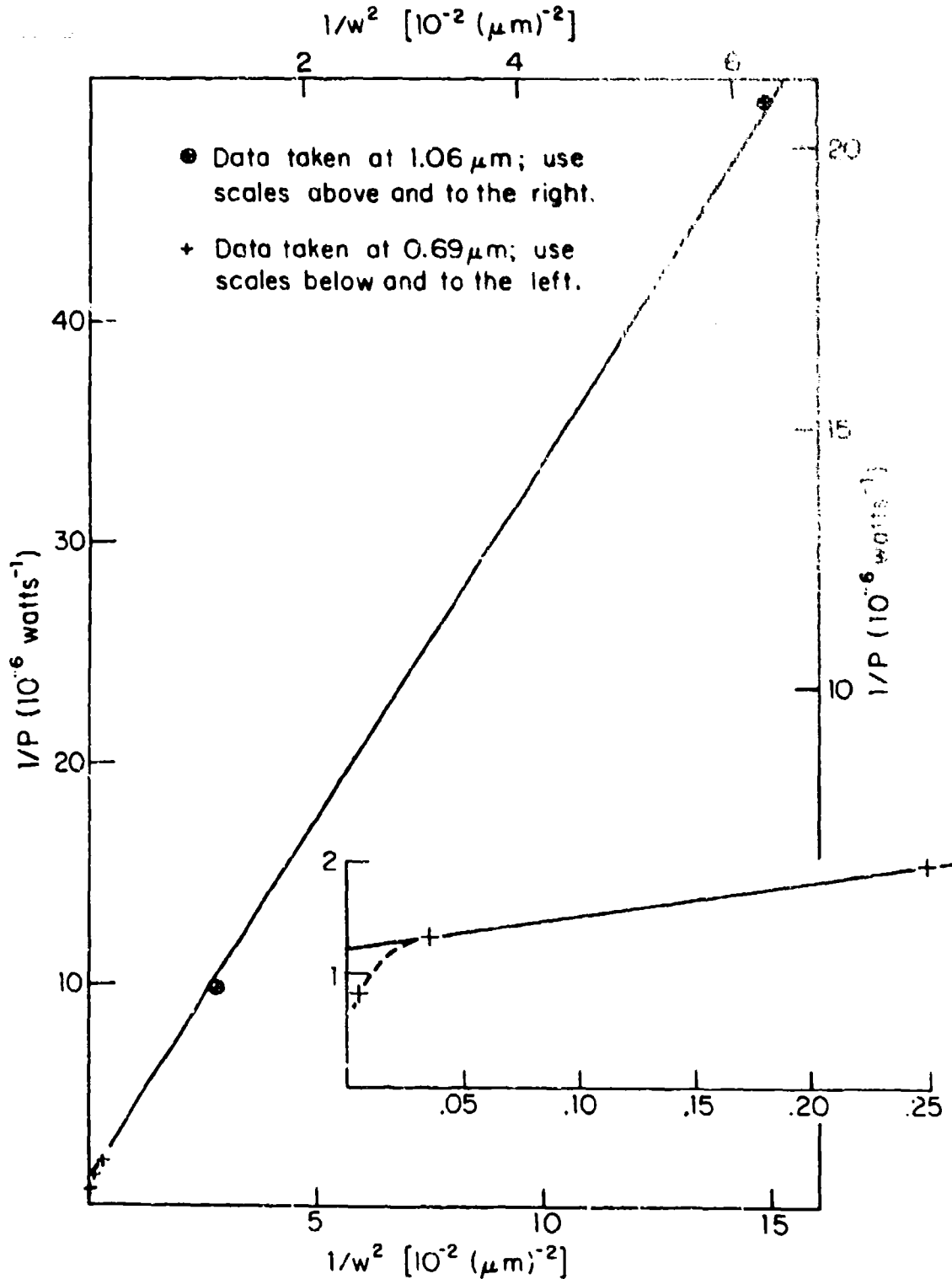
In order to compare the data, the wavelength dependence of  $P_{cr}$  must be considered. It can be seen from Eqs. (2-10) and (2-20) that the data can be plotted together if the coordinate axes for the YAG data are properly scaled relative to those for ruby. In the plot of  $1/P$  versus  $1/a_0^2$  in Fig. 5, the axes are scaled by  $[\lambda_0(\text{YAG})/\lambda_0(\text{ruby})]^2 = 2.35$ . The intercept on the vertical ruby axis is  $P_{cr}$  at  $0.6943 \mu\text{m}$ , and the slope measured relative to either pair of axes, is  $(2/\pi I_d) n_0$ .

$P_{cr}$  is found to be  $0.83 \times 10^6$  watts at ruby wavelength,  $P_c = 3.0 \times 10^6$  watts,  $n_2 = 0.56 \times 10^{-13}$  esu, and  $I_d$  is  $1.1 \times 10^{11}$  watts/cm<sup>2</sup>. The value for  $P_{cr}$  lies within the range of values reported in Ref. 9, and  $I_d$  agrees with the results of Chapt. 7.

The plot in Fig. 5 curves downward when  $1/w^2 \leq 0.02 \times 10^{-2} (\mu\text{m})^{-2}$  because the electrostrictive contribution to the critical power is becoming transient. Even though Eq. (2-20) is not valid for transient effects, we can modify it to approximate slightly transient behavior by using Eq. (2-16). If it is assumed that the electrostrictive nonlinearity is much larger than the electronic effect, a damage power of about  $1.1 \times 10^6$  watts is predicted for  $w = 140 \mu\text{m}$ . Alternately, if the electronic and electrostrictive contributions are equal, the damage power is estimated to be  $1.0 \times 10^6$  watts. Both values compare favorably to the measured value of  $1.2 \times 10^6$  watts in Table I.

Giuliano and Marburger<sup>9</sup> have inferred a range of values

Fig. 5. THE DEPENDENCE OF DAMAGE POWER FOR SAPPHIRE ON BEAM FOCAL DIAMETER



A plot of  $1/P$  as a function of  $1/w^2$  produces a straight line according to Eq. (2-20). In this figure we have used  $w$  to denote the Gaussian beam radius  $a_0$ . For large  $w$  ( $1/w^2 \leq 0.02 \times 10^{-2} (\mu\text{m})^{-2}$ ), departures from a linear relationship are expected because electrostriction becomes transient. This is experimentally observed as seen in the insert where the scales for the ruby data have been expanded.

for the nonlinear index in sapphire of  $0.31$  to  $9.5 \times 10^{-13}$  esu. It is clear from the more recent measurements of Ref. 34, however, that  $n_2$  cannot be as large as  $9.5 \times 10^{-13}$  esu. Giuliano and Marburger's analysis was based on the central assumption that there exists a one-to-one correspondence between a damage spark and a moving self-focus where the latter develops from catastrophic self-focusing. While this is almost certainly true at high input powers, the present analysis and the experiments in later chapters show that a spark and optical damage can occur at low powers where a moving self-focus is absent. It is very likely that their plot of  $P^{\frac{1}{2}}$  versus  $1/z_f$ , where  $z_f$  is the self-focusing distance, deviates from a linear relationship at low powers because damage is occurring without catastrophic self-focusing in this region and not because of transient effects as they suggest. Only data obtained with large values of  $P$ , therefore, can be used within the framework of their analysis to predict  $n_2$ . The lower value of their range of values for  $n_2$  ( $0.31 \times 10^{-13}$  esu) is probably the most meaningful. It is somewhat smaller than the present estimate of  $n_2$ , because under their focusing conditions, the electrostrictive contribution to the nonlinearity may have been transient and therefore smaller than under steady-state conditions. It thus appears that the present measurement of self-focusing parameters in sapphire is consistent with the results of Giuliano and Marburger.

The electronic contribution to  $n_2$  can be determined by the present technique if conditions of measurement are chosen

such that  $t_D/t_R \ll 1$ . Because of the requirement that the input power be less than  $P_{cr}$ ,  $t_D/t_R \ll 1$  cannot be achieved by increasing  $t_R$  through the use of weakly focusing external optics. This extreme transient limit can be achieved, however, by using single, mode-locked laser pulses with time durations of the order of 10 ps. Such pulses must be temporally smooth and hence transform-limited so that a YAG:Nd system is a natural choice for the laser.

In summary, the analysis of Sect. C leads to a useful technique for measuring self-focusing parameters. The ideas which we have developed here not only provide the basis for this technique, but they also help clarify the relationship between self-focusing and optical damage, a relationship which has often been confused in the literature.

## CHAPTER 3

### THE LASER SOURCES AND EXPERIMENTAL TECHNIQUES

#### A. Introduction

In this chapter we will describe the equipment and procedures used in the damage experiments in Chaps. 4-7. Sect. B describes the two Q-switched laser systems, developed by D. Bua and M. Bass of Raytheon Corp., which were used for the nanosecond-pulse studies of damage. Measurements made by the author to characterize these systems will be presented along with an alignment technique that is useful for longitudinal mode selection. The experimental procedures used in the damage studies will also be summarized in this section. In Sect. C a mode-locked laser developed by J. P. Letellier and J. McMahon of Naval Research Laboratories will be described and measurements to characterize its performance summarized.

In the studies of avalanche breakdown, inclusion damage was treated as an experimental problem to be avoided. For this reason techniques for identifying inclusion damage will be considered in this chapter in Sect. D. Without these techniques, several of our damage experiments could not have been completed. The convincing identification of intrinsic processes, in fact, requires that either inclusion damage be known to be absent or that inclusion damage be distinguishable from intrinsic damage at each damage site.

#### B. The Q-Switched Lasers and Beam-Handling Optics

Fig. 6 shows schematically the principal features of the Q-switched laser sources. These systems were pulse pumped and

**Preceding page blank**

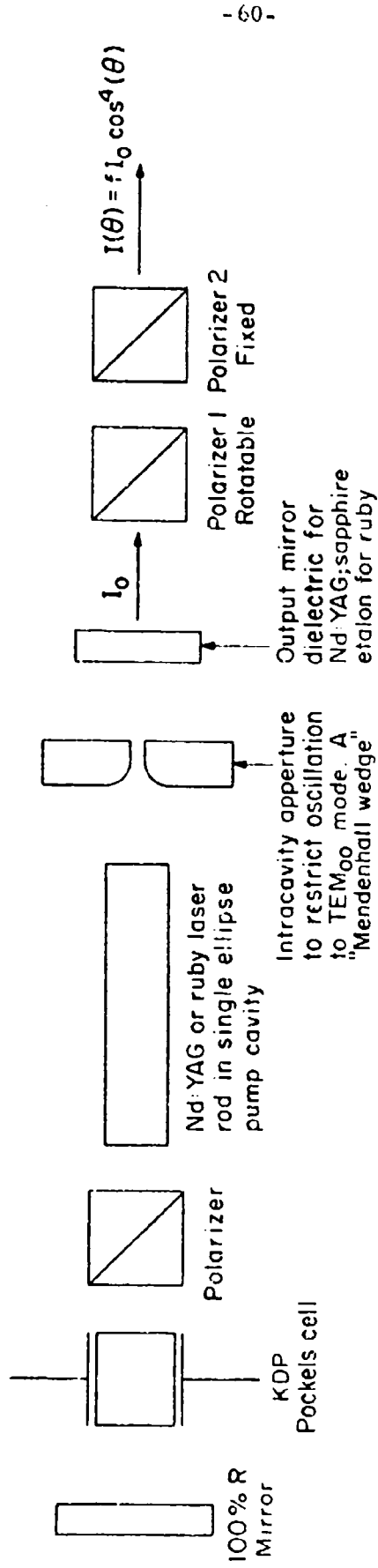


Fig. 6. Q-SWITCHED LASERS AND VARIABLE ATTENUATOR CONFIGURATION FOR DAMAGE STUDIES

Neutral density filters were often used in addition to the Glan prism attenuators.

electro-optically Q-switched. Some important properties of these devices are summarized in Table II.

In order to make meaningful measurements of absolute damage fields, it was essential to restrict the laser transverse structure to a single radial mode. This was accomplished by inserting small circular apertures into the plane-mirror laser cavities. It is well known that diffraction losses are large for a plane mirror cavity so that the use of a circular aperture, which reduces the cavity Fresnel number, can be effective in preventing oscillation in all but the lowest order ( $TEM_{00}$ ) mode.<sup>43</sup> In a confocal cavity, on the other hand, diffraction losses will be relatively unimportant compared to mirror and scattering losses, and an aperture of reasonable size cannot normally produce  $TEM_{00}$  output.

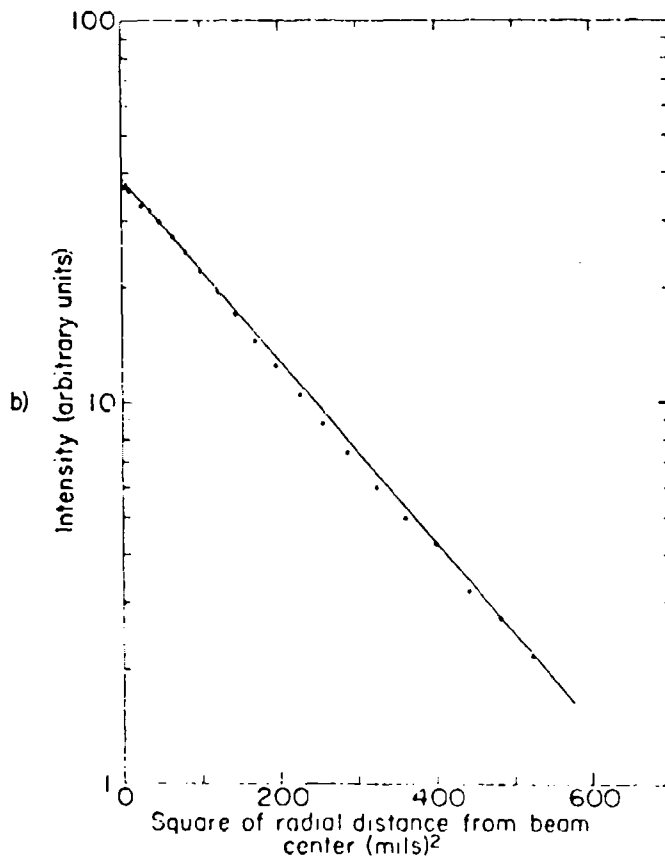
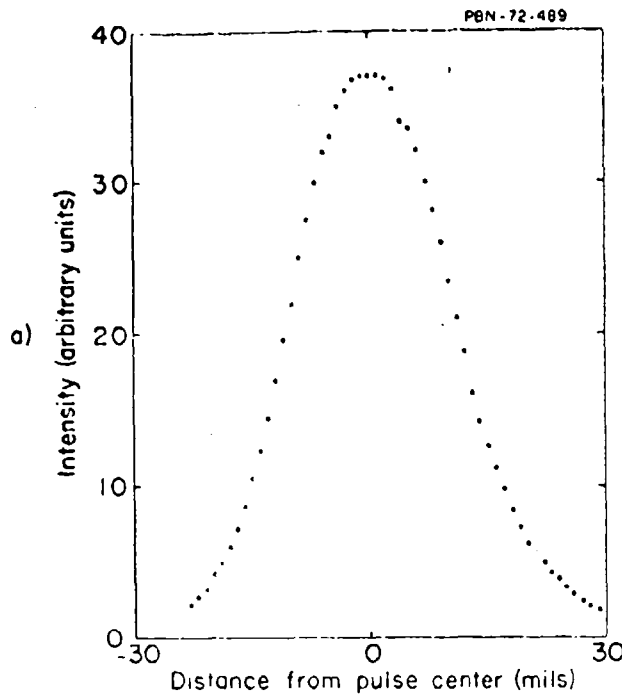
Two techniques were used to verify  $TEM_{00}$  operation. In the first, a 1-mil pinhole was moved across the YAG:Nd beam in 1-mil translation steps and the intensities of successive shots recorded. Fig. 7 summarizes the result of one measurement. Each data point is a visual average of about 5 laser shots. The small dip visible near the center of Fig. 7a could not be reproduced and therefore indicates the experimental errors in the measurement. By plotting the logarithm of the laser intensity as a function of the radial distance squared, it was found that the output of the beam had a Gaussian profile of the form  $I_0 \exp(-2r^2/\sigma^2)$  where  $\sigma$  is measured from Fig. 7b to be about 0.49 mm.

Because the ruby laser was fired less frequently than the

TABLE II

LASER PARAMETERS

Wavelength	Nd:YAG 1.06 $\mu$ m	Ruby 0.694 $\mu$ m
Energy TEM <sub>00</sub> Mode	1.5 mj	2.0 mj
Beam Diameter at Output Mirror TEM <sub>00</sub> Mode	0.8 mm	0.7 mm
Polarization	Linear	Linear
Pulse Repetition Rate	1 pps	1 pulse/5 sec
Pulse Duration in TEM <sub>00</sub> Mode	4.7 nsec (FWHP)	14 nsec (FWHP)
Pulse to Pulse Energy Reproducibility	$\pm$ 7%	$\pm$ 10%

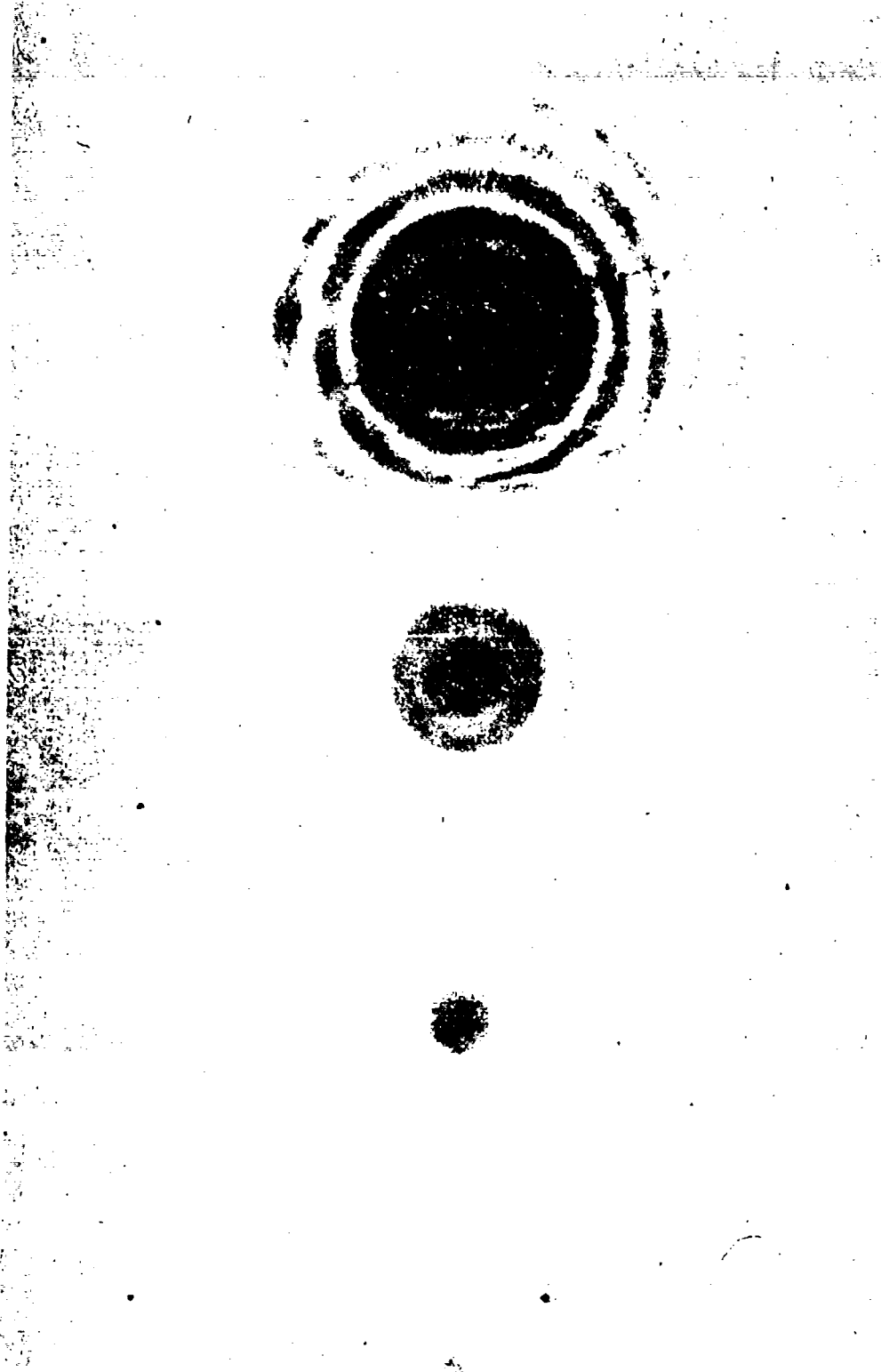


The intensity is found to be of the form  $I(r) = I_0 \exp(-2r^2/\sigma^2)$  with  $\sigma = 0.49$  mm.

Fig. 7. INTENSITY DISTRIBUTION OF THE YAG:Nd LASER AS A FUNCTION OF RADIAL DISTANCE FROM THE BEAM CENTER AT THE POSITION OF THE FOCUSING LENS

YAG and was generally less stable, a second technique for measuring the transverse mode structure was used with the ruby system. A lensless camera was placed in front of the ruby laser with a coated glass plate positioned just before a photographic transparency. The plate was coated in such a manner that the red ruby light was partially reflected at each surface and the light transmitted to the undeveloped transparency consisted of discrete images each attenuated by a factor of 2 from the image above it. Fig. 8 shows the intensity distribution of a single ruby pulse obtained in this manner. It is seen that the intensity distribution of the ruby laser more nearly resembled the far-field pattern of a plane wave than a Gaussian. By imaging the focal plane of the lens used in the damage studies, it was possible to directly measure the intensity distribution of the laser beam when it was tightly focused. This technique was not used with the YAG laser because of the difficulties involved in obtaining and preparing photographic emulsions sensitive to  $1.06 \mu\text{m}$  radiation.

Measurements of the transverse distribution summarized in Figs. 7 and 8 integrate the transverse intensity distribution over the full time duration of the laser pulse. Depletion effects in the rod, however, can cause this distribution to change with time.<sup>44</sup> To verify that such an effect was not occurring on-axis where the laser intensity was greatest and damage was known to commence, the center of the beam was sampled with a 25-micron pinhole and found to have the same



The intensity distribution reproduced here is actually a multiple exposure of several laser pulses. There is no observable variation in the intensity distribution from shot to shot. Each of the four successive images are attenuated by a factor of 2. Strong truncation effects appear which may introduce rapid spatial variations in the intensity distribution near the axis of the beam when it is focused. Imaging the focus in a separate measurement did not reveal such structure, but the spatial resolution of this photographic technique is limited.

Fig. 8. INTENSITY DISTRIBUTION OF THE RUBY LASER TAKEN WITH A MULTIPLE REFLECTION CAMERA

time structure as the entire beam.

The lasing band-width of the lasers was restricted to at most a few adjacent longitudinal modes by using a particularly simple technique that does not require any special optical cavity components such as an output resonant reflector. The technique consists of aligning the front surface of a plane-cut laser rod parallel to the 100 percent reflecting mirror. Fig. 9 indicates the resulting intracavity resonator  $M_1$ -A. The anti-reflection coating on each end of the laser rod has a residual reflectivity of about 0.25 percent and so the passive finesse of resonator  $M_1$ -A is very low. When lasing occurs, however,  $M_1$ -A contains a medium with gain and its effective finesse can be very high. In our ruby laser with a 10 cm rod, for example, the combination of a 0.25 percent reflection surface, A, a laser gain coefficient of  $\approx 0.25 \text{ cm}^{-1}$ , and the 99.9 percent cavity reflector,  $M_1$ , results in a steady-state reflectivity finesse of about 6. All other intracavity elements are placed between surfaces A and  $M_2$  to minimize reflection and scattering losses in the subcavity  $M_1$ -A.

In figures 10 and 11 the effects of rod alignment on the temporal outputs of the Nd:YAG and ruby laser are illustrated as measured by a photodiode-oscilloscope combination having a measured risetime of 0.5 nsec. For the ruby laser, additional mode selection was achieved by using a single sapphire etalon as the output mirror,  $M_2$ .

The detection of a smooth pulse by a limited bandwidth detector may be the result of either single-frequency output

Intracavity resonators

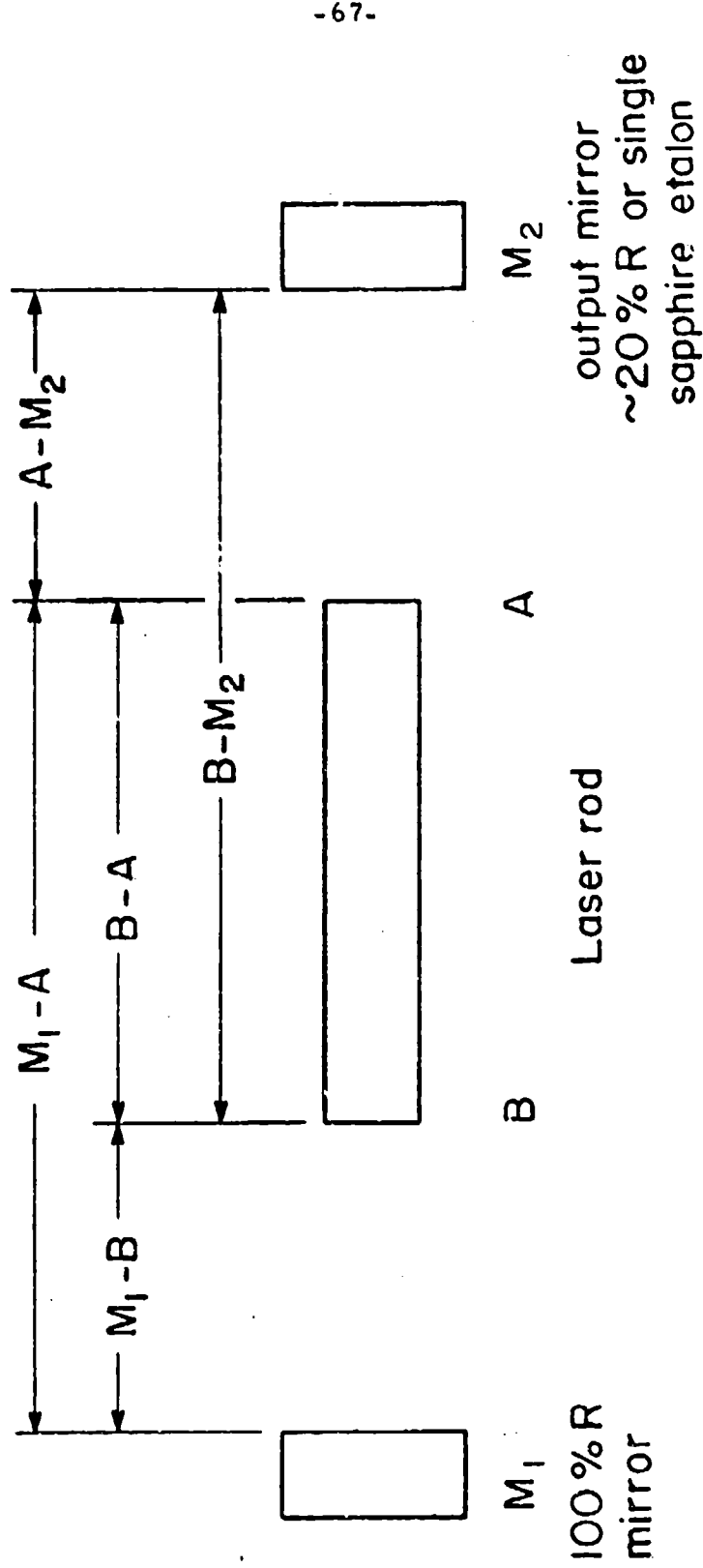


Fig. 9. SCHEMATIC DIAGRAM OF A LASER CAVITY SHOWING MODE-SELECTING INTRACAVITY RESONATOR

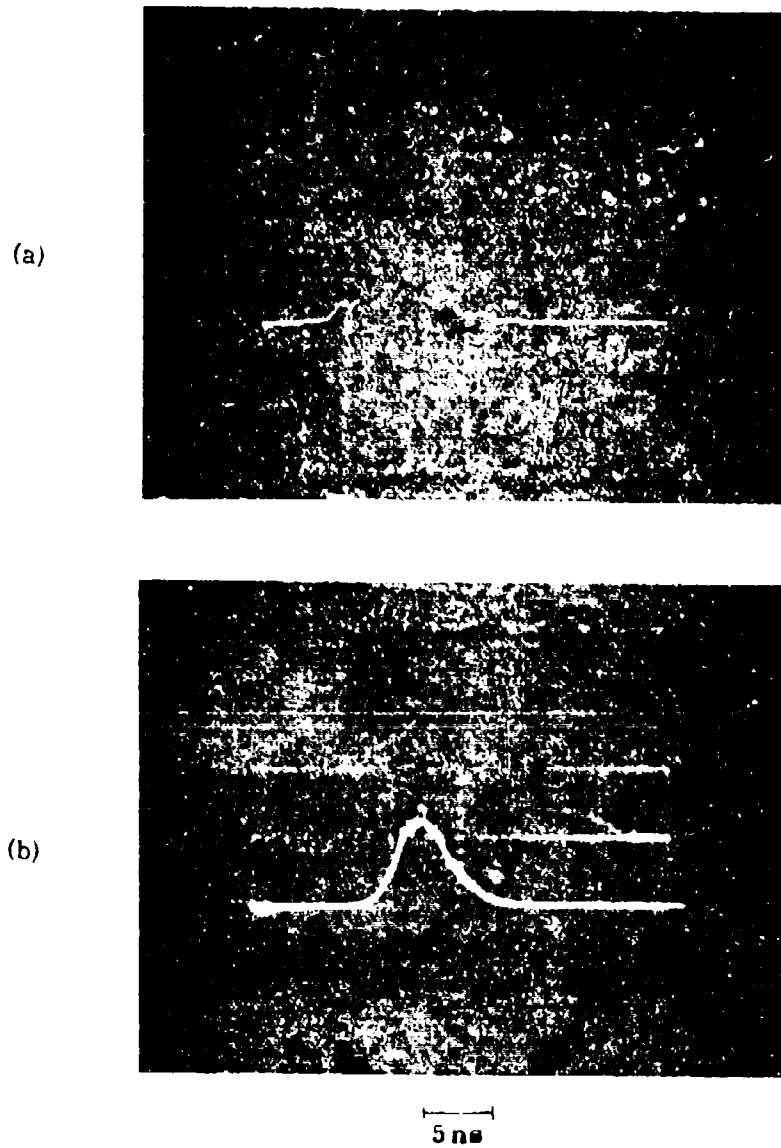
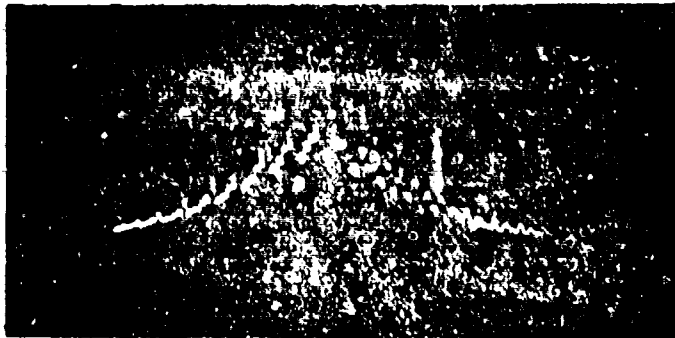


Fig. 10. EFFECT OF ROD ALIGNMENT ON OUTPUT PULSES FOR Q-SWITCHED YAG:Er LASER

- (a) Rod misaligned
- (b) Four successive shots with rod aligned

(a)



Rod badly misaligned

(b)



Rod coarsely aligned

(c)



Rod finely aligned

10  $\mu$

Reproduced from  
best available copy. 

Fig. 11. EFFECTS OF ROD ALIGNMENT ON OUTPUT PULSES  
FOR Q-SWITCHED ROPE LASER

or the simultaneous oscillation of many randomly phased modes. In order to resolve this ambiguity the lasers' output spectra were studied with Fabry-Perot interferometers. The lasing bandwidth narrowed significantly as the rod was aligned to achieve smoother pulses. Unfortunately, our interferometers lacked sufficient finesse to resolve individual laser cavity modes ( $\Delta \nu = 300$  MHz). The longitudinal mode content of a perfectly smooth laser pulse can be inferred, however, by combining the interferometer and pulse waveform data. The observed interferometer limited bandwidth of a smooth ruby laser pulse was  $\approx 1.2$  GHz, implying that a maximum of 4 adjacent modes could have been oscillating. Since the photodiode-oscilloscope combination could detect frequencies as high as  $\approx 3$  GHz, the presence of four adjacent oscillating modes would have been detected through the observation of mode beating as in Fig. 11b. Therefore, our smooth ruby laser pulses, as shown in Fig. 11c, were caused by single longitudinal mode lasing. In support of this conclusion we note that Giuliano et al.<sup>45</sup> reported that perfectly smooth pulses correspond to single mode oscillation while non-smooth waveforms were always associated with two or more oscillating modes. Replacing the sapphire etalon with a wedged output mirror did not qualitatively change the results.

We have found that slight misalignment of a multi-component resonant reflector or of one which employs high reflectivity mirrors often causes transverse mode distortion. The simple technique for obtaining smooth pulses described

above does not have this problem and is quite compatible with TEM<sub>00</sub> mode operation.

When the product of the double-pass gain and the output reflector is less than about 40 percent, it is no longer possible to operate the laser in a single longitudinal mode. A simple modification of the present technique is to misalign the rod and to insert a coated optical flat parallel to the cavity mirrors. One surface of the flat functions as the rod face M<sub>1</sub> above, and its reflectivity can be chosen to be high enough to give high mode discrimination while still low enough so that there is no lasing from that surface. This configuration is identical in basic form to conventional resonant reflectors except that the first surface has a low reflectivity to minimize degradation of the transverse structure. As in the previous technique, mode discrimination is achieved by providing a subcavity containing an active medium.

We thus see that the Q-switched lasers used in the present study produce TEM<sub>00</sub> output with at most a few simultaneously lasing longitudinal modes. Because these systems are well-characterized and stable, it is possible to use them to make accurate determinations of damage fields.

The actual damage measurements were made by focusing the laser beams through a 14 mm focal length lens to approximately 2 mm inside the samples. Care was taken to insure that spherical aberrations from both the lens and the plane entrance surface of the sample being tested were unimportant.

A brief discussion of aberrations is given in the Appendix. A fast photodiode was used to monitor the transmitted light, and an energy monitor recorded the energy in each laser pulse.

The combination of one rotatable and one fixed polarizer resulted in a variable light attenuator which was highly sensitive, quite reproducible, and which did not affect the laser pulse's polarization, spatial distribution, or duration.<sup>12</sup> If the fixed polarizer is oriented to transmit the laser polarization and if  $\theta = 0^\circ$  is the angle of the rotating polarizer which gives maximum transmission through this attenuator, then the transmitted intensity at any other angle of rotation about the beam axis is

$$I(\theta) = bI_0 \cos^4 \theta$$

where  $I_0$  is the incident light intensity and  $b$  is the fraction transmitted when  $\theta = 0^\circ$ . Calibrated neutral density filters were often used in conjunction with the variable Glan attenuator.

### C. The Mode-Locked Laser

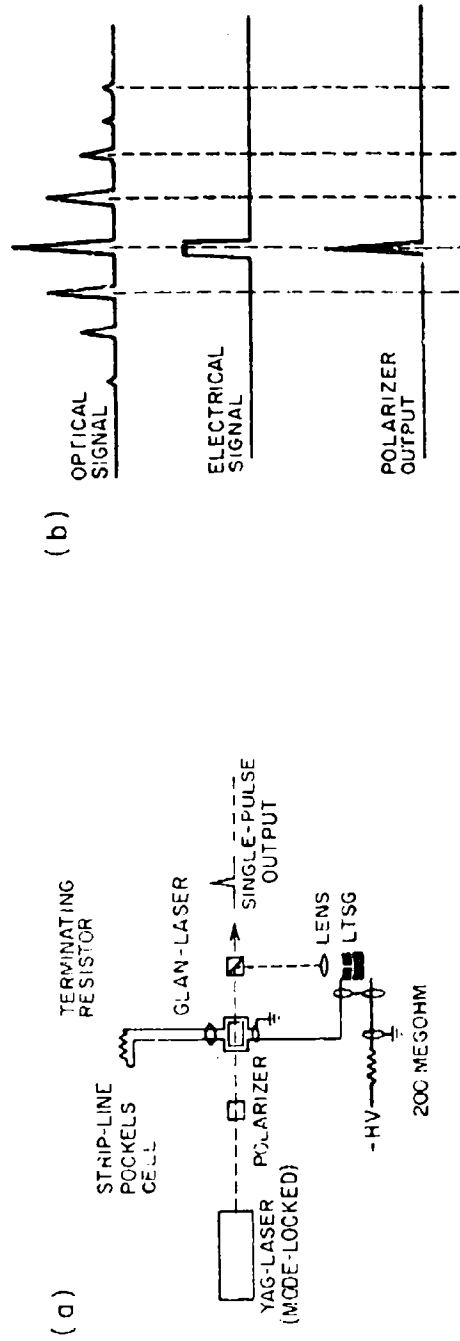
When a large number of randomly phased longitudinal modes oscillate simultaneously, the laser output has an irregular spiked envelope. A phase correlation can be forced on adjacent modes, however, and a train of short pulses produced. The technique most often used for this phase- or mode-locking is to place a saturable organic dye solution inside the cavity.<sup>46</sup> Because the absorption of the dye decreases

for high intensities, the field in the cavity is forced into a high-intensity, short-duration wave-packet, or equivalently, a large number of phase-correlated side-bands are generated which coincide with the longitudinal mode resonances of the cavity and which together produce the desired output.

The mode-locked laser used for the subnanosecond damage study of Chapt. 5 was a YAG:Nd, passively mode-locked laser with Kodak dye 9740 used as the bleachable dye. This system, as opposed to a glass:Nd laser, has the important feature that the individual spikes in the mode-locked train are free of time and carrier-frequency substructure.<sup>38</sup> It is possible, in other words, to establish a phase correlation over the entire lasing band-width with YAG:Nd as the active medium.

In order to allow a large number of longitudinal modes to reach oscillation simultaneously, the ends of the rod were cut at Brewster angle. A circular aperture restricted the radial distribution to a TEM<sub>00</sub> output, and the temperature stabilized dye was carefully circulated through a 1 mm thick cell containing the rear 99.9% reflector. The system was operated at a firing rate of 1 pps with an amplitude stability of about 20% in intensity.

A laser-triggered, electro-optic shutter, positioned just after the laser output mirror, was used to select a single pulse from the mode-locked train.<sup>47</sup> The operation of this device is summarized in Fig. 12. After the pulse train travels through an initially unbiased KDP Pockels cell, it is reflected from a fixed Glan polarizer and focused onto the



(a) The arrangements of the laser and the pulse selection equipment are shown. The Pockels cell, which represents a capacitive load, is biased with a traveling wave pulse. This arrangement, when used with appropriate resistive termination on the coaxial cable, prevents reflections and consequent "ringing" in the transmission of the pulse selector.

(b) The schematic shows the full laser train consisting of subnanosecond pulses under a Q-switched envelope and indicates how the single-pulse switching is accomplished.

Fig. 12. MODE-LOCKED LASER WITH ELECTRO-OPTIC SHUTTER FOR SINGLE PULSE MEASUREMENTS

high-voltage electrode of a pressurized laser-triggered spark gap. When the gas between the electrodes breaks down, a 5 KV voltage spike is transmitted down a coaxial line to the Pockels cell. This voltage spike has a time duration of about 7 ns which coincides with the round-trip cavity time and therefore the temporal separation of the pulses in the train. During this 7 ns time interval, one pulse will enter the Pockels cell. Because of the high voltage applied longitudinally across the KDP crystal, the plane of polarization of that pulse is rotated approximately  $90^{\circ}$  and allowed to pass through the Glan polarizer.

With this design we were able to obtain single pulses of approximately 15 ps duration for the damage studies. By replacing the cavity output mirror with a sapphire etalon, the lasing bandwidth was restricted, and pulses of just under 300 ps duration were obtained. Two-photon absorption measurements established the pulse durations.

The energy calibration posed a problem because a single 15 ps pulse caused optical breakdown inside a calibrated ballistical thermal-pile of the type that had been used to measure the energy of the Q-switched lasers. A planar photo-voltaic cell was finally chosen as an energy monitor. By operating it in an integrating mode and calibrating it with a commercial Q-switched YAG laser, we were able to establish the energy calibration to within about 25%.

This system had been known to operate in a  $TEM_{00}$  mode with an intensity distribution best described as a peaked

Gaussian. (The distortion of the mode probably resulted from the optical characteristics of the dye.) We verified that the mode pattern had not changed by recording successive burn patterns on a commercial blackened paper as the light attenuation was varied in fixed steps.

The actual beam handling optics beyond the electro-optic shutter were the same as with the Q-switched lasers except that laser attenuation was accomplished by calibrated filters alone.

#### D. The Distinction Between Intrinsic and Inclusion Induced Damage

Transparent materials often contain absorbing inclusions which are too small to be easily detected by optical inspection. Calculations in Chapt. 1 have shown that when their diameters are greater than about  $0.1 \mu\text{m}$ , such inclusions can produce local melting of the surrounding material when irradiated with Q-switched laser pulses.

In experiments where intrinsic breakdown mechanisms are to be investigated, damaging inclusions can often be largely avoided by strongly focusing the laser light into small volumes which in general do not contain inclusions. Several techniques have been used in these studies to determine the relative frequency of occurrence of inclusion damage. In the first, one examines the morphology of the residual damage for characteristics related to its cause.<sup>12</sup> This procedure is useful only for bulk studies. The second technique<sup>13</sup>

utilizes the damage statistics described in Chapt. 6 and can be applied to both surface and bulk studies. Its use, however, requires a large number of light probes by a highly stabilized laser. A third technique, which was developed during the present study, allows an immediate determination of the general source of optical damage at individual sites both in the bulk and on the surface. This technique does not require an amplitude stabilized laser and thus simplifies the problem of identifying intrinsic surface and bulk damage. Finally, a number of qualitative observations to be described below are particularly useful as indicators of inclusion damage when subnanosecond pulses are used and the first and third tests cannot be applied.

Yablonoitch<sup>14</sup> first observed the distinctive morphology normally produced by intrinsic bulk breakdown and used it to distinguish between intrinsic and inclusion damage at 10.6  $\mu\text{m}$ . This same technique was used in the bulk breakdown studies at 1.06  $\mu\text{m}$  and at 0.69  $\mu\text{m}$  which are described in Chapt. 4 and 5. It was found that when intrinsic breakdown occurs, a narrow melted region begins at the geometrical focus and increases in cross-section as it grows back a very short distance towards the laser to give a tear-drop appearance. Inclusion damage, on the other hand, generally forms as spherical regions randomly distributed about the focal point. For both mechanisms thermally-induced cracks can develop after the laser pulse has passed.<sup>43</sup> Because of these observations, inclusion and intrinsic damage can be reliably distinguished

in the bulk by examining the damage morphology. Figs. 13 and 14 show examples of this morphology as seen in the damage study described in Chapt. 4.

The second technique for determining the absence of inclusion damage is based on the statistical nature of intrinsic damage as first observed by Bass and Barrett<sup>13</sup> and extended in Chapt. 6. A precisely defined threshold for intrinsic damage does not exist. As a result, intensity levels can be found such that damage occurs on each pulse with some finite probability  $p_1$  defined by

$$p_1 = \frac{\text{total number of damages}}{\text{total number of pulses}} \quad (3-1)$$

By fixing the intensity of the highly-stabilized laser source, a distribution function  $f_N$  can be obtained which describes the fractional number of times  $N$  pulses are required to produce damage. If laser fluctuations can be neglected and  $p_1$  is the same for each laser pulse ( $p_1 = 0$  or  $1$  for inclusion damage),  $f_N$  is given by the probability that no damage has occurred on the first  $N-1$  pulses times the probability it has occurred on the  $N^{\text{th}}$ . I. e.,

$$f_N = (1 - p_1)^{N-1} p_1 \quad (3-2)$$

Since the only way this distribution of  $N$  values can be obtained is if  $p_1$  is constant, the agreement between measured

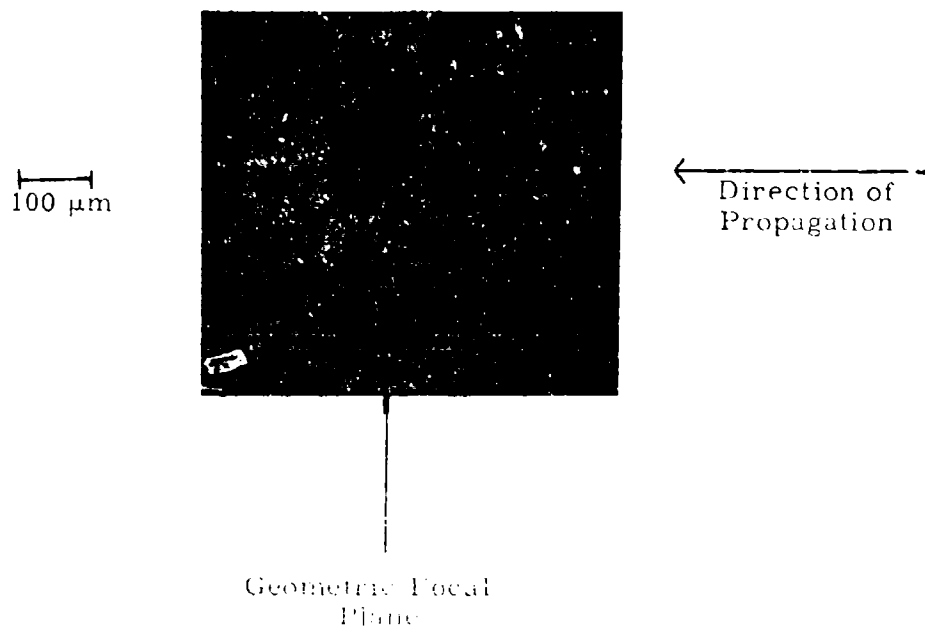


Fig. 13. INTRINSIC DAMAGE IN RBG1

Damage which we have considered to be intrinsic in origin had this basic shape in all the materials tested. This photograph was taken during the experiment of Chapter 6.

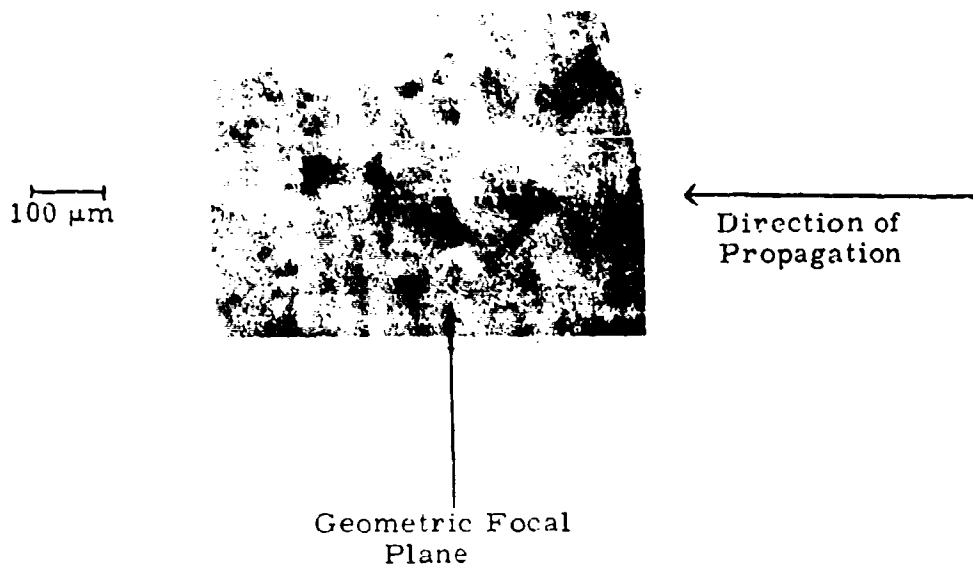


Fig. 14. INCLUSION DAMAGE IN RbCl

Damage which we regarded as due to absorbing inclusions consisted of small spheres randomly distributed about the geometric focal plane. The photograph was taken during the experiment of Chapt. 4.

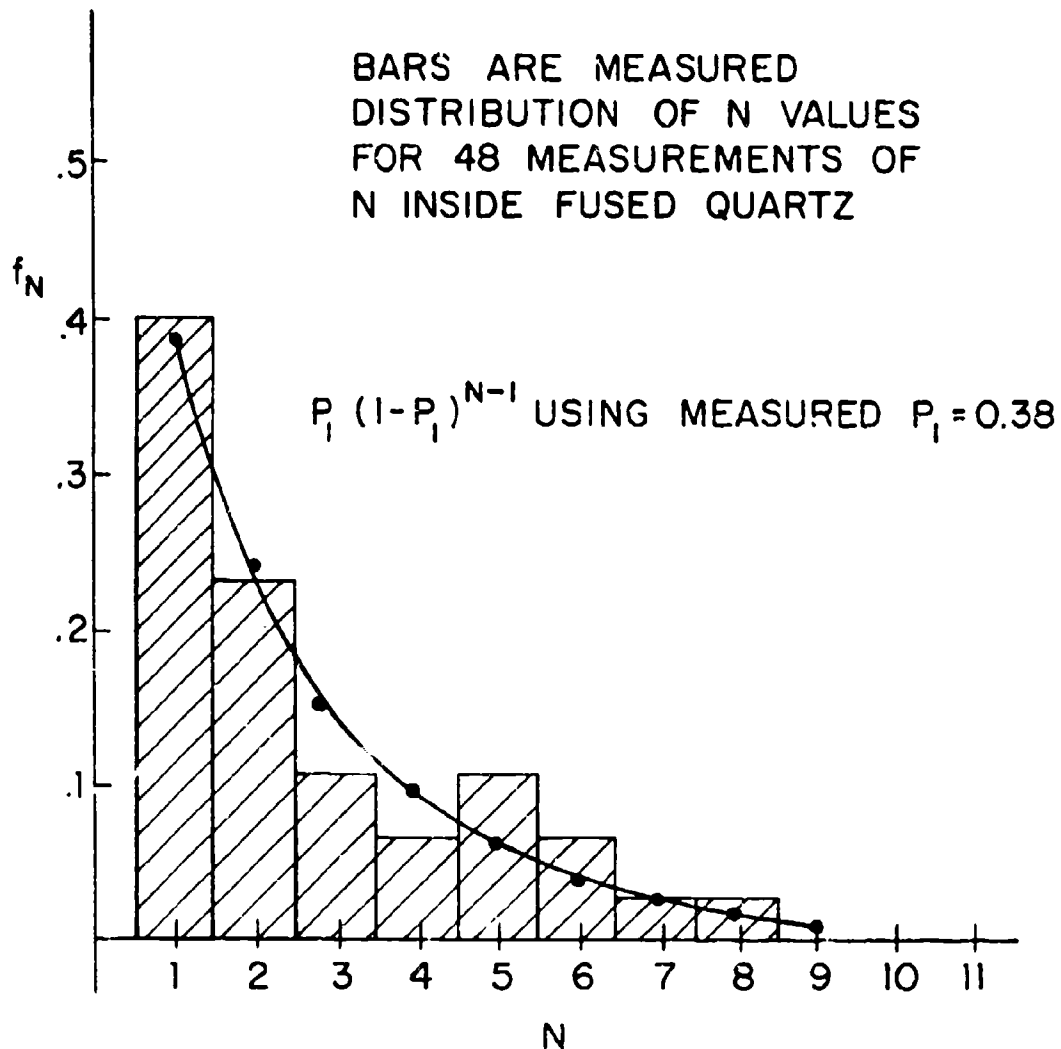
values of  $f_N$  and those computed by Eq. (3-2) indicates that material inhomogeneities were not measurably affecting the damage data and that the laser was sufficiently stable to observe damage statistics. An example of the use of this technique from the measurements of Chapt. 6 is given in Fig. 15 where the measured distribution for bulk damage in fused quartz and Eq. (3-2) are seen to agree.

A third method for distinguishing between inclusions and intrinsic damage was developed and used in the present work. It consists of observing the light transmitted through the sample by using a fast photodiode-oscilloscope combination. When damage occurs, the transmitted laser pulse is attenuated in a manner which is found to be characteristic of the source of damage.

Pulses which are attenuated very rapidly form damage regions in the bulk which are characteristic of the intrinsic mechanism. In addition, for materials which are virtually threshold-like such as those studied in the present work, the intensity at the instant of attenuation for such pulses varies by no more than about 25 percent about some average value. An example of this type of attenuated pulse-shape is given in Fig. 16b.

It was found in the experiments of Chapt. 4-7, however, that a number of damaging pulses were attenuated in a very different manner and produced damage regions that could be identified as resulting from inclusion absorption. For this class of damage events, the attenuation was not as rapid and

Fig. 15. COMPARISON OF MEASURED  $f_N$  WITH  $p_1(1-p_1)^{N-1}$  FOR INTRINSIC BULK DAMAGE IN FUSED QUARTZ



$f_N$  is the fractional number of times  $N$  pulses were required to produce damage, and  $p_1$  is the measured damage probability defined by Eq. (3-1). A least-squares fit to the measured distribution gives  $p_1 = 0.374$  as compared to the measured value of 0.380. This data is taken from the experiments of Chapter 6.



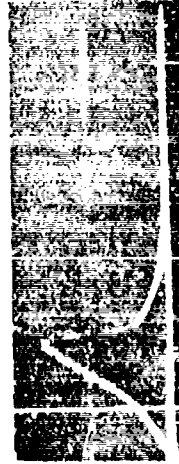
Transmitted pulse which produced bulk damage from inclusion absorption



No damage occurred



Transmitted pulse which also produced bulk damage from inclusion absorption



Transmitted pulse which produced intrinsic bulk damage

10 nsec  
↔

Fig. 16. RUBY LASER PULSES TRANSMITTED THROUGH NaF

as complete as with intrinsic damage nor were the transmitted pulse shape and intensity at the first instant of attenuation as repeatible. Examples of this type of attenuation are given in Figs. 16c and d.

There is, in addition, a small percentage of damage events which could not be unambiguously identified by this scheme or by microscopic investigation of the damage site. In the laser damage studies data obtained from such pulses were not used.

Another distinction between inclusion and intrinsic breakdown involves the intensities of the sparks created by damaging laser pulses. In general, intrinsic events produced bright sparks while damage from inclusions occasionally resulted in sparks which were barely visible.

Except for extremely high laser intensities, intrinsic breakdown occurs near the peak of the laser pulse so that the energy which is available to take part in the damage process is consistently about half the total pulse energy. This was observed experimentally and can be explained by theoretical considerations of avalanche breakdown (see Chapt. 8). It is thus to be expected that the energy deposited in the focal region is reasonably constant for intrinsic breakdown and that the intensity of the sparks which apparently always accompany such damage is, therefore, also reasonably constant.

Figs. 16c and d suggest that these same conclusions do not hold for inclusion damage, and, indeed, there is no reason why they should. Damage from inclusion absorption is energy-

dependent for many different inclusion sizes, and actual material damage may not develop until very late in the laser pulse (i.e., until most of the optical energy has passed through the sample). The focal region may thus be melted but not heated sufficiently to produce a bright spark. A number of experimenters have, in fact, reported material damage without sparks.<sup>45, 49</sup> The arguments advanced here indicate that some type of extrinsic absorptive mechanism such as inclusion absorption very likely caused the damage in their work.

Two of the techniques discussed here--examination of the damage morphology and examination of the transmitted laser light--could not be used in the subnanosecond study of intrinsic damage in NaCl (Chapt. 5) because of the small volumes of the damaged sites and the short durations of the laser pulses. But because breakdown is virtually threshold-like in NaCl, a number of qualitative observations were used to indicate the absence of inclusion damage. For the sample

used to obtain the actual damage data, it was found that the damage field was reasonably well-defined and did not change as different regions of the sample were probed and lenses with different focal lengths were used to focus the radiation. Also, only one faint spark occurred with each damaging laser pulse, and the spark always appeared to form at the geometrical focal plane. These observations contrasted with those obtained under conditions where inclusion damage had been seen in another NaCl crystal irradiated by the same laser and in other

samples irradiated by Q-switched lasers. It was therefore concluded that except possibly for occasional damage sites, inclusion damage was absent in highly pure NaCl under the conditions of measurement described in Chapt. 5.

In summary, then, several techniques have been used to either confirm the absence of inclusion damage or to distinguish between inclusion and intrinsic breakdown when inclusion damage occurs. Intrinsic breakdown cannot be effectively studied without such techniques.

## CHAPTER 4

### INTRINSIC OPTIMAL DAMAGE IN THE ALKALI HALIDES INDUCED BY 1.06 $\mu\text{m}$ RADIATION

#### A. Introduction

Electron avalanche breakdown had been mentioned by a number of authors<sup>50,51</sup> as a possible mechanism for damage. Until the work of Yablonovitch,<sup>14</sup> however, no simple technique had been suggested for identifying the occurrence of avalanche breakdown in solids. The situation was much different in gas studies.<sup>52</sup> Not only had the details of dc avalanches been better understood in gases than in solids,<sup>53</sup> but the ability to vary pressure allowed investigators of gas breakdown to convincingly identify the development of avalanche breakdown and to ascertain the conditions under which multiphoton ionization could develop before an electron avalanche.

Yablonovitch's basic approach was to select transparent materials that had been well-studied for their dc breakdown characteristics and for which damage from multiphoton absorption could not occur. The alkali halide family was a natural choice for laser breakdown studies. Because they have large band-gaps, these compounds are transparent from about 15  $\mu\text{m}$  to about 0.2  $\mu\text{m}$  and optical damage in them from multiphoton absorption is highly improbable until frequencies have been reached that are well into the visible spectrum. The alkali halides have, in addition, been studied extensively in dc damage experiments.<sup>54</sup> Yablonovitch found that the relative root-mean-square damage fields for nine alkali halides at 10.6  $\mu\text{m}$  was the same as had been measured at dc. On the basis of this experimental measurement of breakdown strength plus the prediction that multiphoton absorption could not cause

damage at  $10.6 \mu\text{m}$ , it was concluded that the intrinsic damage process was an electron avalanche, similar in basic character to dc dielectric breakdown.

The discovery that the avalanche breakdown caused by a laser pulse at  $10.6 \mu\text{m}$  in the alkali halides appeared to proceed by the same mechanism and to have the same threshold as dc electric breakdown can be explained if simple impact ionization theories<sup>50, 55</sup> with electron collision times shorter than the light period are correct. As discussed in Chapt. 1, the electron avalanche develops because electrons are heated by an electric field in the presence of phonon collisions that primarily change the electron momentum. Altering the frequency of the applied field should have little effect on this heating until the field reverses direction in a time comparable to the electron-phonon collision time. If only the rate of conduction-band electron heating determines the avalanche characteristics, the avalanche should therefore appear to be in its dc limit as long as  $\omega \leq \tau^{-1}$  where  $\omega$  is the laser angular frequency and  $\tau$  is the average electron-phonon collision time. (This behavior is displayed by Eq. (1-1) of Chapt. 1.) An upper limit  $\tau_{\text{max}}$  to the collision time in NaCl can be estimated by using the low-field mobility<sup>56</sup> ( $10 \text{ cm}^2/\text{volt-sec}$ ) and setting it equal to  $e\tau_{\text{max}}/m_e$  where  $m_e$  is the free-electron mass and  $e$  is the electronic charge. We find that  $\omega\tau_{\text{max}} \approx 1$  for  $10 \mu\text{m}$  radiation. In electric fields approaching breakdown values, the average electron drift energy can be shown to be comparable to the longitudinal optical (LO) phonon

energy, and since the scattering is enhanced near the LO resonance,<sup>57</sup>  $r$  should be less than  $r_{\max}$ . Thus Yablonovitch was working at a frequency where  $\omega r$  was probably still a small quantity compared to unity and where simple impact ionization theories would predict essentially dc behavior.

We have extended Yablonovitch's work to  $1.06 \mu\text{m}$  by using a Q-switched YAG:Nd laser to induce damage. The intent of this work was, first, to determine if the relative intrinsic damage fields of the alkali halides are different at  $1.06 \mu\text{m}$  than they are at  $10.6 \mu\text{m}$  and at dc and, second, to demonstrate the feasibility of conducting near-IR and visible bulk optical damage studies at low powers without catastrophic self-focusing. It will be shown below that the relative breakdown strengths in fact change very little at  $1.06 \mu\text{m}$  and that a number of additional time-related observations support the conclusion that intrinsic breakdown is occurring by a time-dependent electron avalanche.

Self-focusing is potentially more of a problem at  $1.06 \mu\text{m}$  than it is at  $10.6 \mu\text{m}$ . As discussed in Chapt. 2, the amount of beam distortion from the self-focusing nonlinearity depends on  $P/P_{\text{cr}}$ . Since it is desirable to have as little beam distortion as possible,  $P/P_{\text{cr}}$  should be kept small. As the wavelength increases, however,  $P_{\text{cr}}$  decreases as  $\lambda^2$ , so that to maintain the same value of  $P/P_{\text{cr}}$ ,  $P$  must also scale as  $\lambda^2$ . Because the breakdown intensity is approximately independent of  $\lambda$ , the requirement that  $P/P_{\text{cr}}$  be held constant is equivalent to requiring that the area of the focal spot--

$-(\lambda/d)^2 f^2$  where  $d$  is the incident beam diameter and  $f$  is the lens' focal length--also scale as  $\lambda^2$ . But the diameter of a TEM<sub>00</sub> mode depends on both wavelength and cavity design, being on the order of 1 cm for the 10.6  $\mu\text{m}$  laser of Ref. 14 and 0.1 cm for our 1.06  $\mu\text{m}$  system. In order to maintain a constant value of  $P/P_{\text{cr}}$  as  $\lambda$  is decreased, it is necessary to focus more tightly with an external lens or to design the cavity optics to compensate for the dependence of  $d$  on wavelength.

In the present work it was not possible to focus sufficiently to maintain the same value of  $P/P_{\text{cr}}$  that Yablonovitch had been able to achieve at 10.6  $\mu\text{m}$ .  $P_{\text{cr}}$  changes by a factor of 100 as  $\lambda$  is decreased from 10.6  $\mu\text{m}$  to 1.06  $\mu\text{m}$ , and the minimum value of  $f$  that could be used was limited by aberrations to about  $\frac{1}{4}$  inch as compared to  $f = 1$  inch for the lens that Yablonovitch had used. As a result, self-focusing was potentially more of a problem in our measurements, and it was necessary to conduct simple tests to confirm the absence of significant self-focusing effects. The designs of these tests were discussed in Chapt. 2, and their results are summarized in the next section.

## B. The Experiment

The laser sources and experimental arrangement for the present work are summarized in Section B of Chapt. 3. In this section we will summarize the actual experiment, including both the self-focusing tests and the measured breakdown fields

of nine alkali halides at  $1.06 \mu\text{m}$  and one at  $0.69 \mu\text{m}$ .

As discussed in detail in Chapt. 2, self-focusing effects can lead to significant beam distortion. Because accurate measurements of breakdown fields are desired, it is necessary to take great care to avoid such distortion by restricting the laser input power. Theoretical self-focusing parameters were defined and derived in Chapt. 2 where quantitative corrections from the index nonlinearity at powers below  $P_c$  were discussed. Table III summarizes the numerical results. The input power is the experimental power at the peak of the laser pulse and is more than one order of magnitude below  $P_c$ . From a purely theoretical viewpoint, therefore, catastrophic self-focusing is impossible, and it can be shown using Eq. (2-15) that beam distortion from the index nonlinearity introduces at most a few percent correction in the measured electric field strengths. If catastrophic self-focusing does occur, then the breakdown damage data is a measure of the critical powers rather than the intrinsic breakdown field. The measured threshold intensity will then scale with the square of the calculated focal diameter if the process is steady-state and will depend on the pulse width if the process is transient. (The diameter dependence in the steady-state results from the existence of a constant critical power  $P_c$  which does not vary with beam diameter.)

Two experiments were conducted to test our belief that self-focusing was absent. In the first the relative field strength threshold for damage in NaCl was measured with three

TABLE III

Calculated Steady-State, Self-Focusing Parameters and  
Experimental Values of Pulse-Widths and Peak Power

	Wavelength (microns)	$t_R$ ( $10^{-9}$ sec)	$t_p$ ( $10^{-9}$ sec)	$n_2 \times 10^{22}$ (mks)	$P_{cr}$ ( $10^3$ watts)	$P_c$ ( $10^3$ watts)	$P_{input}$ ( $10^3$ watts)
NaCl	10.6	5.5	200		48,000	175,000	120
	1.06	2.7	4.7	2.3	480	1,750	30
	0.69	2.0	14		204	746	26
Rbl	10.6	11.2	200		13,200	50,000	20
	1.06	5.4	4.7	8.1	132	500	8.1

For  $P_{input} < P_c$  catastrophic self-focusing will not occur.

The 10.6  $\mu\text{m}$  data is taken from reference 14.

See Chapt. 2 for definitions of  $t_R$ ,  $n_2$ , and  $P_{cr}$ . To convert  $n_2$  to esu units, multiply by  $0.91 \times 10^9$ .

different focusing lenses, corrected for spherical aberrations, and having focal lengths of 1.4, 2.5 and 3.8 cm. The experiment was conducted at  $1.06 \mu\text{m}$ . If steady-state self-focusing were present, the observed damage threshold would have scaled with the inverse of the focal length. It did not, and, in fact, to within 5 percent the field strength was independent of focal length. This effectively eliminated the possibility of steady-state self-focusing. Since  $t_p/t_R > 1$  from Table III, self-focusing should not be transient. Eq. (2-17) however, predicts the results observed when transient self-focusing is present. For this reason a measurement was made of the damage threshold as a function of pulse duration with the beam diameter held essentially constant.

By changing the pumping level for the YAG laser, we were able to extend the pulse width by a factor of 2.3 to 10.8 nsec. In addition, the breakdown strength at  $0.69 \mu\text{m}$  was measured with ruby laser pulses of 14-nanosecond duration and a focused diameter 25 percent smaller than that obtained with the YAG laser. The same 1.4 cm focal length lens was used in all three measurements, and to compute the ruby value, we assumed the same transverse intensity variation as that present at  $1.06 \mu\text{m}$ . To within 15 percent no change was noted in the threshold field despite the pulse-width dependence in Eq. (2-17). The agreement for the ruby pulses was especially reassuring, because the critical power varies with wavelength squared. If transient self-focusing were present, we would have seen a change by a factor of 18 in the measured intensity--an effect

which would have been quite dramatic. A factor of nine comes from the pulse-width dependence of the transient critical power and a factor of 2 from the wavelength dependence.

Perhaps the best experimental check for self-focusing is the actual measurement of breakdown strengths. Self-focusing theory appears to be totally unable to account for the experimental results given below in which both relative and absolute values of breakdown strengths show striking similarities to 10.6  $\mu\text{m}$  values. We thus conclude that prior to the onset of material damage, self-focusing has been effectively eliminated as a competing nonlinearity.

The possibility may exist that self-focusing occurs after a sufficient number of electrons have been generated to cause intense local heating of the sample. We note, however, that in our measurements any late developing nonlinearity is unimportant.

To measure the breakdown strengths of the alkali halides, the laser beam was focused approximately 2 mm into each sample and the number of laser pulses necessary to produce internal damage at various power levels was recorded. In every case where damage occurred, a white spark was produced, and the damage was later carefully inspected with a microscope. Because of the small volume damaged by our highly focused 1.06  $\mu\text{m}$  pulses (less than  $2 \times 10^{-8} \text{ cm}^3$ ), a large number of data points (40 to 100) could be taken with each sample.

Defining threshold as that value of incident power necessary to produce intrinsic damage in a single shot for

50 percent of the positions probed, we calculated the rms, on-axis electric field at the measured threshold in NaCl. Corrections were made for reflections from various surfaces and the changes in the beam diameter due to the effect of the index nonlinearity. This was the basic calibration, and all other values of threshold were measured relative to  $E_{\text{NaCl}}$ . In order to avoid errors from daily power fluctuations and possible alignment changes, a single sample of NaCl was tested with each alkali halide. It was readily determined that a slight misalignment of the focusing lens had no measurable effect on the relative breakdown strengths.

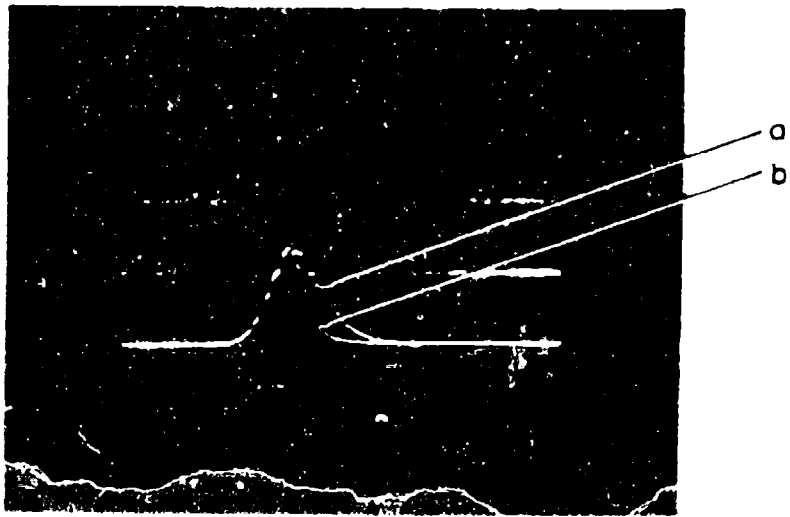
Visual inspection and the breakdown statistics suggested that spatial inhomogeneities from inclusions were not affecting the results except in the single case of RbCl (see Sect. D of Chapt. 3). Damage which we regarded as intrinsic consisted at each damage position of a single pointed region which began at the geometrical focus and extended a very short distance back toward the laser, increasing in cross-section to give a tear-drop appearance. A typical example is indicated in Fig. 13 in Chapt. 3. In RbCl, on the other hand, regions with low breakdown thresholds consisted typically of one or more spherical voids randomly distributed about the focus (Fig. 14 in Chapt. 3). A number of points, however, did appear visually to have intrinsic damage and were consistently more difficult to breakdown. These data points were used for the RbCl results.

Finally, a fast photodiode detector system with a 0.5 nsec

risetime monitored the transmitted light as shown in Fig. 17 and was used to confirm threshold levels in NaCl and KCl as well as to establish the approximate time structure and stability of the laser output.

Values for the breakdown field obtained at  $1.06 \mu\text{m}$  are summarized in Table IV and in Fig. 18 along with both the  $10.6 \mu\text{m}$  data collected by Yablonovitch<sup>14</sup> and accepted dc results.<sup>54</sup> These results are normalized to the respective values of field necessary to damage NaCl listed in Table V. This allows the striking similarity in trends of breakdown field to be easily observed and the possible systematic deviations at  $1.06 \mu\text{m}$  to be recognized. The quoted errors at  $10.6 \mu\text{m}$  are  $\pm 10$  percent, and our random experimental errors in relative fields are estimated to be no more than  $\pm 10$  percent with possible errors due to microscopic strains adding another  $\pm 5$  percent. Two different samples of both NaCl and KBr from two different manufacturers gave nearly identical results.

The breakdown strength of NaCl was also measured with a ruby laser to confirm the absence of self-focusing as noted above. Table V records the average of about 50 damage measurements. Although the laser was normally operating in a single longitudinal mode as indicated by Fabry-Perot and photodiode studies, each laser shot during the measurement was monitored with a fast photodiode and recorded.



8- 10 11

Fig. 17

SECTION III

14

15

16  
17  
18  
19  
20

21  
22  
23  
24  
25



TABLE IV

RELATIVE BREAKDOWN FIELDS - NORMALIZED TO

$E_{NaCl} \approx 2 \times 10^6 \text{ V/cm}$

	<u>NaI</u>	<u>NaBr</u>	<u>NaCl</u>	<u>NaF</u>
DC	0.460	0.553	1	1.60
10.6 $\mu\text{m}$	0.405	0.476	1	
1.06 $\mu\text{m}$	(0.29)*	0.67	1	1.64
	<u>KI</u>	<u>KBr</u>	<u>KCl</u>	<u>KF</u>
DC	0.380	0.460	0.667	1.27
10.6 $\mu\text{m}$	0.369	0.482	0.713	1.23
1.06 $\mu\text{m}$	0.27	0.38	0.57	
	<u>RbI</u>	<u>RbBr</u>	<u>RbCl</u>	
DC	0.327	0.387	0.553	
10.6 $\mu\text{m}$	0.323	0.400	0.472	
1.06 $\mu\text{m}$	0.40	0.55	0.67	

\*Crystal was extremely hygroscopic and no final check was made with the microscope to determine if inclusions were responsible for the damage observed.

PBN-72-491

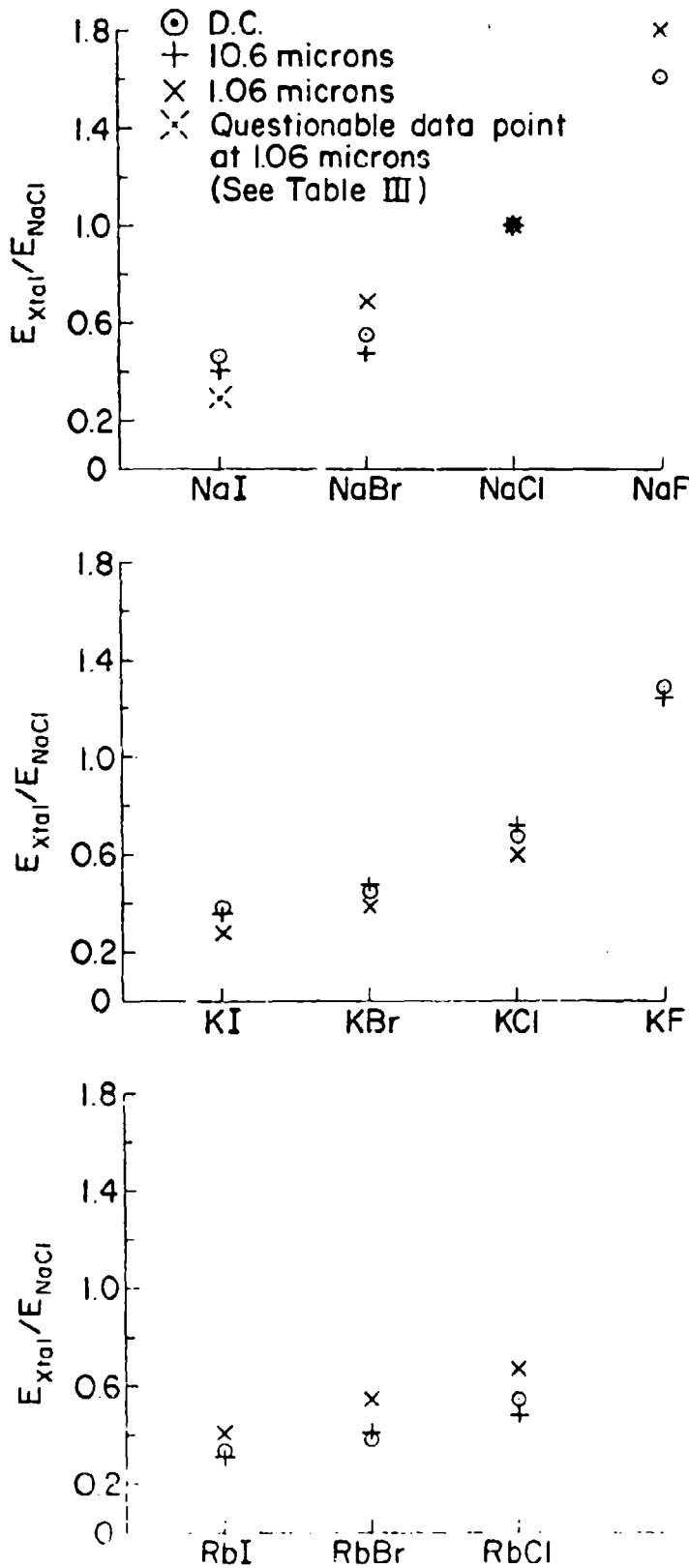


Fig. 18. COMPARISON OF BREAKDOWN STRENGTHS FOR VARIOUS ALKALI HALIDES STUDIED AT DC, 10.6  $\mu\text{m}$ , and 1.06  $\mu\text{m}$

Values for 10.6 and 1.06  $\mu\text{m}$  are root-mean-square field strengths and not peak fields. The data at dc is taken from Ref. 54 and the 10.6  $\mu\text{m}$  data is taken from Ref. 14. The damage fields for the three experiments have been normalized to the respective values of the damage field in NaCl.

TABLE V

ABSOLUTE BREAKDOWN STRENGTH  
OF NaCl

$E_{\text{peak}} \text{ (dc)}^*$	1.50	$\times 10^6 \text{ V/cm}$
$E_{\text{rms}} \text{ (10.6 } \mu\text{m)}^*$	$(1.95 \pm 0.20)$	$\times 10^6 \text{ V/cm}$
$E_{\text{rms}} \text{ (1.06 } \mu\text{m)}$	$(2.3 \pm 0.46)$	$\times 10^6 \text{ V/cm}$
$E_{\text{rms}} \text{ (0.69 } \mu\text{m)}$	$(2.2 \pm 0.44)$	$\times 10^6 \text{ V/cm}$

\* These values are taken from Refs. 54 and 14

### C. Discussion of Results

The experiments reported here were performed under carefully controlled conditions using stable, well-characterized lasers and optical systems for which aberrations were unimportant. Because we were able to probe each sample in many different positions, random fluctuations in breakdown strength were averaged out. It was possible to distinguish between inclusion and intrinsic damage by inspection of the residual damage sites and to correct for the effects of inclusions in the one material for which they were important. In addition, experimental tests showed that catastrophic self-focusing was absent and, consistent with theory, that the index nonlinearity did not affect the results to within experimental error. It is therefore concluded that the results of the 1.06 and 0.69  $\mu\text{m}$  study as summarized in Fig. 18 and Table V represent accurate measurements of intrinsic bulk damage.

Because the techniques of this study are virtually identical to those of reference 14, direct comparison can be made to breakdown strengths at 10.6  $\mu\text{m}$ . It has already been observed that the damage thresholds for the alkali-halides at 1.06  $\mu\text{m}$  follow a trend nearly identical to that observed with the CO<sub>2</sub> laser and, in fact, to the dc measurements of reference 54. It thus appears that the intrinsic process of laser-induced damage for the alkali-halides has the same fundamental character as both ac damage in the infrared and dc avalanche breakdown. Moreover, the consistency of the optical breakdown strengths at 0.69  $\mu\text{m}$  suggests that this

same process may dominate up to frequencies approaching  $4 \times 10^{14}$  herz.

Data from Fig. 18 and Table V have established the relationship  $(E_{1.06})_{rms}$  is about  $1.5 \times E_{dc}$  for ten different compounds. The precise value of the factor 1.5 is not important since dc measurements are known to be somewhat sensitive to experimental techniques.<sup>58, 59</sup> It is important, on the other hand, that consistent measuring techniques have measured roughly the same factor of 1.5 for all ten alkali halides.

Additional support for an avalanche mechanism comes from three experimental observations concerning the time-structure of the laser probe pulses. The first is that increasing the pulse width of the YAG laser output by a factor of 2.3 resulted in a 14 percent average drop in threshold intensity for NaCl. Averages were taken at about 20 shots at each pulse width. This change, though small, is probably real, because the test was made on a single sample of high-quality NaCl and thereby avoided a major source of experimental uncertainties arising from material variations. The second observation, noted at both 1.06 and 0.69  $\mu m$ , is that high-frequency time-structure on the pulse has little measurable effect on the breakdown strength. And finally, after adjusting the power level so that damage occurred regularly near the top of the laser pulses, the probe intensities were increased by a factor of about three by changing the beam attenuation. When this was done, the intensity at which the transmitted

light dropped (see Fig. 16) was higher by 25 percent or more than it had been with the lower intensity pulses. This was interpreted to mean that increasing the effective risetime of the optical field raises the measured breakdown strength. To understand both this set of observations and the results from Table V, some discussion of existing electron avalanche theories is given. This discussion will be extended in Chapt. 8.

An electron avalanche in solids is a rapid multiplication of conduction-band electrons in which an initially low density  $N_0$  of free carriers interacts with an intense electric field in the presence of phonons. The number of electrons increases with time as

$$N(t) = N_0 \exp \left[ \int_0^t \alpha(E) dt \right] . \quad (4-1)$$

The gain coefficient  $\alpha(E)$  is a strongly-varying function whose value can be inferred from dc measurements of breakdown strength as a function of sample thickness for extremely thin specimens. For Eq. (4-1) to be valid the rate at which electrons are lost by trapping and diffusion out of the focal volume must be small compared to the rate at which they are generated. For Q-switched laser pulses, the electron losses are, in fact, negligible.<sup>18</sup>

Two important conclusions develop from such an analysis. The first is that the entire process of avalanche and damage involves energy exchange between the field and the electrons which, as has already been discussed, is approximately

described by the well-known formula for ac conductivity given by Eq. (1-1). Eq. (1-1) shows that the energy input to the electrons scales with frequency and field as  $E^2/(1 + \omega^2 \tau^2)$ , and because the details of energy input determine the electron distribution function and hence  $N(t)$ , the threshold for damage will scale in the same manner. This justifies the use of root-mean-square fields in Table V. It also indicates that the ac breakdown strength will increase for frequencies near  $1/\tau$ . An estimate of  $\tau$  for NaCl<sup>55</sup> indicates that frequency dispersion should begin to occur somewhere near that of the ruby laser.

The second relevant conclusion from an analysis of avalanche breakdown is that if insufficient time exists for the electron density to reach values necessary to damage, then damage will not occur even though electron recombination losses have been exceeded and an electron avalanche is underway. Damage will only be produced when the field is subsequently raised above the steady-state breakdown field and the gain coefficient  $a$  is correspondingly increased. Such an effect has been observed in dc experiments by varying the thickness of thin ( $< 50 \mu\text{m}$ ) samples.<sup>60, 61</sup> In such experiments transit effects limit the build-up time.<sup>58</sup>

The field dependence of the gain coefficient, or ionization rate, has been measured experimentally in NaCl by using subnanosecond laser pulses. This measurement will be presented in Chapt. 5. For present purposes we merely note that our observations of a pulse-width dependence to breakdown, the

insensitivity of threshold to fast time structure, and the increase in breakdown strength for rapidly rising pulses all indicate that the intrinsic damage process is time-dependent as expected from an electron avalanche and that the process has an effective time constant on the order of 1 ns. Such temporal considerations may explain part of the difference in damage field between dc and laser measurements as summarized in Table V.<sup>62</sup> A more likely explanation for most of this difference involves space charges and will be discussed in Chapt. 5.

The essential details of the breakdown studies reported here are thus fully explained by the process of avalanche breakdown.

In summary, careful measurements of laser-induced bulk damage have been made in nine alkali-halides without the confusing effects of self-focusing. Comparison of the results to studies at dc and at  $10.6 \mu\text{m}$  indicate that the process of ac avalanche breakdown, similar in fundamental character to dc avalanche breakdown is responsible for the damage observed. Analysis of time-related observations confirms this conclusion.

## CHAPTER 5

### THE EFFECTS OF LASER FREQUENCY, PULSE DURATION AND CRYSTAL DISORDER ON INTRINSIC OPTICAL DAMAGE FIELDS

#### A. Introduction

In the last chapter the intrinsic breakdown mechanism was identified in the alkali halides for  $1.06 \mu\text{m}$  radiation. This process, an electron avalanche, has been studied at dc for over forty years. Despite the extensive investigation avalanche breakdown has attracted, very little progress has been made in understanding the microscopic details of its development. Not only is the proper modeling of this highly complex process beyond the present level of solid state theory,<sup>63</sup> but experiments on dc breakdown are difficult to conduct and often yield very limited information.<sup>58</sup> No estimates can be obtained, for example, of effective electron collision rates from dc experiments, and the time dependence of the avalanche can only be studied indirectly.<sup>18</sup> Laser damage techniques, on the other hand, are comparatively simple, and the great versatility of the laser can be exploited to probe aspects of an avalanche that are inaccessible to dc investigators.

In this chapter we extend the damage measurements in the alkali halides to higher frequencies and shorter pulse widths. It will be shown, in particular, that frequency dispersion begins to develop at  $0.69 \mu\text{m}$  and that the damage field in NaCl increases as expected with decreasing pulse width. These two observations provide an experimental estimate of the high-field electron-phonon collision frequency and an experimental measure of the avalanche ionization rate. An apparent anomaly in the frequency dispersion suggests the possibility

**Preceding page blank**

that deep lying exciton levels may affect the breakdown strength of NaF. A comparison of the optical frequency ionization rate to estimates based on dc data<sup>18</sup> show at least qualitative agreement. The results of a short experiment will also be described in which the effects of lattice disorder on the intrinsic breakdown strengths of materials were studied.

#### B. Avalanche Breakdown Induced by Ruby Laser Light

We have completed measurements of intrinsic bulk breakdown in nine single crystal alkali halides using a TEM<sub>00</sub>, single-longitudinal mode ruby laser. Self-focusing was absent in these studies, and damage from inclusion absorption was distinguished from intrinsic damage. It was found that at 0.69  $\mu\text{m}$  the relative breakdown strengths of the alkali halides have begun to differ from values obtained at 1.06 and 10.6  $\mu\text{m}$  and at dc. The onset of this frequency dispersion in the avalanche breakdown process enables one to estimate the high-field electron-phonon collision frequency.

The laser system and techniques for avoiding and confirming the absence of self-focusing have been described in detail in Chapt. 2 and 3. Damage from inclusions was distinguished from intrinsic damage by examining both the morphology of the damage sites and the temporal shape of light pulses transmitted through the sample. (See Sect. D of Chapt. 3.) The latter technique employed the fact that a damaging light pulse is attenuated in a manner which is characteristic of the cause of damage. Only data obtained from intrinsic

damage events were considered in the present work.

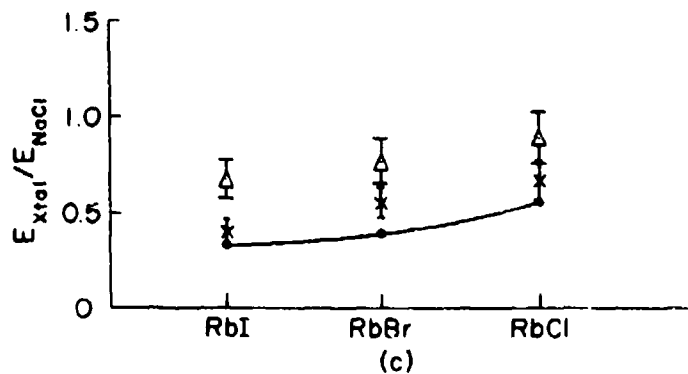
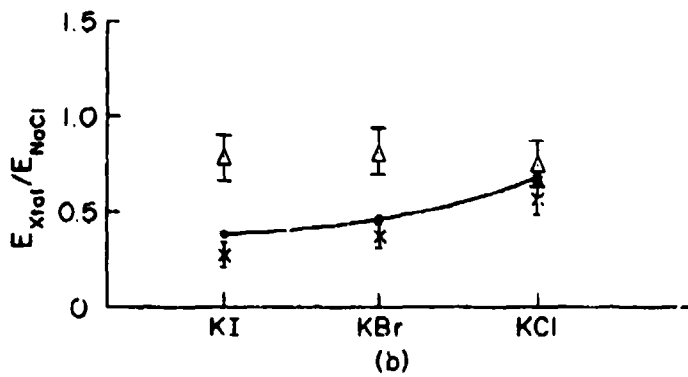
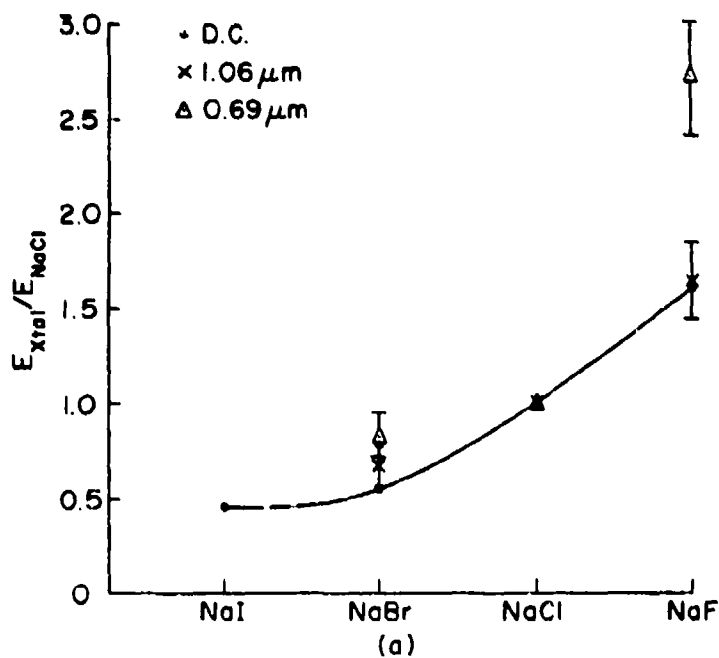
To measure the breakdown strengths of the alkali halides, we focused the laser beam inside the sample about 1.5 mm from the front surface. The focal spot diameter was about  $15\ \mu\text{m}$ . When the incident power was sufficiently high, a bright white spark was produced and a small volume of the material ( $\leq 10^{-8}\ \text{cm}^3$ ) was melted. Because a well-defined threshold could not be found (see Chapt. 6) we again defined the damage field as that value of rms electric field inside the material which was necessary in order to induce damage on a simple pulse with a probability of 0.5. The incident power necessary to reach this field in NaF under our conditions of focusing was 146 KW. For the other crystals, the input power was between 20 KW (for NaCl) and 9.2 KW (for RbI).

A large number of data points were taken for each sample (40 to 100), but normally less than half of these damage sites could be unambiguously identified as resulting from intrinsic processes. The remainder were apparently caused by the presence of absorbing inclusions.

As in Chapt. 4, the rms on-axis damage field was determined for NaCl using the measured intensity distribution at the focus of the 14 mm focal-length lens. This measurement was the basic calibration, and in order to avoid errors from possible alignment changes, damage fields for the other materials were measured relative to  $E_{\text{NaCl}}$ . The same sample of NaCl was tested with each alkali halide.

Figure 19 and Table V (Chapt. 4) summarize the results

PBN-72-1170



The dc data is taken from Ref. 54 and the 1.06  $\mu\text{m}$  data is taken from Chapt. 4.

Fig. 19. RMS ELECTRIC FIELDS NECESSARY TO INDUCE DAMAGE IN NINE ALKALI HALIDES NORMALIZED TO THE DAMAGING FIELD FOR NaCl

of this study, the  $1.06 \mu\text{m}$  data from Chapt. 4, and accepted dc results.<sup>54</sup> In Fig. 19 the damage fields of the various alkali halides are normalized to that of NaCl at the appropriate frequency. This makes the variation in trends between the  $1.06 \mu\text{m}$  and the  $0.69 \mu\text{m}$  measurements more easily seen. The relative breakdown strengths at  $1.06 \mu\text{m}$  are virtually identical to those measured at dc. Although the corresponding data at  $10.6 \mu\text{m}$ <sup>14</sup> are not displayed, they too follow the same trend. This is not the case at  $0.69 \mu\text{m}$ , however, even when the 10 to 15 percent measurement errors are considered.

Table V lists the rms damage fields of NaCl for these experiments. The agreement found in the four experiments is heartening because there are particular difficulties in determining the absolute damage fields in dc measurements.<sup>58, 59</sup> Root-mean-square values of the electric field strength are given because for laser pulses of this intensity, the build-up time of an electron avalanche to damaging levels is on the order of  $10^3$  to  $10^4$  cycles of the optical field. (See next Section.) Heating of the electron population is thus effectively averaged over many cycles.

Because the measured breakdown strength of NaCl was the same within experimental error at  $1.06 \mu\text{m}$  and  $0.69 \mu\text{m}$ , the ordinate in Fig. 19 could be changed to read in absolute field units with virtually no change in the relative positions of the  $1.06 \mu\text{m}$  and  $0.69 \mu\text{m}$  data points. Absolute field units were not used, because the resulting error bars on the altered plot would be much larger. They would include not only the

experimental uncertainty in field values relative to NaCl, as displayed in Fig. 19, but they would also include the comparatively large experimental uncertainty in the absolute damage field for NaCl as summarized in Table V. It is the change in trends of damage fields which is most meaningful, and we have chosen to display the data and experimental uncertainty in a manner which will best underscore this change.

A complete theoretical description of avalanche breakdown has not been developed. The onset of frequency dispersion can be qualitatively understood, however, by using the results of models based on relaxation time approximations which we have briefly considered in Chaps. 1 and 4 and which we will consider in more detail in Chapt. 5. These models predict that the damage field will scale with frequency as

$$E_{\text{break}}(\omega) = (1 + \omega^2 \tau^2)^{1/2} E_{\text{dc}} \quad (5-1)$$

where  $\omega = 2\pi\nu$  is the laser radian frequency and  $\tau$  is an effective, high-field, electron-phonon collision time. Since each material has a different value of  $\tau$ , the relative breakdown fields for the alkali halides should begin to change at high frequencies. Data such as shown in Figure 19 can be used to infer approximate relative values of  $\tau$  for a variety of theoretical models.

Perturbation calculations of  $\tau$  have been performed which are applicable for electron energies greater than the longitudinal optical photon energies.<sup>69</sup> If  $\omega\tau > 0.5$  for NaCl, then the results of these calculations can explain qualitatively

the change in relative breakdown strengths observed at ruby frequencies for most of the alkali halides. The collision time for NaCl under this assumption is about  $2 \times 10^{-16}$  sec. For NaF these calculations predict that the relative breakdown field ( $E_{\text{NaF}}/E_{\text{NaCl}}$  in Fig. 19) will decrease at ruby frequencies, contrary to the change which is experimentally observed. This discrepancy may be the result of the inadequacy of the perturbation calculations or it may indicate that the frequency dependence of the electron avalanche is not determined by the electron-phonon collision frequency alone.

Seitz<sup>65</sup> has suggested that the presence of deep-lying exciton bands may influence the dielectric strength of alkali halide crystals. If this is the case, then as the field frequency  $\omega$  is increased, direct excitation out of these bands becomes possible and the damage field will decrease. NaF, which has the deepest lying bands (1.5 - 2.0 eV) of the materials studied,<sup>56</sup> will experience this effect at a higher frequency than the other alkali halides. Such considerations of the relative importance of the exciton bands may explain the observed large increase in the relative NaF damage field at  $0.69 \mu\text{m}$ .

Multiphoton absorption directly across the bandgap cannot explain the changes in relative breakdown strength which have been observed. In addition, theoretical calculations of the fields at  $0.69 \mu\text{m}$  necessary to induce damage from multiphoton ionization or from its low-frequency limit, tunnel ionization, give damage fields which are about an order of

magnitude larger than those measured.<sup>18, 65</sup>

In conclusion, we have measured the intrinsic optical breakdown fields of nine alkali halides using a ruby laser. Although the absolute and relative threshold fields are comparable to the thresholds observed at  $1.06 \mu\text{m}$  and at dc, differences are observed which suggest that at  $\nu = 4.3 \times 10^{14} \text{ sec}^{-1}$ , avalanche breakdown is no longer identical to dc dielectric breakdown. Current theories of avalanche breakdown do not appear to explain the details of this observed difference.

#### C. The Pulse-Width Dependence of Optical Avalanche Breakdown

Measurements are reported here of optical damage induced by subnanosecond laser pulses. These measurements were performed by focusing mode-locked YAG:Nd laser pulses having durations of 15 and 300 picoseconds inside single crystal NaCl. Because the experimental procedures used in the present work were identical to those used in the studies of Chapt. 4 with a Q-switched YAG:Nd laser, the subnanosecond measurements can be directly compared to the results of those studies. It was found that the intrinsic breakdown field increased by almost an order of magnitude to over  $10^7$  volts/cm as the laser pulsewidth was decreased from 10 ns to 15 ps.<sup>66</sup> The dependence of the damage field on laser pulse duration is used to calculate a field-dependent ionization rate which is compared to the predictions of Yablonovitch and Bloembergen<sup>18</sup> who estimated the ionization rate from published measurements of the dc dielectric strength of NaCl for thin samples with

varying thickness. Qualitative agreement is found.

The laser used for the present work (see Fig. 12 in Chapt. 3) was a passively mode-locked YAG:Nd laser operating in a TEM<sub>00</sub> mode at 1.06  $\mu\text{m}$ . Without intercavity etalons, this oscillator produced bandwidth-limited light pulses of 15 picosecond duration. When the cavity output mirror was replaced with a sapphire etalon, the pulsewidth was lengthened to about 300 picoseconds. Two-photon-fluorescence measurements failed to detect substructure with pulses of either duration. A laser-triggered spark gap was used to select a single light pulse which, after attenuation, was focused through a 14 mm focal length lens about 2 mm into the sample. Care was taken to insure that spherical aberrations from both the lens and the plane entrance surface of the sample being tested were unimportant. An energy monitor recorded the energy in each laser pulse.

Although the intrinsic damage process in transparent materials is an inherently statistical process<sup>12</sup> (see Chapt. 6), it is virtually threshold-like in NaCl. Consistent with Chapt. 4, a damage field can be defined as that value of root-mean-square electric field inside the sample which produced damage on a single shot with a probability of 0.5. Damage was identified by the occurrence of a faint spark and was accompanied by a small melted region ( $\leq 2 \times 10^{-9} \text{ cm}^3$ ) inside the crystal. At least 20 data points were taken for each pulse duration at the 0.5 probability point.

Beam distortion from self-focusing was avoided by

confining the laser input powers to well below the calculated critical powers for catastrophic self-focusing. (See Table VI.) To verify the absence of self-focusing, two different lenses (focal lengths of 14 mm and 25 mm) were used to focus the laser radiation. As expected from diffraction effects alone, the input damage powers scaled with the square of the focal lengths. If catastrophic self-focusing had been present with the subnanosecond pulses, the input damage power would have been independent of focal length. The absence of inclusion damage was confirmed in the manner discussed in Sect. D of Chapt. 3.

Table VI summarizes the results of the present measurements and those of Chapt. 4. An increase in breakdown strength was observed as the duration of the laser pulse was decreased. As the pulse duration was changed from 10.3 ns to 15 ps, there was a total change by a factor of 5.8 in damage field strengths or a factor of 33 in damage intensity. The experimental points are plotted in Fig. 20 along with the semi-empirical predicted curves from Ref. 18.

The existence of a pulse-width dependence to intrinsic damage is qualitatively explained by classical theories of electron avalanche ionization.<sup>58, 67-68</sup> These theories, which are summarized in Chapt. 8, predict that the density of conduction-band electrons,  $N(t)$ , increases with time as

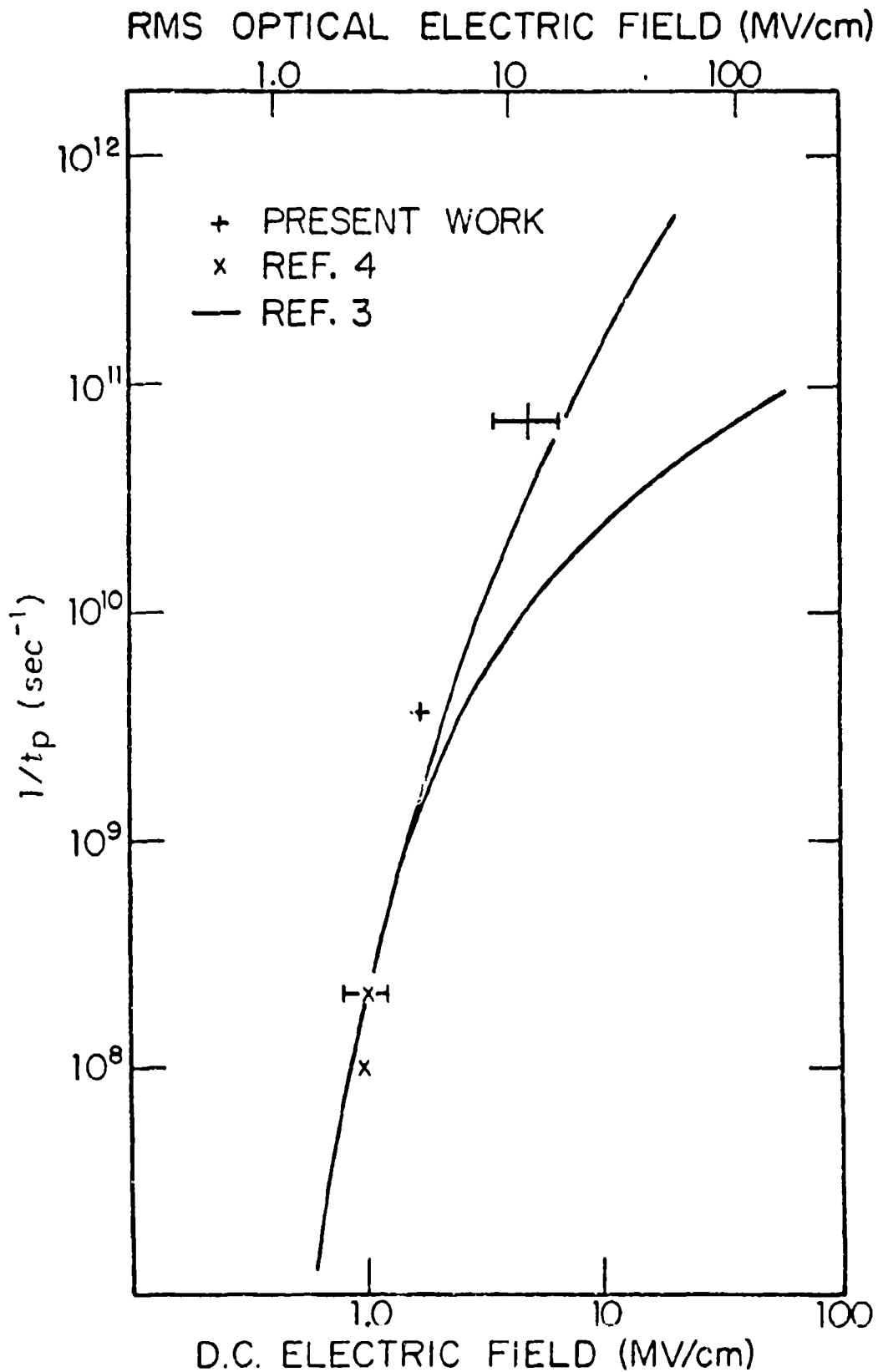
$$N(t) = N_0 \exp \left[ \int \alpha(E) dt \right] = M_c(t) \quad (5-2)$$

TABLE VI

Experimental Breakdown Fields and  
Calculated Self-Focusing Parameters in NaCl

Pulsewidth ( $10^{-12}$ sec)	$P_{\text{input}}$ ( $10^6$ watts)	$P_c$ ( $10^6$ watts)* electrostriction	electronic	$E_{\text{rms}}$ ( $10^6$ volts/cm) relative	absolute
15	1.5	$2.9 \times 10^4$	18	E(15 ps)/E(300 ps)	$12.4 \pm 3.7$
300	0.22	82	18	= $2.6 \pm 0.7$	4.7
$4.7 \times 10^3$	0.030	1.8	18	E(4.7 ns)/E(10.3 ns)	$2.3 \pm 0.4$
$10.3 \times 10^3$	0.033	1.8	18	= $1.1 \pm 0.05$	2.1

\*  $P_c$  is the calculated critical power for catastrophic self-focusing.



The two branches of the solid curve correspond to two limits on the high-field electron drift velocity which were used in Ref. 18 to calculate the dc ionization rate. Corresponding laser data at 1.06  $\mu\text{m}$  is plotted. It should be noted that the changes in the damage field as the pulse duration is lowered from 300 to 15 ps and from 10.3 to 4.7 ns are known to higher precision than the absolute field strengths. The error bars reflect the experimental uncertainties in the absolute field strengths. (See Table VI.)

Fig. 20. THE RATE OF IONIZATION IN NaCl AS A FUNCTION OF ELECTRIC FIELD

Eq. (5-2) is valid when, as is the case with laser breakdown,<sup>18</sup> electron diffusion and trapping can be ignored.  $N_0$  is the low density of conduction electrons before the application of the electric field and  $\alpha$  is the ionization rate which increases monotonically with increasing electric field. Breakdown occurs when the density of electrons becomes high enough to cause a material irreversibility such as a phase change. (See Chapt. 1.) As the time available for the avalanche to develop to damaging proportions decreases, the rate of ionization and hence the electric field must be increased in order to produce damage.

It is desirable to compare the laser data to dc results. Such a comparison cannot be made directly, because impulse dc measurements with subnanosecond impulse durations have not been made. As Yablonovitch and Bloembergen<sup>18</sup> have suggested, however, dc measurements on samples with varying thickness provide an indirect comparison because the maximum duration of the dc avalanche is limited to the electron drift time from cathode to anode.<sup>58</sup> By considering limits on the electron drift velocity, Yablonovitch and Bloembergen have calculated  $\alpha(E)$  for dc fields using Eq. (5-2) and previously published measurements of dc damage fields in thin samples of NaCl.<sup>60, 61</sup> Breakdown was assumed to occur when  $M_0$  in Eq. (5-2) reached a value of  $10^8$ . The ionization rates for the laser data can be found by replacing the integral in Eq. (5-2) by  $\alpha(E_{rms})t_p$  where  $E_{rms}$  is the root-mean-square field on axis at the peak of the laser pulse and  $t_p$  is the laser pulsewidth. Then

$\alpha(E_{rms})$  is given by

$$\alpha(E_{rms}) = \frac{1}{t_p} \ln M_c \approx 18/t_p \quad (5-3)$$

This relation has been used to convert the quantity  $\alpha(E)$  used along the vertical axis in the figure of Ref. 18 to our figure which used  $t_p^{-1}$ . We have shifted the curves along the horizontal axis to obtain agreement with the experimental values for the breakdown field  $E_{rms}$  for the long pulses.

It should be noted that the damage fields for the dc studies of Refs. 60-61 are approximately a factor of 2.3 lower than the corresponding values for laser-induced damage. There are two reasons to suspect that this factor is a systematic error in determining absolute field strength at dc rather than an indication of a fundamental difference between dc and laser-induced breakdown.<sup>69</sup> First, this factor of 2.3 is nearly the same for all nine alkali halides studied at  $10.6 \mu m^{14}$  and  $1.06 \mu m$ , and second, dc field values are average values given by the voltage difference between anode and cathode divided by their separation without regard for field inhomogeneities from effects such as space charges which can be important in dc experiments. Some evidence in fact exists in the literature that space charge effects are influencing dc breakdown. For example, dc impulse experiments have been performed<sup>70</sup> in which the duration of the applied field was reduced to about 10 ns, a time interval too short to allow the development of ionic space charges.<sup>71</sup> It was found that the damage field in

NaCl increased from about 1 MV/cm, its steady-state value, to just over 2 MV/cm, a value which agrees closely with the laser measurements. The time-related considerations discussed in this section do not explain this change. In other experiments the start of an avalanche has been observed to vary in a statistical manner with average lags of 1  $\mu$ s or more.<sup>72, 73</sup>

This effect has been interpreted as resulting from space charge development.<sup>73</sup> A complete understanding of space charge effects, electrode effects, and other factors which can affect dc measurements of breakdown has not emerged, and thus we should regard absolute measurements of dc breakdown with some caution, preferring instead to compare trends in absolute field strengths as different materials are investigated or as parameters are varied.

In Fig. 20 the four laser measurements are plotted with the computed curve from Ref. 18. The two branches to the computed curve correspond to two limits on the high-field electron drift velocity. Within experimental error, the laser data overlap the upper curve of Ref. 18 which was derived on the assumption that the mobility in the hot electron gas is independent of  $E_{rms}$ . Quantitative agreement should not be emphasized, however, because the present analysis is based on at least two important assumptions which may not be valid over the range of damage fields considered. The first assumption is that factors in the dc experiments such as space charges and electrode effects do not change as the sample thickness is reduced to approximately a micron. And the

second assumption is that the same intrinsic mechanism dominates over the range of laser pulsewidths in Table VI. Another intrinsic mechanism--multiphoton ionization<sup>74</sup>--may cause damage at lower fields than required for avalanche breakdown when the laser pulsewidth is extremely short. Estimates for 1.06  $\mu\text{m}$  radiation in NaCl indicate that when the laser pulsewidth is less than about a picosecond, multiphoton ionization is responsible for intrinsic damage.<sup>18</sup> Since the shortest pulsewidth considered in the present work is 15 ps, the neglect of multiphoton ionization appears to be justified. If the estimates of Yablonovitch and Bloembergen are inaccurate, however, and damage from multiphoton ionization is occurring, the ionization rate determined from the 15 ps pulse is an upper bound for the actual value of  $\alpha$  at  $E_{\text{rms}} = 12.4 \text{ MV/cm}$ .

In summary, intrinsic laser-induced damage has been shown to be a time-dependent process. As the laser pulsewidth was decreased to 15 ps, the damage field in NaCl increased to over  $10^7 \text{ v/cm}$ . From the pulsewidth dependence of the optical damage field, a field-dependent ionization rate was determined and found to agree at least qualitatively with experiments using dc fields. The agreement underscores the basic similarity between intrinsic laser-induced damage at 1.06  $\mu\text{m}$  and dc dielectric breakdown.

#### D. Effects of Disorder on the Intrinsic Damage Field

Measurements are reported here of optical bulk damage in

three disordered systems--polycrystal KCl, a single-crystal KBr-KCl (67%-33%) alloy, and fused quartz. In each case the damage field for the disordered system is compared to the optical strength of the corresponding crystal. These measurements were made in order to determine if the optical breakdown field increases with severe lattice disorder as had been observed in dc breakdown experiments<sup>75, 14</sup> and as predicted by simple theories of avalanche breakdown.<sup>58</sup>

The laser system and the experimental techniques used here were identical to those of Chapt. 4 except that inspection of the transmitted laser light, rather than microscopic inspection of the damaged crystal, was used to distinguish inclusion damage.

It was found that the damage field of the large-grain (20  $\mu\text{m}$ ) polycrystal was the same as that measured in the single crystal and that the alloy damage field was about 20 percent larger than the damage field measured in the majority constituent, KBr. In the quartz system, on the other hand, the disordered (amorphous) phase was noticeably stronger than the crystal, the ratio of damage intensities being  $5 \pm 1$ . This ratio is identical to the corresponding ratio of surface damage fields measured by Bass and Barrett.<sup>12</sup>

It is to be expected that the large-grain polycrystal should have the same damage field as the single crystal. The average grain diameter (20  $\mu\text{m}$ ) and the laser focal diameter are comparable so that in the high intensity region near the beam axis where breakdown is observed to initiate (see Fig. 13

in Chapt. 3), the sample looks like a single crystal.

By a simplified argument we can predict the approximate crystallite size necessary to affect the breakdown strength. Classical theories of avalanche breakdown (see Chapt. 8) predict that the dynamics of electrons with energies greater than the longitudinal optical (LO) energy determine the characteristics of the avalanche. The LO energy in the alkali halides corresponds to electron momenta of about 0.1 times the reciprocal lattice vector  $G$  so that the important electrons have  $k \geq 0.1 G$ . Phonons with values of  $q \geq 0.1 G$  will interact most strongly with these electrons.<sup>76</sup> Because such lattice vibrations have wavelengths equal to 10 lattice constants or less, we expect that unless crystal disorder appears on the scale of about 10 lattice constants ( $\sim 100\text{\AA}$ ) or less the damage field should be unaffected by disorder.

Amorphous systems are, of course, disordered on such a scale. Our observation that the glass is more resistant to damage is, therefore, consistent with the argument just presented. The behavior of the quartz system can be explained in somewhat more quantitative terms by an equivalent argument. Referring to Eq. (1-1) on p. 1-3, it is seen that the rate of energy input into the electron population decreases with decreasing electron mobility  $\mu$ . It is known that the mobility of disordered systems is less than the crystal mobility<sup>76</sup> so that it should be more difficult to heat the electron distribution in the glass. As we have observed, then, the damage field for glass should be higher than the crystal

damage field.

The breakdown field of the KBr-KCl alloy, measured relative to the breakdown of NaCl, was  $0.45 \pm 0.06$ . This value compares to 0.38 for pure KBr, 0.57 for pure KCl, and 0.44 for the average breakdown field  $E_{avg}$  weighted according to the alloy composition:  $E_{avg} = 0.67 E_{KBr} + 0.33 E_{KCl}$ . It may be fortuitous that the measured breakdown strength of the alloy and  $E_{avg}$  agree. On the other hand, the average lattice constant of this alloy determined by X-ray diffraction scale with composition,<sup>77</sup> and other material parameter such as bandgap, dielectric constant, and reststrahlen frequency probably scale in the same linear manner. Since the breakdown field depends on these various material parameters,<sup>58, 67-68</sup> it is reasonable that the breakdown field should also scale with composition--provided that the crystal disorder resulting from the mixed composition does not affect the breakdown strength. More alloy systems must be studied before firm conclusions can be drawn concerning the effects of alloying on the breakdown strength of materials.

It thus appears that only extreme lattice disorder such as present in amorphous systems has a measurable effect on intrinsic damage fields. Future work is needed, however, to ascertain any general correlations between lattice disorder and breakdown fields. Such work is important not only to an understanding of avalanche breakdown but it is also important from a practical viewpoint to the design of more damage-resistant optics.

## CHAPTER 6

### LASER DAMAGE STATISTICS

#### A. Introduction

In a recent study by Bass and Barrett<sup>72</sup> it was found that the resistance of surface to optical damage has a statistical character. This observation, which could apparently not be explained either by laser fluctuations or by fixed material inhomogeneities, was interpreted in terms of an electron avalanche model. Previously a number of investigators had measured a statistical character to dc breakdown in both gases<sup>78</sup> and solids.<sup>72, 73</sup> Statistics in dc experiments were assumed to arise either from the details of an electron avalanche or from the dynamics of space charge formation.<sup>71</sup>

The laser damage techniques of the present work can be applied to the study of breakdown statistics. There are, in fact, several advantages to using these techniques. First, the intrinsic damage process has been identified, at least in the alkali halides. Secondly, because damage from absorbing inclusions can be distinguished and space charges will presumably not develop in optical fields, major experimental uncertainties in the surface studies and dc measurements are avoided. And finally, the bulk of crystals is far better characterized than surfaces in terms of structure and composition.

In the next section, after briefly reviewing the results of Bass and Barrett, we will present new experimental evidence to support the conclusion that there exists a statistical nature to laser-induced damage both in the bulk and on the surfaces of transparent materials. It will be shown that the

new experimental data is compatible with the results of Ref. 12. Some new arguments will be presented in Sect. C to support the original conclusion that the surface damage statistics are intrinsic in origin, and possible sources of statistics within the avalanche process will be discussed.

#### B. Experimental Measurements of Laser Damage Statistics

Bass and Barrett<sup>12</sup> observed that a precisely defined threshold for laser induced surface damage does not exist in the ten different solids which they studied. Instead, there is a range of power levels within which damage can develop on each shot with some finite probability  $p_1$  such that  $0 < p_1 < 1$ . The damage probability  $p_1$  at some power level was defined as the ratio of the total number of damage sites to the total number of laser shots. (See Eq. (3-1).) By varying the power level of the highly-stabilized laser source, they were able to measure  $p_1$  as a function of the laser power. Fig. 21, which summarizes their experimental results, shows that the data appears to satisfy the relationship

$$p_1 \propto \exp(-K/E). \quad (6-1)$$

An analysis of the statistical distribution  $f_N$  (see Eq. (3-2)) confirmed that the statistics were not resulting from either material homogeneities fixed in position or from laser fluctuations.

Additional evidence for the probabilistic nature of

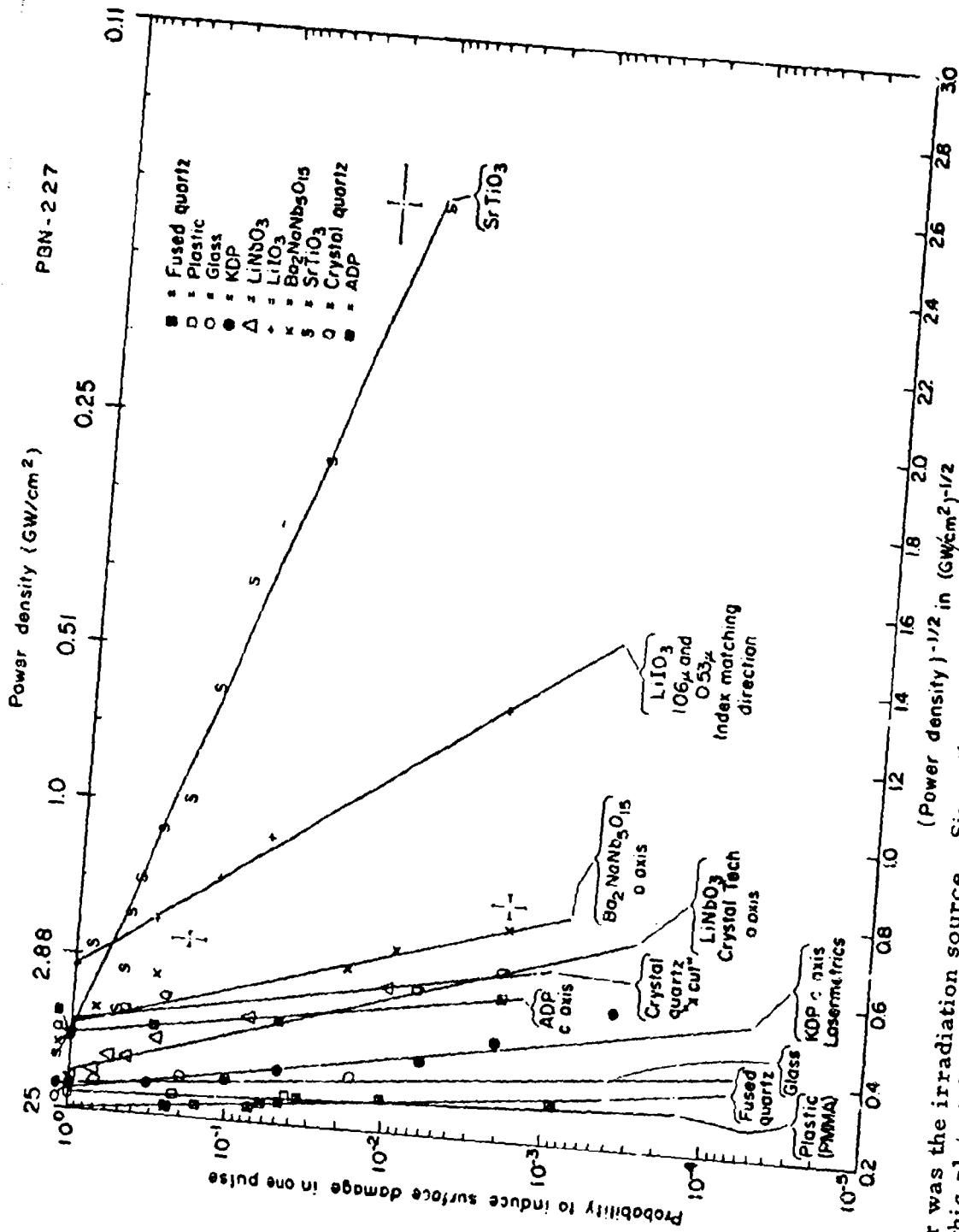


Fig. 21. THE SURFACE DAMAGE PROBABILITY  $P_1$  AS A FUNCTION OF LASER POWER (Bass and Barrett, 1972)

A YAG:Nd laser was the irradiation source. Since the lower abscissa is proportional to the reciprocal of the electric field, this plot, taken from Ref. 12, serves to test for a dependence of the form  $P_1 \propto \exp(-\text{const}/E)$ . The powers are not corrected for the materials' indices of refraction.

laser damage was obtained in experiments in which an image converter streak camera was used to measure the distribution of breakdown starting times for surface damage to two different materials. (The time at which a visible spark first appeared was assumed to be the breakdown starting time.) If the breakdown process were completely described by a well-defined threshold, then this distribution should be very narrow. The data, however, showed broad distributions, particularly when the applied field was such that  $p_1 < 1$ . In all cases the most probable starting time for breakdown occurred before the time of maximum field.

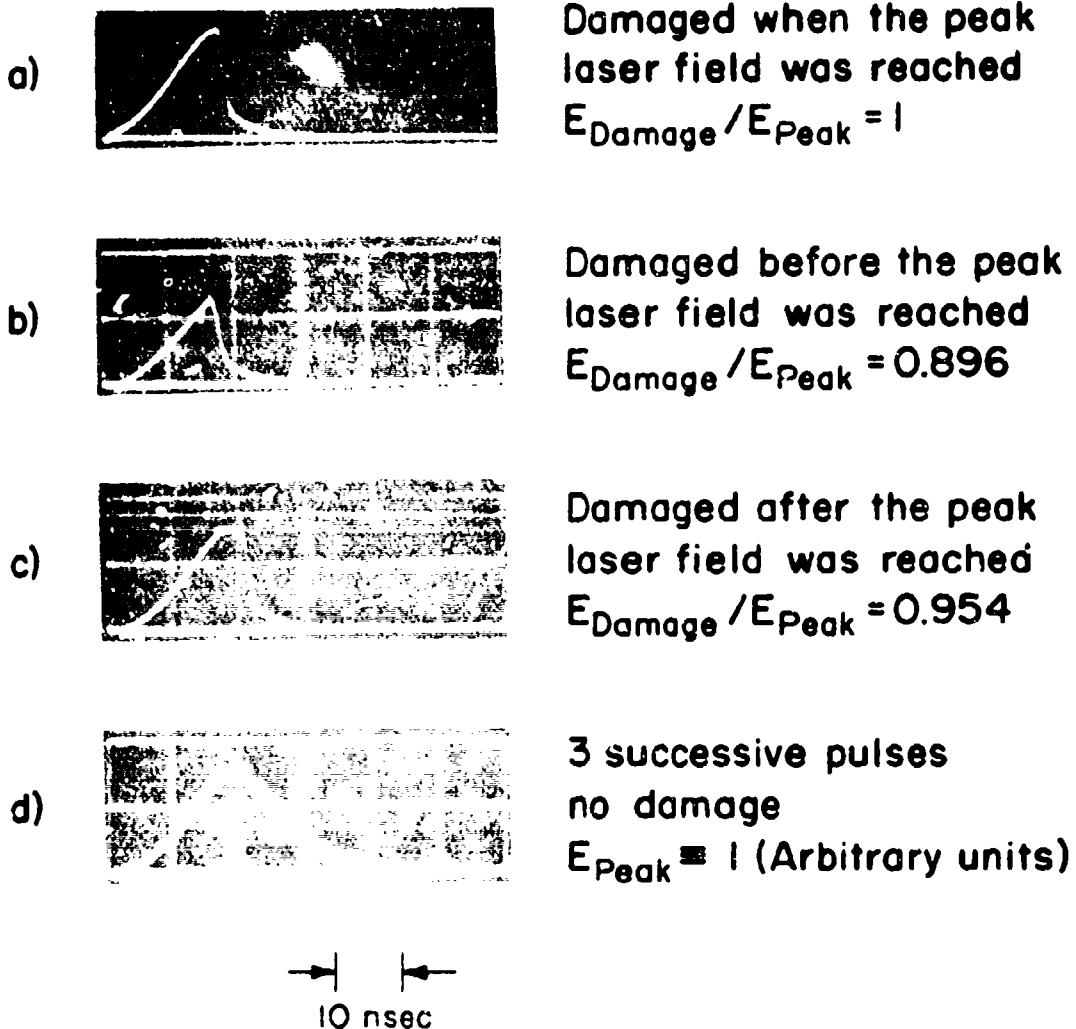
Damage statistics develop because there exists a statistical time lag to the damage process as confirmed by Bass and Barrett's streak camera measurements. When lasers are used to induce damage, the electric field is applied for only a short time interval so that late-starting avalanches may not be able to develop to damaging proportions before the laser pulse has passed. Avalanche breakdown induced by a continuous laser source, on the other hand, should have a well-defined threshold for damage instead of a statistical threshold as indicated by Eq. (6-1).

During the Q-switched damage experiments on the alkali halides (see Chaps. 4 and 5), evidence was recorded which supports the statistical viewpoint. By monitoring the transmitted laser light with a fast photodiode-oscilloscope combination (risetime  $\approx 0.5$  ns), we observed that the laser light is attenuated when damage develops. The first instant of

measurable attenuation can occur before, at, or after the peak of the laser pulse, so that no well-defined relationship exists between the laser intensity and the first instant of attenuation. Fig. 22 shows examples of such observations made with a ruby laser beam focused to produce damage inside NaCl. The laser pulses are fully time-resolved as verified by Fabry-Perot studies. In Fig. 23 another ruby laser pulse was focused into NaCl but did not cause damage whereas a second pulse, apparently identical to the first, did induce damage when focused into the same volume of the crystal. Nothing was moved between the two laser shots, and the laser was firing automatically at a repetition rate of about 1 pulse/5 sec. A similar observation was recorded at  $1.06 \mu\text{m}$  in Fig. 17 of Chapt. 4 where the automatic firing rate was just over 1 pps.

The relationship between laser light attenuation and the size of the electron avalanche is difficult to establish. A reasonable estimate indicates that the transmitted light is unaffected by the avalanche until the density of conduction-band electrons reaches a level of about  $10^{18} \text{ cm}^{-3}$ . It is not strictly correct, therefore, to associate the first instant of attenuation with the breakdown or avalanche starting time. But as noted below, there should be essentially no random character to the time delay between the avalanche starting time and the first instant of attenuation.<sup>55</sup> We will assume as a simplification that the two instants of time are identical within experimental error. It should be noted, incidentally,

P8N-72-430



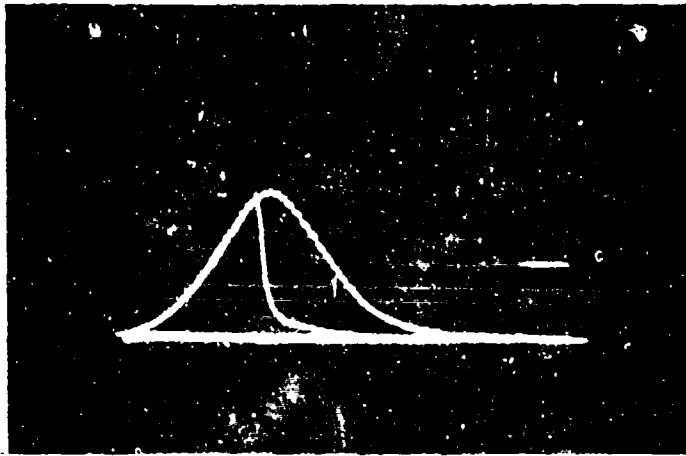
THE OCCURRENCE OF INTERNAL DAMAGE IN NaCl

A TEM<sub>00</sub> mode ruby laser with total pulse energy of 0.3 mJ was focused inside the inclusion free sample with a 14 mm focal length lens

The laser intensity transmitted through the sample is shown in these photographs.

Fig. 22. THE OCCURRENCE OF INTERNAL DAMAGE IN NaCl DUE TO RUBY LASER IRRADIATION

PBN-72-543



→ | ←  
10 nsec

**Ruby laser pulses in NaCl with no self-focusing. The first pulse caused no damage. Five seconds later the second pulse caused damage before peak field was reached.**

About 5 seconds passed between the apparently identical laser pulses. Because nothing was moved during this time interval, the same volume of material was irradiated by both pulses.

Fig. 23. INTRINSIC BULK DAMAGE OCCURRING IN NaCl ON THE SECOND OF TWO RUBY LASER PULSES

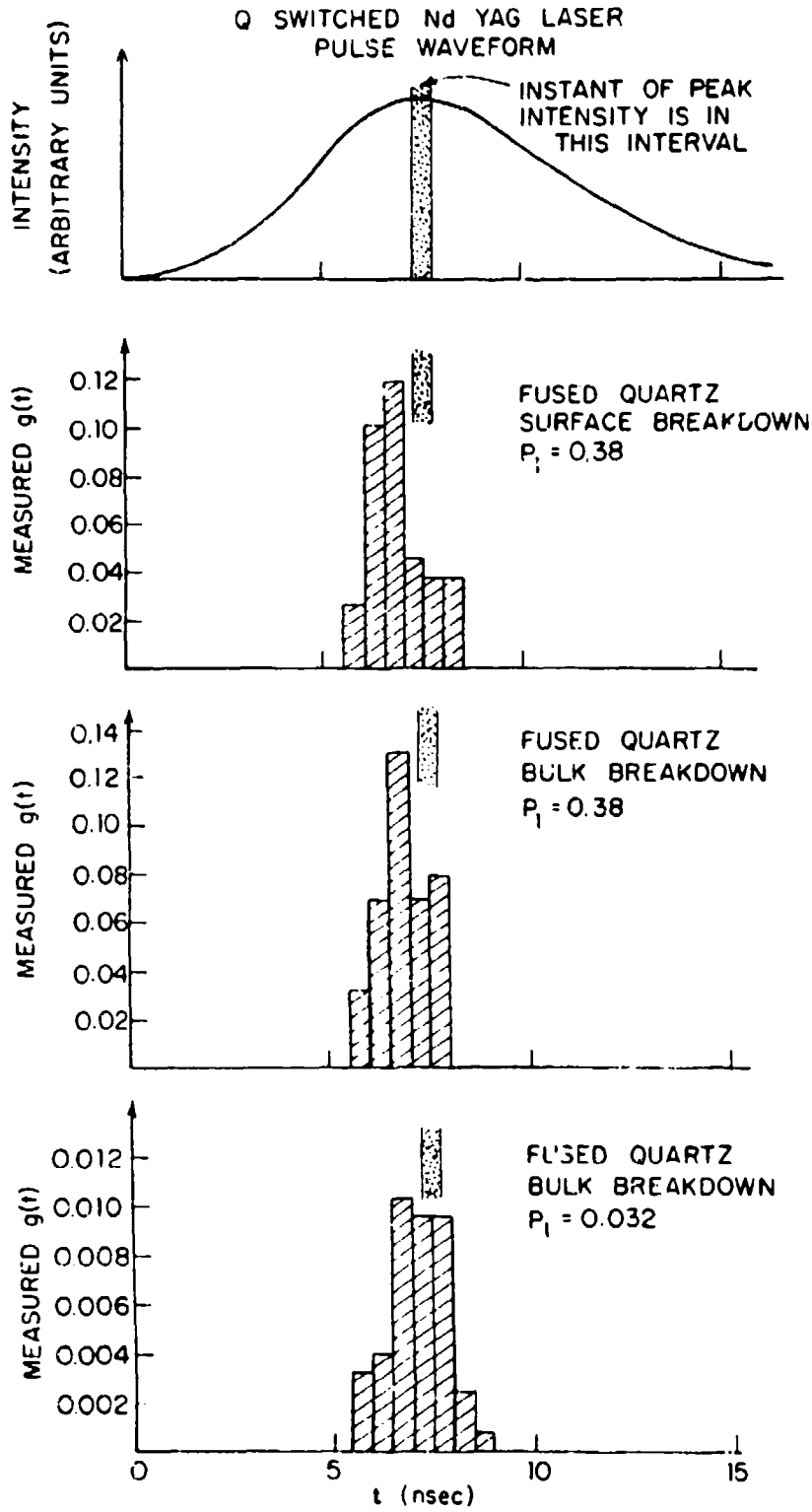


that the time interval over which the transmission drops from effectively unity to nearly zero may have no simple relationship to the ionization rate  $\alpha(E)$  defined in Chapt. 5. Because the density of electrons is quite high by the time measurable attenuation occurs, electron-electron collisions may alter the avalanche development and reflection from the plasma may become important, particularly at longer laser wavelengths.

Encouraged by our experimental observations, we decided to conduct a careful measurement of the statistical time lag in a number of materials. Figs. 24-26 summarize measurements made in fused quartz at  $1.06 \mu\text{m}$ , in NaF at  $0.69 \mu\text{m}$ , and in sapphire at  $1.06 \mu\text{m}$ . As usual, self-focusing was found to be absent under the conditions of our measurements. In each case 30 to 50 damage events were recorded, and  $p_1$  was defined by Eq. (3-1). The position of the peak of the laser pulse could be identified to within intervals of 0.5 ns for the  $1.06 \mu\text{m}$  pulses and 1.0 ns for the  $0.69 \mu\text{m}$  pulses. Fig. 15 of Chapt. 3 and the techniques of Chapt. 3 (Sect. D) were used to verify that the statistics were not occurring because of the presence of point-to-point material inhomogeneities such as inclusions.

The distributions of breakdown starting times for surface and bulk damage to fused quartz are shown in Fig. 24 to be virtually identical for the same value of  $p_1$ . These distributions have the same characteristics as those reported by Bass and Barrett for entrance surface damage. The breakdown can begin at any time over a relatively long interval which

PBN-72-1172



The histograms represent experimental measures of  $g(t)$  as discussed in the text.

Fig. 24. MEASURED DISTRIBUTIONS OF BULK BREAKDOWN STARTING TIMES FOR FUSED QUARTZ USING YAG:Nd LASER IRRADIATION

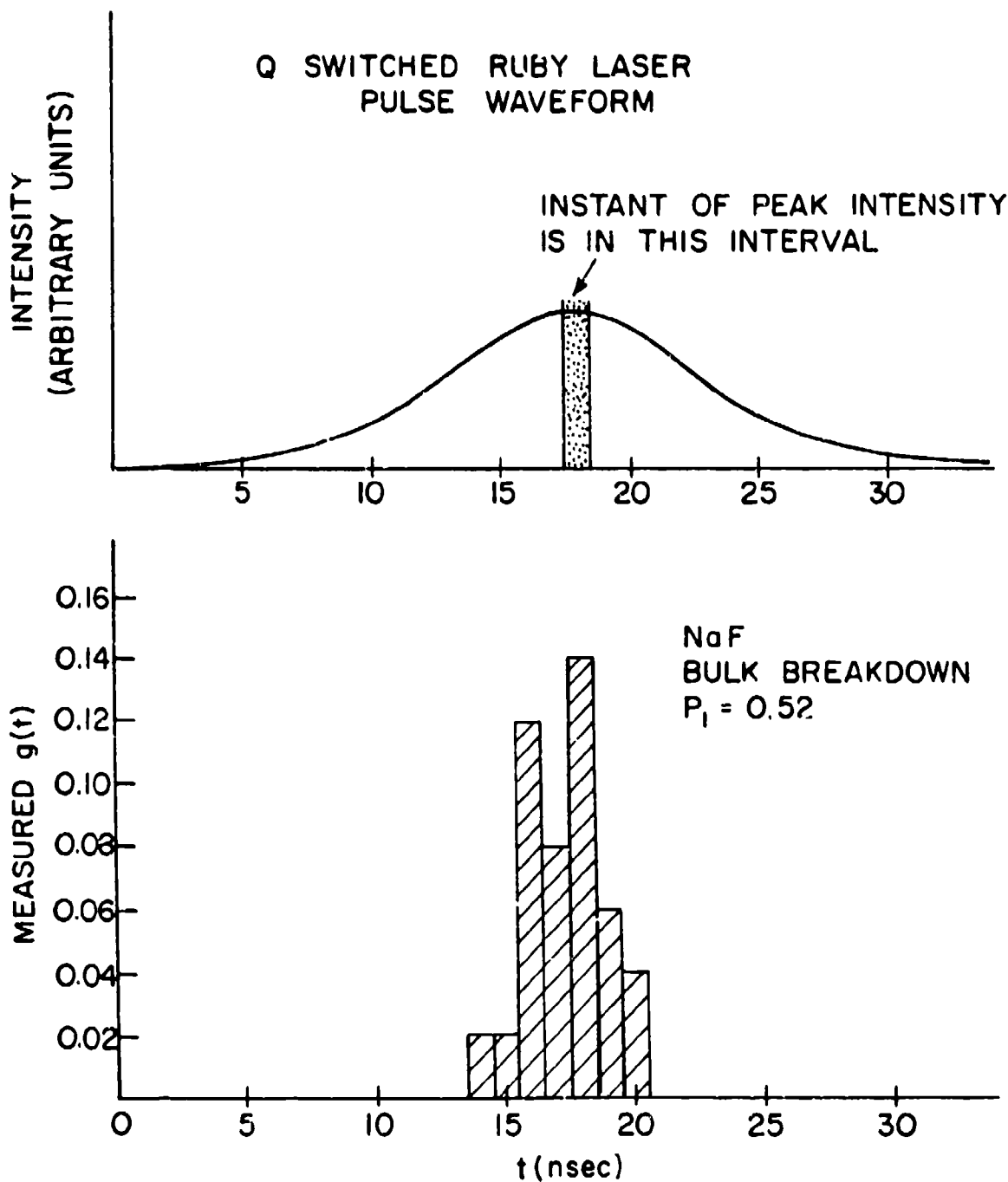


Fig. 25. MEASURED DISTRIBUTION OF BULK AND SURFACE BREAKDOWN STARTING TIMES FOR NaF USING RUBY LASER IRRADIATION

Q-Switched YAG:Nd Laser  
Pulse Waveform

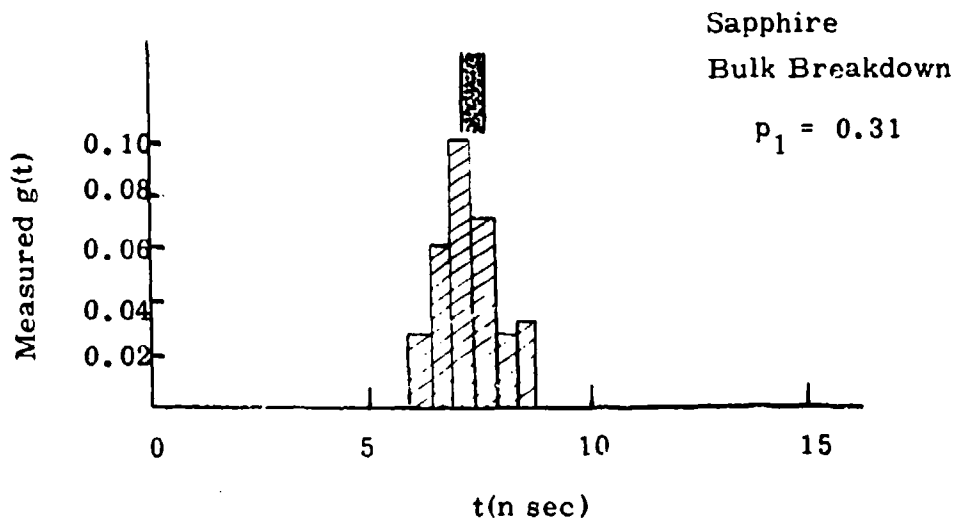
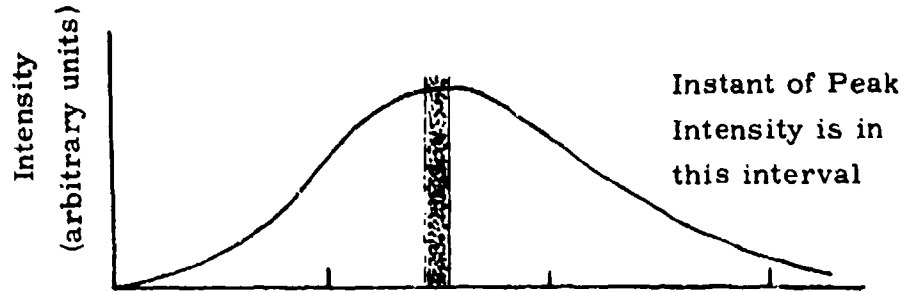


Fig. 26. MEASURED DISTRIBUTION OF BULK BREAKDOWN STARTING TIMES FOR SAPPHIRE USING YAG:Nd LASER IRRADIATION

includes times after the peak intensity in contrast to the very sharply defined breakdown starting time expected for a threshold-like process. The most probable time for damage is in all cases before or at the instant of maximum intensity or optical field, and as the applied field is reduced ( $p_1$  is lowered), the time of maximum damage probability shifts to the peak of the pulse. (Compare Figs. 24c and d.) These qualitative properties were shown in Ref. 12 to be explained by the probabilistic point of view.

Quantitative comparison can be made between the present results and the earlier studies by using an expression for the distribution of breakdown starting times  $g(t)$  which was derived by Bass and Barrett. It was shown in Ref. 12 that  $g(t)$  is given by the compound probability that breakdown occurs at a particular instant given that it has not occurred before that time or

$$g(t) = h(t) \exp\left(-\int_{-\infty}^t h(t') dt'\right) \quad (6-2)$$

where  $h(t)$  is the probability per unit time that the applied laser field  $E(t)$  causes breakdown. The probability  $p_1$  in Eq. (3-1) is related to  $g(t)$  by

$$p_1 = \int_{-\infty}^{\infty} g(t) dt \quad (6-3)$$

and the histograms in Figs. 24-26 are experimental measures of  $g(t)$ . If the damage rate  $h(t)$  can be expressed quantitatively, then  $g(t)$  can be computed and compared to our

experimental data.

Eq. (6-1) suggests that the damage rate should be of the form<sup>12</sup>

$$h(t) = A_0 \exp(-K/E(t)) \quad (6-4)$$

$A_0$  is a normalization constant, and  $K$  is the experimentally determined quantity in Eq. (6-1).  $E(t)$  is determined from the peak laser field  $E_0$  and the electric field waveform.

If, as Bass and Barrett had assumed, a damaging avalanche could form for all values of  $E(t)$ , then Eq. (6-4) would be an appropriate choice for  $h(t)$ . It was demonstrated in Sect. C of Chapt. 5, however, that the avalanche is time dependent. When  $E(t)$  is less than some minimum field  $E_{min}$ , the time required for the avalanche to reach damaging proportions will exceed the pulse duration and the damage rate must vanish. In a pulsed field which reaches  $E_{min}$  at  $t_{min}$  and falls below  $E_{min}$  at  $t_{max}$ ,  $h(t)$  is therefore effectively zero when  $t < t_{min}$  and  $t > t_{max}$ . Assuming that the avalanche formation time is negligibly small ( $\leq 0.1$  ns) when  $E(t) > E_{min}$ , then Eq. (6-4) should be replaced by

$$h(t) = \begin{cases} 0 & ; \quad t < t_{min} \\ A_0 \exp(-K/E(t)) & ; \quad t_{min} \leq t \leq t_{max} \\ 0 & ; \quad t > t_{max} \end{cases} \quad (6-5)$$

An estimate for  $E_{min}$  can be made from the measured form of  $g(t)$  by setting  $E_{min}$  equal to the lowest electric field value at which breakdown has been observed to occur in a particular

material. The times  $t_{\min}$  and  $t_{\max}$  can then be determined from the pulse waveform.

In order to complete the numerical comparison, values are needed for the normalization constant  $A_0$  and the slope  $K$ . We have found  $K$  experimentally in fused quartz by measuring  $p_1$  at three different field values. The value so obtained--  $71 \times 10^8$  v/cm--compares favorably to the earlier measurement of  $61 \times 10^8$  v/cm which Bass and Barrett obtained from their surface studies in fused quartz.

The computation of  $A_0$  is simplified by introducing the function  $v(t)$ , defined as the fractional number of tests where no damage has occurred by the time  $t$ . When the laser pulse is passed,  $v(t)$  must equal  $1 - p_1$ , the probability that no damage was produced. In Ref. 12,  $v(t)$  was shown to be

$$v(t) = \exp\left(-\int_{-\infty}^t h(t') dt'\right) \quad (6-6)$$

Bass<sup>79</sup> has calculated  $A_0$  from Eqs. (6-5) and (6-6) and the final condition on  $v(t)$  and has found that

$$A_0 = -\ln(1-p_1) / \left( \int_{t_{\min}}^{t_{\max}} \exp(-K/E(t)) dt \right) \quad (6-7)$$

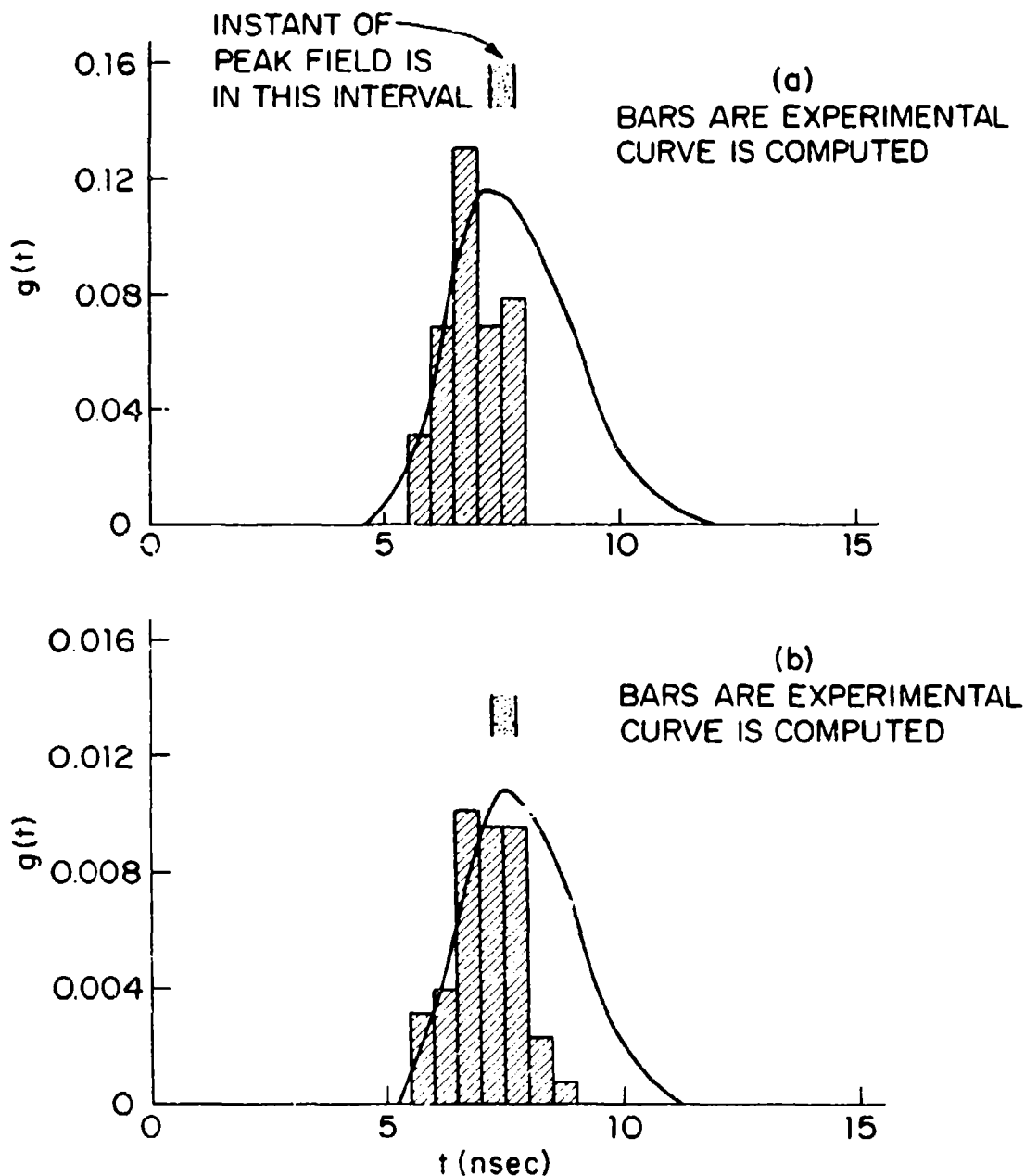
$A_0$  can thus be evaluated from experimental parameters. If the damage rate assumed in Eq. (6-5) is consistent with the experimental data, then  $A_0$  should be a constant for a particular material.

Eqs. (6-3), (6-5), and (6-7) can now be used to calculate

the predicted distribution of breakdown starting times for bulk damage in fused quartz which can be compared to the experimental results of Fig. 24. Using numerical techniques, Bass obtained the curves in Fig. 22. The data used to compute these curves are summarized in Table VII.

Fig. 27 shows good qualitative agreement between the model based on Bass and Barrett's experimental results as summarized by Eq. (6-1) and our own experimental data in fused quartz. There is, however, some deviation between the two for times after the peak of the laser pulse, that is, for times when  $E(t)$  decreases to  $E_{\min}$ . The form used for  $h(t)$  when  $t_{\min} < t < t_{\max}$  assumed that the avalanche formation time was negligibly small whenever the field was greater than  $E_c$ . As  $E(t)$  decreases, however, the formation time must increase at an increasing rate. This means that at such times  $h(t)$  will be decreased over the value in Eq. (6-5) at a rate which increases as  $t \rightarrow t_{\max}$ , and the computed values of  $g(t)$  will be reduced accordingly. The effect of allowing for finite formation time, then, would make the computed curves in Fig. 27 decrease more rapidly for times past the peak of the pulse and thereby improve the qualitative agreement in that figure.

The agreement between model and experiment which has already been achieved is strengthened by the results in Table VII. There we find that both cases were computed with nearly the same value of  $A_0$ . The  $\pm 20$  percent experimental error in  $K$  and  $E_0$  can easily account for the 10 percent



The parameters relevant to these figures are listed in Table VII.

Fig. 27. MEASURED AND CALCULATED DISTRIBUTIONS OF BREAK-DOWN STARTING TIMES FOR BULK DAMAGE IN FUSED QUARTZ USING A YAG:Nd LASER

TABLE VII

Parameters Used to Calculate  $g(t)$  in Fig. 27

Materials Studied: Fused Quartz

	Experimentally Determined				Calculated
	$p_1$	$E_o^{(a)}$	$K$	$A_o$	$\int_{t_{\min}}^{t_{\max}} g(t) dt$
Fig. 27a	0.380	$7.3 \times 10^8$ V/m	$71 \times 10^8$ V/m	2599.8	0.373
Fig. 27b	0.032	$5.7 \times 10^8$ V/m	$71 \times 10^8$ V/m	2776.4	0.031

(a)  $E_o$  is the peak value of the applied optical field within the medium. The electric field waveform is the square root of the waveform in Fig. 24a.

difference between the  $A_0$ 's. As a further check on the consistency of the model, we also computed the time integral of  $g(t)$  since, by definition, it should equal the experimentally determined value of  $p_1$ . In Table VII we find that this condition is also satisfied. These computations do not involve any fitted parameters and as such are a useful test of the consistency of the model with the experimental data.

Finally, it should be noted that the breakdown statistics should depend on the size of the focal volume. This conclusion, discussed in Ref. 13, follows from a general model which assumes that the statistics arise because of fluctuations in the formation of the first few hot electrons in the small focal volume. As larger volumes are probed, the number of potential starting electrons increases and breakdown statistics should become less important. Comparable statistics can only be obtained, therefore, from experiments in which approximately the same volumes of material are irradiated.

In conclusion, the present work confirms the existence of a statistical nature to the laser induced intrinsic damage process and supports the notion that the damage mechanism both on the surface and in the bulk is an electron avalanche with statistical starting properties.

### C. Sources of Damage Statistics

It was shown in the last section that the optical breakdown process has a statistical character which leads to an experimentally measurable probability of the form of Eq. (6-1).

Bass and Barrett explained this behavior by using a simplified model for avalanche breakdown. In their model it was assumed that statistics for the entire process were determined by the heating of the first electron in the avalanche. This assumption was based on the expectation that the secondary electrons produced by an ionizing collision have energies much greater than the thermal energy  $kT$  and are therefore more easily accelerated to ionizing energies than is the starting electron. Using a classical collision model, similar in conceptual form to a dc model by Shockley,<sup>80</sup> they were able to derive Eq. (6-1) for a laser pulse of constant intensity.

The model of Bass and Barrett is greatly oversimplified in computational details because of the use of a classical relaxation time approximation with an energy-independent collision rate. In addition, the most pronounced damage statistics in their study are observed with the pathological crystal  $\text{SrTiO}_3$  which is known to possess large surface strains and enormous local field effects.<sup>81</sup> Yet the idea that the heating of starting electrons determines the observed damage statistics is an intriguing one, and their model is consistent with experimental results. We will reconsider the matter of starting electrons after looking for other sources of damage statistics in addition to the dynamics of the electron avalanche.

It was observed by tests such as those summarized in Sect. D of Chapt. 3 that the damage statistics do not result from inclusions and fixed material inhomogeneities. A

measurement has been made of the density of inclusions on the surface of fused quartz to show that this conclusion is reasonable. At our request Dr. O. J. Guentert of Raytheon Corp. conducted an electron microprobe survey of the surface of a piece of conventionally polished fused quartz used in the actual damage measurements of Ref. 12. He found that there were no more than about 100 impurities per  $\text{cm}^2$ . The microprobe could sense impurities with diameters  $\geq 1 \mu\text{m}$  and to a depth of  $5 \mu\text{m}$ . In the surface damage measurements of the last section and those of Bass and Barrett, the high intensity (1/e) region of the focused laser beam was about  $10 \mu\text{m}$  in diameter, and damage was observed to commence within a few  $\mu\text{m}$  of the surface. On the average, then, the probability of intercepting a large inclusion was about  $10^{-4}$  per shot. If we assume that the density of potentially damaging inclusions with diameters  $d$  such that  $0.1 \mu\text{m} < d < 1 \mu\text{m}$  is about 100 times as great as Guentert had measured for large inclusions, then the probability increases to  $10^{-2}$ , a value which is still much less than unity. We thus see that the experimental confirmation of the absence of inclusion damage on the surface is consistent with the measured density of inclusions. A similar result holds for bulk damage. It should be noted, incidentally, that the use of small beam diameters resulting from tightly focusing external optics is necessary in order to avoid inclusion damage. Many studies of optical damage have been conducted with laser beam diameters  $< 100 \mu\text{m}$ <sup>10, 45, 49</sup> and, therefore, probably reflect

characteristics of inclusion damage rather than characteristics of intrinsic processes.

It has been suggested that dust particles settling on the surface could lead to surface damage statistics.<sup>82</sup> While dust may affect the results of surface studies, it is difficult to see how statistics from the settling of dust can have the form of Eq. (6-1). Also, statistics have now been observed in the bulk where surface dust does not present a problem.

Another possible source of statistics is from thermally-induced migration of absorbing impurities.<sup>83</sup> This process can lead to statistical distributions at fixed laser power of the form of Fig. 15 in Chapt. 3. Let us attempt to model such a process. It might be expected that some activation energy  $\epsilon_g$  exists for the migration. The driving force is a heat pulse injected by a small residual absorption of the laser light. If large volumes are considered, the temperature rise  $\delta T \sim I t_p$ , such as we found for inclusions in Chapt. 1, and if small volumes are considered,  $\delta T \sim$  the laser intensity  $I$  or, equivalently,  $\delta T \sim E^2$ . The probability that such a migration will occur by laser irradiation is proportional to a Boltzman-like factor  $\exp(-\epsilon_g/k T)$ . At first glance this factor appears to be of the form of Eq. (6-1) but with closer study we realize that the present exponential function depends on  $E^2$  and not  $E$  as observed in Fig. 21 and as summarized by Eq. (6-1). This is a general result: Physical observables from a thermal process should be functions of  $E^2$  and not  $E$ . The damage probability  $p_1$  is a function of  $E$ , however, so that

we can conclude that no simple thermal process is causing the damage statistics.

There are other possible sources of damage statistics. In dc experiments it is very likely that damage statistics result from space charge development which intensifies the local field.<sup>73</sup> But space charges should not develop in optical fields or, for that matter, in quasi-dc fields of nanosecond duration so that this model cannot explain our results. A cumulative effect from the trapping of electrons in low lying states may in principle influence the experimental results,<sup>55</sup> but it was found that the damage statistics were not a function of repetition rate as that rate was varied from about 1 pps to 4 pps. Also, the life-time of such trapped states is less than a second.<sup>55</sup>

Statistics in laser-induced gas breakdown can occur because there may be no free electrons in the irradiated volume.<sup>84</sup> Let us consider this mechanism as a source for damage statistics in solids. In an insulator the density of thermally excited conduction electrons in zero field is of the order of  $10^{12}/\text{cm}^3$  or more. The high-intensity region of the focused laser beam where bulk damage commences (see Fig. 13 in Chapt. 3) is about  $10^{-9} \text{ cm}^3$  in volume so that about  $10^3$  quasi-free electrons should exist in that volume. This number is adequate to insure that at least one ionized electron is present in the focal volume. Multiphoton ionization of impurities should, in fact, increase this number. It thus appears that an initially ionized (conduction-band) electron

will always be present in the focal volume.

Bass and Barrett have recently made an observation which gives further support to the conclusion that statistics are present in the avalanche itself.<sup>13</sup> When  $\text{LiIO}_3$  and  $\text{SrTiO}_3$  were damaged with ruby laser light, no intrinsic statistics could be seen. This was not the case, however, with three other materials studied at  $0.69 \mu\text{m}$ . The interpretation given for the abrupt change in damage characteristics was that another intrinsic mechanism, multiphoton absorption, was responsible for damage in  $\text{LiIO}_3$  and  $\text{SrTiO}_3$  by ruby laser light. Damage from multiphoton absorption is not expected to have a measurable statistical character because multiphoton ionization does not require a sequence of improbable events. This is not the case with avalanche ionization, however, because the development of the avalanche requires some electrons to be heated to energies well in excess of the average electron energy. (See Chapt. 8.) In support of their interpretation, Bass and Barrett noted that two-photon absorption is possible in  $\text{LiNbO}_3$  and  $\text{SrTiO}_3$  at  $0.69 \mu\text{m}$  but it is not possible at  $1.06 \mu\text{m}$ . The other materials studied at both wavelengths have band-gap energies in excess of 3.6 eV so that two-photon absorption is not possible in them at either  $1.06 \mu\text{m}$  or  $0.69 \mu\text{m}$ . If this interpretation is correct, these measurements represent the first experimental confirmation of the competition between multiphoton absorption and avalanche breakdown in solids. (See the discussion at the end of Chapt. 1.)

The source of the damage statistics thus appears to be in the electron avalanche itself--through the details of the initial electron heating, because of the chance termination of incipient avalanches, or because of fluctuations in the ionization rate  $\alpha$ . Yablonovitch<sup>55</sup> has shown that the latter process cannot lead to measurable statistics. The second possibility is virtually identical to the first because it is unlikely that an avalanche which has produced more than a few generations can terminate with any reasonable probability. We are thus left with the basic hypothesis of Bass and Barrett, that measurable damage statistics can develop from the first generations in the avalanche.

Bass and Barrett have suggested a description of those first generations. A relatively simple improvement of their model would be to use an energy-dependent collision rate such as discussed in Chapt. 8. Alternately, it may be possible to show that the statistics of the first events do not result from the heating of the first electron to the ionization energy  $I$  but, rather, they result from the heating of the electron to energies just greater than the longitudinal optical phonon (LO) resonances at about  $0.01 I$ . Thornber and Feynman<sup>57</sup> have shown that electron energy losses to the lattice are extremely high near the LO energies. These resonances, therefore, represent barriers to electron heating and may effectively produce low-energy electron traps. Because there are probably only of the order of  $10^4$  quasi-free electrons in the focal volume at the start of the laser

pulse, there may be no electrons initially present with energies past the L0 resonances. Once an electron moves past this barrier because of a sequence of favorable but improbable collisions with the lattice, the heating may be rapid. Products of the ionization will probably have energies which are much greater than the L0 energy so that the avalanche, once begun, will not terminate.

We thus see that there is ample evidence that optical avalanche breakdown has a measurable statistical character. From a practical viewpoint, however, it is not clear that damage statistics such as we have measured are important to laser system design. It is the author's experience that when inclusion damage develops, variations in optical strength are normally much more pronounced than the statistics we have observed from intrinsic damage. In fact, the observation of a reasonably well-defined damage threshold is itself an indication that intrinsic damage is occurring. (See Sect. D of Chapt. 3.) Intrinsic damage statistics have been observed because inclusions have been largely avoided in our measurements and in those of Ref. 12, stable single-mode laser sources have been used, great care has been taken in recording damage levels and only small focal volumes have been irradiated.<sup>85</sup> From a fundamental viewpoint, on the other hand, the study of avalanche statistics may give us valuable insight into the details of the avalanche formation, insight which could not be gained by observation of other damage parameters.

## CHAPTER 7

### OPTICAL SURFACE DAMAGE

#### A. Introduction

In the experiments of Bass and Barrett,<sup>12, 13</sup> the laser beams were focused to about 25  $\mu\text{m}$  in diameter ( $1/e^2$  in intensity) in order to induce damage on the surface. For such focal diameters the laser beam was effectively collimated over a distance of about 50  $\mu\text{m}$  near the focus,<sup>86</sup> and yet damage was consistently observed to develop within the first 0.25  $\mu\text{m}$  of material. Because surface contaminants were apparently not responsible for damage in this study (see Chapt. 6), this surprising result indicated that the surfaces of conventionally polished solids have a lower intrinsic threshold than the bulk. Giuliano observed in a later work with a weakly focused ruby laser beam<sup>87</sup> that the surface damage field for sapphire was increased when the surface was ion-beam polished, a procedure that removed most but not all of the polishing scratches on his samples.

A quantitative relationship between surface damage fields and those of the bulk was not established experimentally in these or in any other published study, because, to the author's knowledge, until the work of Yablonovitch<sup>14</sup> and the present work, no accurate measurements of intrinsic optical bulk damage had ever been made. Using the bulk damage techniques of Chapt. 4-6 and the surface focusing scheme of Ref. 12, we have completed a study of surface damage at 1.06  $\mu\text{m}$  in which surface damage fields were measured for a variety of surface preparations and compared to bulk damage fields. A simple model proposed by Bloembergen<sup>15</sup> is found to be fully

Preceding page blank

capable of explaining the experimental results.

## B. The Experiment

The laser source and experimental procedures for studying intrinsic bulk damage were discussed in detail in Chapt. 3 and 4. A simple scheme for accurately focusing on the surfaces of solids was developed in Ref. 12 and applied in the present work. In this scheme the focusing lens for the laser beam is used as a microscope objective. Laser light enters the microscope between the eyepiece and objective and is reflected off a beam-splitter towards the objective lens. By inducing a spark with laser light on the surface of a piece of steel shim stock, it is possible to accurately place the shim stock at the focus of the objective lens. When the separation of the two lenses in the eyepiece is adjusted to bring the surface of the shim stock into a sharp visible focus, a calibration is established such that the focused object plane for the observer who uses the total eyepiece-objective system is the same as the focal plane for the laser light which enters only the objective lens. In this manner the separation of the objective lens and the sample was adjusted by simple visual inspection to accurately focus the laser light on the sample surface.

For each sample studied, the surface damage field  $E_S$  was measured, and by bringing the sample about 1 mm closer to the objective lens, the bulk damage field  $E_B$  was determined for that same sample. All field measurements were made relative to the bulk damage field of NaCl which was known from the

experiment of Chapt. 4 to an accuracy of 20%. Relative measurements of damage fields were made to an accuracy of better than 10%. The damage field itself was defined in the usual manner as that value of rms electric field which produced damage half of the time on a single shot (i.e.,  $E_1 = 0.5$ ).

Table VIII summarizes the measured ratios  $E_d/E_g$  for three materials whose surfaces have been prepared by various means. These data show that the clean but conventionally polished surface (Fig. 28a) of a transparent medium is generally more easily damaged than the bulk. On the other hand, when care is taken to achieve imperfection-free surface finishes such as shown in Fig. 28b, the bulk and surface damage fields are equal.

The morphology of the residual entrance surface damage gives additional support for the preceding conclusions. When a spark was observed during laser irradiation, very small pit damage<sup>37</sup> was found on a conventionally finished surface. Imperfection-free surfaces showed more extensive damage including a region of cracks surrounding the melted irradiated volume (Fig. 29). Such damage extends many microns into the material and is very similar to a cross-section of bulk damage as recorded in Fig. 13 of Chapt. 3.

Since the focused laser light was effectively collimated over several microns near the surface, high intensity light extended into the bulk, and it was possible for the light to cause internal or bulk damage. A conventionally finished surface, however, damages more easily than the bulk. Because

Material	Finishing Procedure Finish Quality (a)	Spherical Void	Predicted Ratio $E_B/E_S$ Cylindrical Groove	"Vec" Groove	Measured $E_B/E_S$	Surface Damage Morphology
Fused Quartz	Conventional #1 Standard 0-0 (see Fig. 28a)	1.21	1.35	2.1	$1.3 \pm 0.1$	b
	Conventional #2 Standard 0-0	"	"	"	$1.5 \pm 0.1$	b
	"Bowl" feed finish See Fig. 28b	"	"	"	$1.0 \pm 0.1$	c
	Ion beam polish Standard 0-0 with final 1.25 $\mu\text{m}$ removed by Ar ion beam	"	"	"	$1.0 \pm 0.1$	c
Sapphire	Conventional Many scratches and digs with 50X mag and dark field	1.29	1.50	3.00	$2.0 \pm 0.2$	b
	Conventional Standard 0-0	1.23	1.39	2.25	$1.3 \pm 0.1$	b
BSC-2 Glass	"Bowl" feed finish See Fig. 28c	"	"	"	$1.0 \pm 0.1$	b, c

- a. All surfaces were cleaned with collodion
- b. Very faint pit  $\sim 20 \mu\text{m}$  in dia. and  $\sim 0.25 \mu\text{m}$  deep
- c. Extensive cracking out to  $\sim 150 \mu\text{m}$  with central hole  $\sim 20 \mu\text{m}$  dia. and  $\sim 3-10 \mu\text{m}$  deep

TABLE VIII

Comparison of Bulk and Surface Damage Fields for Different Samples and Surface Finishes

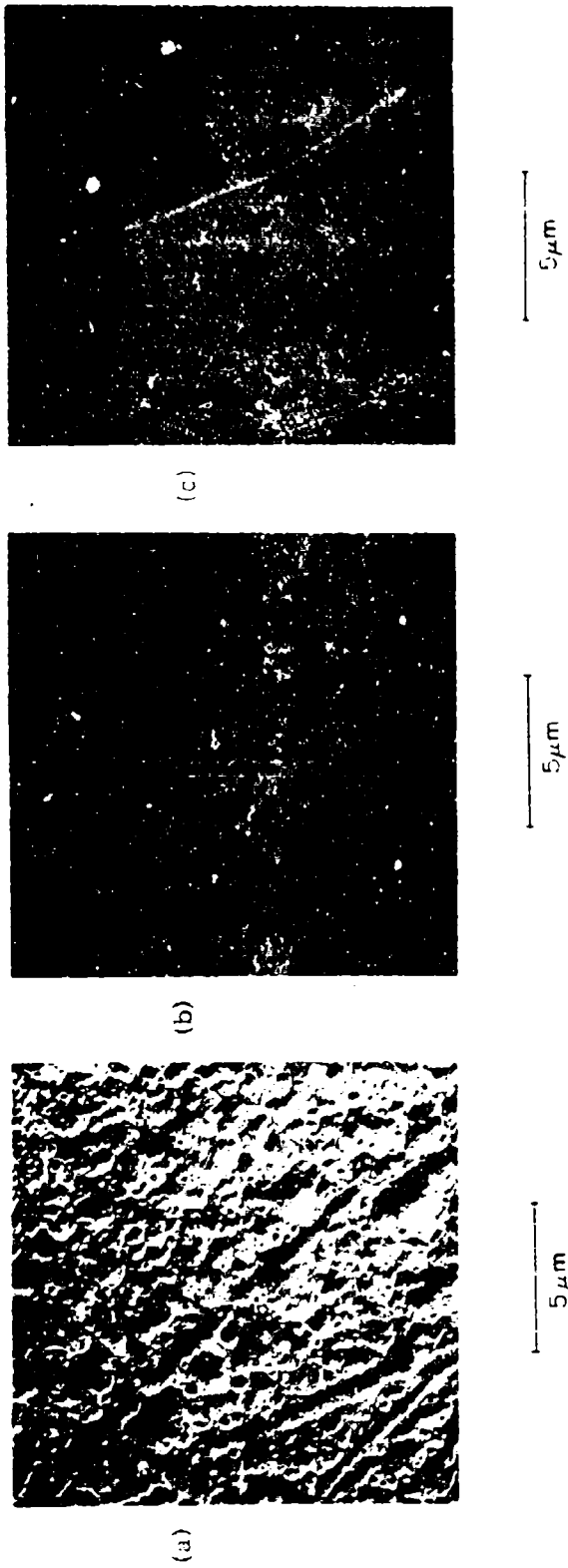
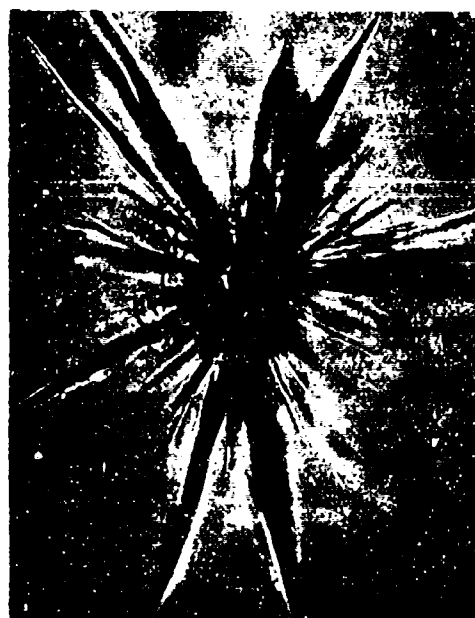


Fig. 28. ELECTRON MICROGRAPHS OF THE SURFACES OF FOCUSED QUARTZ AND BSC-2 GLASS

- (a) Conventionally polished fused quartz (no. 1)
- (b) Bowl-feed ("superpolished") finished fused quartz
- (c) Bowl-feed finished BSC-2 glass

Fig. 29. RESIDUAL SURFACE DAMAGE ON ION-BEAM  
POLISHED FUSED QUARTZ



100  $\mu$ m

Surface which were effectively imperfection-free produced the form of damage morphology pictured here. Cracks surround a small molten region about  $10 \mu\text{m}$  in diameter. Bass<sup>37</sup> has observed a similar morphology when damage occurs from self-focusing inside the bulk and breaks out through the surface.

the onset of damage is accompanied by a strong attenuation of the transmitted beam, surface damage on conventionally finished samples is localized on the surface. If, on the other hand, a more highly finished surface does not damage any more easily than the volume of the medium, it is possible for intense light to reach the bulk. Damage can then commence anywhere within the effective focal volume. Occasionally damage will begin within  $0.25 \mu\text{m}$  of the surface and produce a faint pit, but more often it will begin somewhere in the bulk several microns from the surface. When bulk damage occurs, the molten region grows back towards the laser and breaks out of the entrance surface producing the morphology recorded in Fig. 29. These morphological observations, which are valid only when inclusion induced damage is absent, show that if very small pit damage is normally produced, then that surface is more easily damaged than the bulk. The observations that damage on imperfection-free surfaces appears to be bulk damage which erupted from within the medium might explain Giuliano's report of more extensive surface damage on ion-beam polished sapphire than on a conventionally polished sample.<sup>87</sup>

The morphology of damage on the bowl feed ("superpolished") surface of BSC-2 glass was generally of the small pit type though more extensive damage was detected occasionally. The measured ratio of bulk to surface damage fields,  $1.0 \pm 0.1$ , implied a perfect surface, but based on the damage morphology we decided that the surface was, in fact, not as uniformly imperfection-free as possible. Not long after this conclusion

was reached, we received the electron micrograph shown in Fig. 28c which confirmed our interpretation of the surface quality. Faint residual scratches can still be seen in that figure.

Bloembergen has completed a simple but intriguing model<sup>15</sup> which predicts that the apparent optical strength of surfaces will normally be less than the optical strength of the bulk. He recognized that the dielectric discontinuity occurring at structural defects can enhance the electric field over its average value. The following values are predicted for the ratios  $E_p/E_s$ :

Spherical void	$3\epsilon/(2\epsilon + 1)$
Cylindrical groove	$2\epsilon/(\epsilon + 1)$
"Vee" groove	$\epsilon$

where  $\epsilon$  = optical frequency dielectric constant. These expressions were used to obtain the predicted ratios in Table VIII.

It is seen that except for sapphire the measured ratios for conventionally polished samples lie within the range of values which Bloembergen predicts for spherical voids and cylindrical grooves. Actual defects on conventionally polished surfaces probably have more complicated shapes than Bloembergen has considered. But a high density of subsurface voids and surface pits does result from standard abrasive

polishing<sup>83</sup> as seen in Fig. 28a, so that the reasonable agreement between the first two predicted ratios and experiment is impressive. The sapphire sample had visible scratches that, as Bloembergen predicted, result in a large damage ratio. Finally, the bowl-feed and ion-beam polished samples appear to have only gentle variations in surface topography (Fig. 28b) which should lead to little if any measurable field enhancement according to Bloembergen's model. Again there is experimental agreement. It should be noted, incidentally, that good quality conventional polishes (Fig. 28a) appear spatially uniform to a 20  $\mu\text{m}$ -diameter laser beam. Intrinsic damage on such a surface will produce damage statistics of the form of Fig. 15 in Chapt. 3.

Another point of interest in Table VIII is the fact that the first and third fused quartz samples were purchased from the same manufacturer at the same time. These were described as "1/20 wave interferometer flats." Ion beam polishing of the fourth sample removed material to a depth greater than 3 times the smallest grit size used in the mechanical polishing process, and a large increase in the surface damage field resulted. The ion beam polisher employed  $\text{Ar}^+$  ions at 10 kV and incident at  $60^\circ$  to the surface normal to remove 1.25  $\mu\text{m}$  of material.

Table IX gives the measured bulk damage fields for the samples in Table VIII. These values were measured relative to the damage field for NaCl, and most of the assumed errors in Table IX are due to the experimental uncertainty in that

TABLE IX

Measured Bulk Damage Fields at 1.06  $\mu\text{m}$

Material	$E_B$ (MV/cm) <sup>(a)</sup>
Fused Quartz	Conventional #1
	Conventional #2
	Bowl feed finish
	Ion beam polished
Sapphire	$5.2 \pm 1.3$
Sapphire	$6.3 \pm 1.6$
BSC-2 Glass	$4.7 \pm 1.2$

(a) RMS field values are listed

Measurements were made relative to  $E_B$  in NaCl

latter value.

In conclusion, we see that the incident laser fields for entrance surface and bulk damage to transparent solids are the same for imperfection-free surfaces. When structural imperfections are present, they enhance the optical field locally so that the surface damages more easily than the bulk. Improved surface finish quality is recognized as essential to minimizing the problem of scattering in optical systems. The results of this work show that it is also critical in the problem of laser induced surface damage.

## CHAPTER 8

### THEORIES OF DC AND OPTICAL ELECTRIC BREAKDOWN

#### A. Introduction

Electric breakdown is one of the most difficult problems of modern solid state theory. As is probably the case with most hot electron phenomena in solids, the process is understood only in qualitative terms. The basis of the difficulty in modeling breakdown is the fact that the relevant interactions cannot be treated separately. It is not strictly correct, for example, to speak of electron excitations as being distinct from those of the lattice. The electron-phonon interaction in NaCl, for example, is so strong that the effective collision time appears to be  $\sim 2 \times 10^{-16}$  sec. (Sect. B of Chapt. 6) which implies an electron energy uncertainty of the order of the ionization energy. In addition, distortion from electric fields having rms values  $\sim 10^6$  volts/cm cannot properly be treated as a perturbation on the energy spectrum of the electron-lattice system.

A number of theories have been formulated which largely ignore these difficulties. Many such theories use a relaxation time approximation with the electron-phonon collision time calculated from perturbation theory. Despite their lack of rigor, such models appear to explain many features of the process.

In this chapter we will briefly review some of the published models of dc and optical electric breakdown and compare their predictions with the experimental results of Chaps. 4 and 5. A recent work by Holway<sup>67, 68</sup> will be considered in which the high-field electron distribution function is

**Preceding page blank**

calculated from a classical Fokker-Planck equation. Although Holway's model greatly simplifies the optical breakdown process, it demonstrates that electric breakdown may not be an average electron phenomenon. The model, in addition, can provide a useful framework for evaluating many untested theoretical ideas concerning electric breakdown.

### B. Historical Review of Breakdown Theories

The literature on breakdown distinguishes between two general types of dielectric failure called intrinsic breakdown and avalanche breakdown.<sup>58</sup> In intrinsic breakdown theories, the quasi-free electron density is seen to jump discontinuously to damaging proportions from a low steady-state level as the external field is raised by a small amount. Calculated thresholds are independent of sample thickness (dc) or duration of the applied field. Avalanche theories, on the other hand, consider a time-dependent electron multiplication whose threshold is sensitive to the time available for the avalanche. As the sample thickness is decreased or as the time duration of the applied field is reduced, the electric field necessary to induce damage will increase.

Experimental evidence suggests that the idealized intrinsic mechanism does not exist. Materials such as the alkali halides and mica, which were originally believed to fail by intrinsic breakdown, have been shown to have a time-dependent damage field at dc and, as we saw in Chapt. 5, at optical frequencies. Yet the conceptual distinction between an

intrinsic instability and a time-dependent avalanche persists in the recent theoretical literature, and in this section we will group breakdown theories according to this distinction.

Intrinsic breakdown theories consider a balance between electron energy gain  $A$  from the field and electron energy loss  $B$  to the lattice. Equilibrium exists when the relationship

$$A(E, \beta) = B(\beta) \quad (8-1)$$

can be satisfied in a physically acceptable manner.<sup>58</sup>  $E$  is the external electric field and  $\beta$  symbolizes various material parameters that determine  $A$  and  $B$ . When the field is raised to a critical value  $E_c$ , Eq. (8-1) can no longer be satisfied in a physically acceptable manner and breakdown is assumed to develop.  $E_c$  is identified as the breakdown field. Various theories of intrinsic breakdown differ in two basic aspects--the modeling of the manner in which the electron population is coupled to the lattice (i.e., in the calculation of  $B$ ) and the explicit assumption of what constitutes a physically acceptable condition. We will consider important examples of such theories.

One of the most frequently referenced theories of dc breakdown is the original model of Fröhlich.<sup>64</sup> In this work Fröhlich considered ionic insulators and assumed that the electron-lattice coupling arises entirely from the interaction between electrons and longitudinal-optical (LO) phonons. A perturbation calculation of the electron-phonon interaction leads to an effective collision frequency  $\nu_i = 1/\tau$  which

decreases with increasing electron energy  $\epsilon$  for  $\epsilon$  greater than the LO phonon energy  $\hbar\omega_{LO}$ . In particular, when  $\epsilon > \hbar\omega_{LO}$ .

$$v_z(\epsilon) \propto \begin{cases} \epsilon^{-1/2} & k < G \\ \epsilon^{-3/2} & k > G \end{cases} \quad (8-2)$$

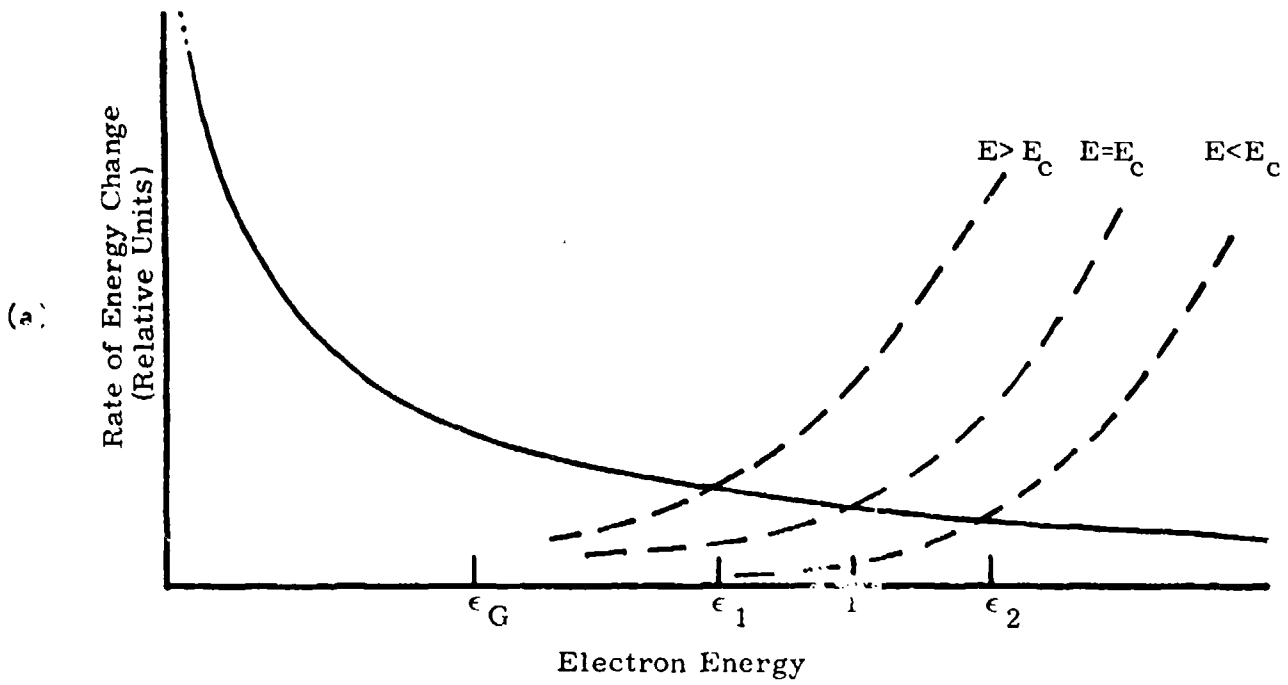
where  $k$  is the free electron wave vector and  $G$  is the reciprocal lattice wavevector. For NaCl,  $\hbar^2 G/2m \approx 0.5 I$  where  $m$  is the free electron mass and  $I$  is the ionization energy. The term  $B(\beta)$  in Eq. (8-1), which describes the energy transfer to the lattice, is proportional to  $v_z$  times a factor depending logarithmically on the electron energy.<sup>64</sup> That is,

$$B \approx v_z(\epsilon) \quad (8-3)$$

$A(E, \beta)$  has the form of Eq. (1-1) with  $\mu = e\tau/m$ . At dc ( $\omega = 0$ ) the energy gain for each electron is

$$A = \left( \frac{e^2 E^2}{m} \right) \frac{1}{v_z(\epsilon)} \quad (8-4)$$

Fröhlich defined the breakdown field  $E_c$  as that value of electric field for which  $A$  and  $B$  intersect at the ionization energy  $I$ . When  $E > E_c$ , the point of intersection is at  $\epsilon_1 < I$ , and when  $E < E_c$ , the point of intersection is at  $\epsilon_2 > I$ . This behavior is shown schematically in Fig. 30a. At  $E = E_c$ , electrons with energies greater than  $I$  gain more energy on the average from the field than they lose to the



--- A( $\epsilon$ ) energy gain from field  
 — B( $\epsilon$ ) energy loss to lattice

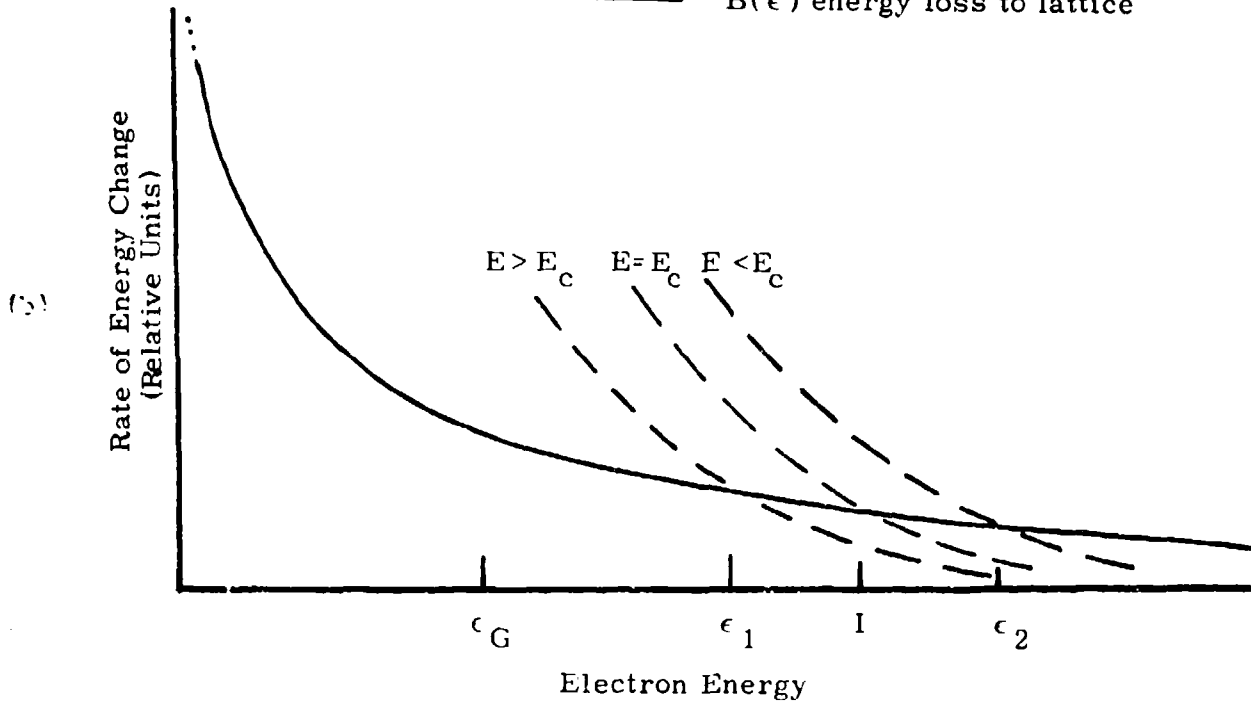


Fig. 30. THE ENERGY BALANCE IN AVERAGE-ELECTRON BREAKDOWN THEORIES

lattice, and electrons with  $\epsilon < I$  lose more energy on the average to the lattice than they gain from the field.

The basis for defining  $E_c$  in this manner, is the intuitive notion that a steady-state can only exist when collision ionization is balanced by the inverse process of recombination. If  $E < E_c$ , then a high energy electron ( $\epsilon = I$ ) created by recombination will lose its energy to the lattice, but if  $E > E_c$ , the high energy electron created by recombination will continue to gain energy on the average from the field until it produces another ionization. The precise manner in which low energy electrons reach  $\epsilon = I$  and cause ionization is not specified.

Fröhlich has thus considered a possible electron instability, but he did not relate this instability to the actual dynamics of electron multiplication and eventual material damage. An earlier theory by von Hippel,<sup>54</sup> which was developed further by Callen,<sup>88</sup> is based on the far more stringent requirement that  $E$  must be sufficiently large to move the point of intersection of the curves for A and B to  $\epsilon = \hbar\omega_{LO} = 0.01 I$ . The Fröhlich model predicts breakdown fields about an order of magnitude larger than experimentally observed.

Zverev et al.<sup>50</sup> have considered the Fröhlich model in the high frequency limit by setting  $\omega \gg \nu_l$  in Eq. (1-1). This changes A ( $E, \beta$ ) to

$$A = \frac{e^2 E^2}{m\omega^2} \nu_l(\epsilon) . \quad (8-5)$$

$B(\beta)$  is again given by Eq. (8-3). In the energy range of interest, the collision frequency  $\nu_c(\epsilon)$  is given by the second (high momentum) form of Eq. (8-2).

Fig. 30b shows the functional form of A and B. It is seen that, in this high frequency limit, when  $E = E_c$ , electrons with  $\epsilon > I$  lose energy to the lattice while those with  $\epsilon < I$  gain from the field on the average--the opposite of the dc behavior. The intuitive basis for defining  $E_c$ , therefore, is not valid in the limit Zverev et al. have considered. In addition, their calculated breakdown strength for sapphire is about an order of magnitude larger than we have measured at  $1.06 \mu\text{m}$ . (See Table IX in Chapt. 7.)

A second group of intrinsic breakdown theories use a Boltzmann equation to calculate an electron distribution function  $f(\epsilon)$ . We will consider these theories only briefly. As before, the perturbation results of Eqs. (8-2) and (8-3) are used to model the energy transfers among the field, the electrons, and the lattice. A general solution for  $f(\epsilon)$  is expanded in terms of spherical harmonics with only the first two terms retained. Breakdown is assumed to occur when either an effective electron temperature increases without limit or when the distribution function can no longer be normalized. The minimum electric field which produces these conditions is defined to be the damage field  $E_c$ .

A number of authors, including Fröhlich,<sup>89-91</sup> have used this formalism to describe dc breakdown. The simplification is normally made that  $f(\epsilon)$  is essentially a Boltzmann

distribution even though this assumption is valid only at low fields or under conditions where the electron density  $n \geq 10^{18} \text{ cm}^{-3}$ .<sup>63</sup> A high frequency (optical) extension of this formalism was carried out by Wasserman who assumed that  $\omega r \gg 1$  in Eq. (1-1).<sup>51</sup> He found that an effective electron temperature could not be found in NaCl when  $E \geq 2 \times 10^7$  volts/cm. This field, assumed to be the damage field, is the same magnitude as the critical fields obtained in the dc theories, but it is a factor of 10 larger than the optical breakdown field we measured in Chapt. 4 and 5.

Avalanche breakdown theories consider damage to develop when a time-dependent electron multiplication has increased the conduction band density to damaging proportions. As was the case with intrinsic breakdown theories, the modeling generally takes one of two forms, either calculations of average electron dynamics or calculations of the high-field electron distribution function.

A phenomenological dc breakdown model due to Shockley<sup>80</sup> displays some simple features of an electron avalanche. According to Shockley, the ionization rate at dc (see Eq. (5-2)) is proportional to the probability  $P(t_1)$  that a low energy electron avoids phonon collisions for a sufficiently long period of time  $t_1$  to be accelerated by the dc field to the ionization energy  $i$ .

We can find  $P$  by the following argument.<sup>58</sup> The probability that an electron will avoid collisions for the period  $(t + dt)$  is given by the compound probability that it avoids collision

for the period  $t$  and the probability that it does not collide with a phonon during the interval  $dt$ . That is

$$P(t+dt) = P(t)(1 - \nu_c(t) dt) \quad (8-6)$$

The solution to Eq. (8-6) is

$$P(t_1) = \exp \left[ - \int_0^{t_1} \nu_c(\epsilon) dt \right] \quad (8-7)$$

Time and energy are related for a free electron in a dc field by

$$\frac{e\epsilon}{dt} = m v \left( \frac{dv}{dt} \right) = (2m\epsilon)^{1/2} \frac{eE}{m} \quad (8-8)$$

which can be inserted into Eq. (8-7) to give

$$P(t_1) \propto \exp(-K/E) \propto \frac{1}{N} \frac{dN}{dt} \equiv \alpha \quad (8-9)$$

$N$  is the density of conduction band electrons. The constant  $K$ , which has the dimension of a field, can be calculated from Eqs. (8-7) and (8-8). This simple dependence has the same functional form as the Townsend coefficient in gas breakdown.<sup>92</sup>

Baraff<sup>93</sup> calculated  $\alpha(E)$  from a nonlinear Boltzmann equation by assuming that  $\nu_c(\epsilon)$  is a constant independent of energy. He found that Eq. (8-9) approximately describes the functional dependence of  $\alpha(E)$  at low fields but that  $K$  is actually higher than Shockley had calculated. The physical reason for this discrepancy is that Shockley implicitly assumed that each electron colliding at intermediate energies returns to zero energy before attempting another flight to high

energy.<sup>93</sup> This assumption leads to an underestimate of the number of electrons which reach ionizing energies. In high fields the ionization coefficient was found by Baraff to be approximately proportional to  $\exp(-K'/E^2)$ . Baraff's calculations were intended to describe avalanche multiplication in semiconductors such as Ge although his choice of an energy-independent  $\nu_i$  is probably more suggestive of breakdown in gases.

Pass and Barrett<sup>12</sup> have shown that Shockley's model can be applied to breakdown from optical electric fields by considering a sequence of "lucky" collisions that reverse the electron momentum at about the instant when the field changes direction. In this manner a "lucky" electron will continually remain in phase with the field and be accelerated to ionizing energy. A probability was calculated which has the same functional dependence on field as does Eq. (8-9). Although this simple model was advanced to explain laser breakdown statistics (see Chapt. 6), it leads to a prediction of the ionization rate  $\alpha(E)$  in the same manner that Shockley's calculation of  $P(t_I)$  leads to  $\alpha(E)$ . This model suffers from the same simplifications as Shockley's--the assumption of a constant  $\nu_i$  and an underestimate of the number of electrons which reach ionizing energy.

Seitz has written one of the classic papers on dc electron avalanche breakdown.<sup>65</sup> His description of the avalanche contains the famous "40 generations" model and is generally based on physical arguments rather than on formal mathematical

modeling. This work contains many important ideas that had not previously been considered in breakdown theory.

Seitz recognized that the LO phonon interaction (or Fröhlich interaction) may not realistically model the electron-lattice coupling. In all solids the electron can be coupled to the lattice by a deformation potential interaction. This interaction increases with increasing energy and may dominate the LO phonon interaction in ionic solids when  $\epsilon \geq 10 \hbar \omega_{LO} = 0.1$  I. A perturbation calculation that considers both types of coupling can be applied to calculate an effective  $\nu_i(\epsilon)$  as shown schematically in Fig. 31.

The "40 generations" model is an estimate of the number of progeny which a single electron must produce in order to create a damaging avalanche. With simple arguments, Seitz demonstrated that if a single electron, starting its flight at the cathode, produces 40 secondary electrons before the avalanche is terminated at the anode, then enough energy will be deposited from joule heating into the medium near the anode to destroy the material. This description leads naturally to the prediction, later verified,<sup>60, 61</sup> that the breakdown field will depend on sample thickness. If the specimen thickness is reduced, the ionization rate per unit distance must increase in order to compensate for the reduced spatial extent (or time duration) available for 40 secondaries to be produced. In Chapt. 6 we in effect considered the basic concept of the "40 generations" model by defining breakdown as the growth of the multiplication factor  $M_c$  to a critical size. (See

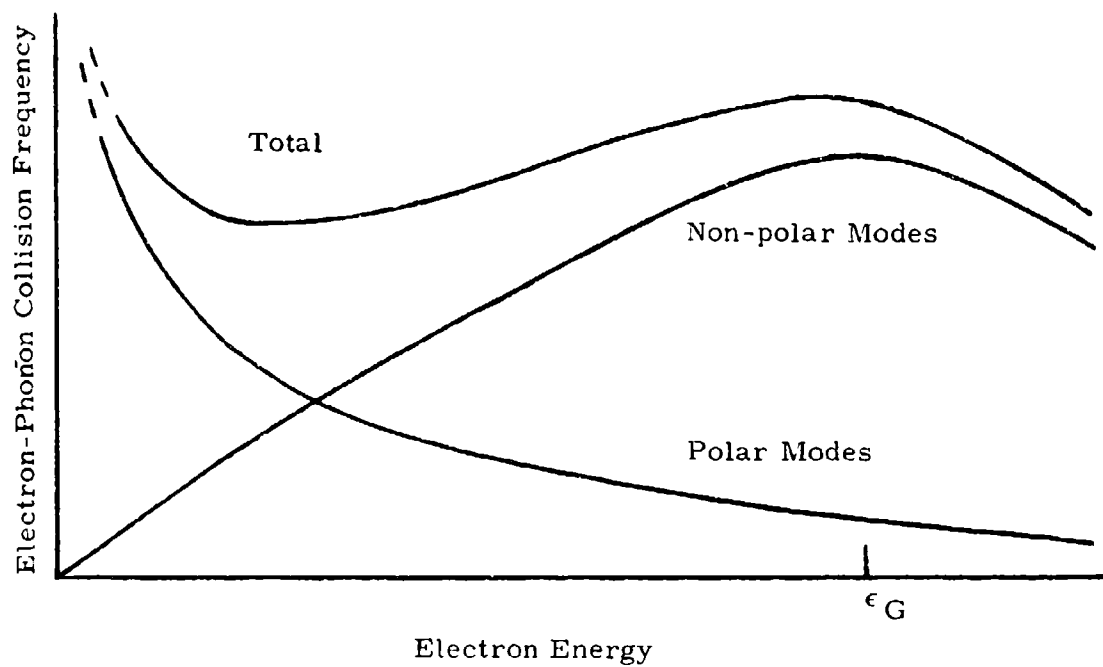


Fig. 31. SCHEMATIC OF THE ELECTRON-PHONON COLLISION FREQUENCY AS A FUNCTION OF ENERGY FOR BOTH POLAR AND NONPOLAR INTERACTIONS (Seitz 1949)

Eq. (5-2).) Our choice of  $M_c = 10^7$  corresponds to 23 generations.<sup>94</sup>

The damage field for NaCl predicted by the "40 generations" model is about an order of magnitude larger than experimentally observed. Seitz explained this discrepancy by showing that avalanche breakdown may not be an average electron phenomenon. Fluctuations in electron energies can substantially lower the breakdown threshold. This same result was demonstrated several years later in the calculations of Baraff<sup>93</sup> and Holway.<sup>68</sup>

Seitz considered the effects of exciton states on breakdown, a concept introduced in Sect. B of Chapt. 5. He also attempted to explain the origin of noisy dc pre-breakdown currents that had been observed experimentally, and he considered the possibility that Bragg reflection at the Brillouin zone boundary (Umklapp processes) might affect the breakdown strength of some materials.

A recent model by Holway,<sup>67</sup> developed by analogy to gas breakdown, provides a relatively simple mathematical formalism for evaluating many theoretical ideas suggested by Seitz's work. This model, which will be considered again in the next section, can be applied at dc and at optical frequencies. Holway calculated a high-field electron distribution function by using a classical Fokker-Planck equation and a relaxation-time model for the electron-phonon interaction. The calculation used Eq. (8-5) for  $A(\epsilon)$  and Eq. (8-3) for  $B(\epsilon)$ , and only the high energy form for the collision frequency in Eq. (8-2). Two important results were obtained. First, the growth of

the electron density was found to proceed in the manner indicated by Eq. (5-2) so that an ionization rate could be calculated. Second, the term in the Fokker-Planck equation describing the average electron energy was found to be unimportant to the avalanche dynamics. As Seitz had suggested<sup>65</sup> and as Baraff had found<sup>93</sup> with a more complicated Boltzmann equation calculation, the avalanche appears to develop because of electron diffusion to higher energies and not because the average electron has been heated sufficiently to produce ionization.

Finally, we mention two more calculations related to breakdown. In the first, Thornber and Feynman<sup>59</sup> treated the Fröhlich interaction quantum mechanically to a high degree of precision over the energy extending to about twice the LO phonon energy. Their results, which are quite involved mathematically, are not directly applicable to avalanche breakdown. As Seitz has observed, the LO interaction described approximately by the Fröhlich Hamiltonian, may not completely describe the electron-phonon coupling over the energy range of interest. We also realize that avalanche breakdown is a statistical process, and it appears to be necessary to calculate an electron distribution function before any realistic predictions of breakdown strength can be made. The details of the electron-phonon interaction near the LO resonance may not even be important to an understanding of the avalanche development. Since the cross-section for impact ionization will not be large until  $\epsilon = 1.2 I$ , the products of the ionization

event may have energies much greater than  $\hbar\omega_{LO}$ .

The last theory of breakdown we will consider is Zener tunneling which at high frequencies becomes multiphoton absorption.<sup>18</sup> Even though this process is not an electron avalanche, it can cause breakdown, and we, therefore, consider it briefly here. Zener<sup>20</sup> originally introduced the concept of field emission breakdown, and Franz<sup>95</sup> put the idea on a more quantitative basis for dc fields. An approximation to Franz' results, given by O'Dwyer,<sup>58</sup> predicts a breakdown field in volts/cm of

$$E_c \approx \frac{4 \times 10^7 I^{3/2}}{\ln(10^{20} t_p^2)} \quad (8-10)$$

where  $I$  is the band-gap (ionization) energy in eV and  $t_p$  is the duration of the applied field in microseconds. Eq. (8-10) is probably a useful approximation to optical tunneling field at  $1 \mu\text{m}$  in NaCl.<sup>20</sup> For  $t_p = 10 \text{ ns}$ , Eq. (8-10) predicts  $E_c = 3 \times 10^7$  volts/cm, and for  $t_p = 15 \text{ ps}$ ,  $E_c = 5 \times 10^7$  volts/cm. These values compare to  $0.2 \times 10^7$  volts/cm and  $1.2 \times 10^7$  volts/cm measured at  $1.06 \mu\text{m}$  in Chapt. 5. This process thus appears to have a weaker pulse-width dependence than optical avalanche breakdown and should therefore be observed when extremely short laser pulses ( $t_p = 10^{-12}$  sec.) are used to induce damage.

### C. Implications of Experimental Results to Theory

In Chapt. 4 and 5 we observed that the avalanche break-

down process has a time and frequency dependence and that it appears to be affected by severe crystalline disorder. We were also able to determine accurate values of breakdown fields which were not confused by the many experimental uncertainties of dc measurements.

The observation of a time dependence to damage suggests that the breakdown models which we called "intrinsic breakdown theories" in the last section are not applicable to the materials we have studied. It appears, in fact, that the distinction between intrinsic breakdown and avalanche breakdown is entirely artificial. Breakdown in materials must have a time dependent aspect.

Our data on the time dependence to the damage field can be compared to the simple prediction of Eq. (8-9) using the definition of  $\alpha$  given in Eq. (5-3). This comparison is made in Fig. 32 where it is seen that the functional form of Shockley's model is not an unreasonable approximation to the experimental data.

A weak frequency dependence to the damage field was observed in the alkali halides in Chapt. 5. In Sect. F of Chapt. 2, a comparison between the sapphire damage field at  $0.69 \mu\text{m}$  measured indirectly by Guiliano et al.<sup>21</sup> and our own measurement at  $1.06 \mu\text{m}$  (Table X in Chapt. 7) indicates that the sapphire damage field is still effectively in its dc limit at ruby frequency. These surprising results suggest that the effective electron-phonon collision times in these materials are of order  $10^{-16}$  sec, a value so short that the

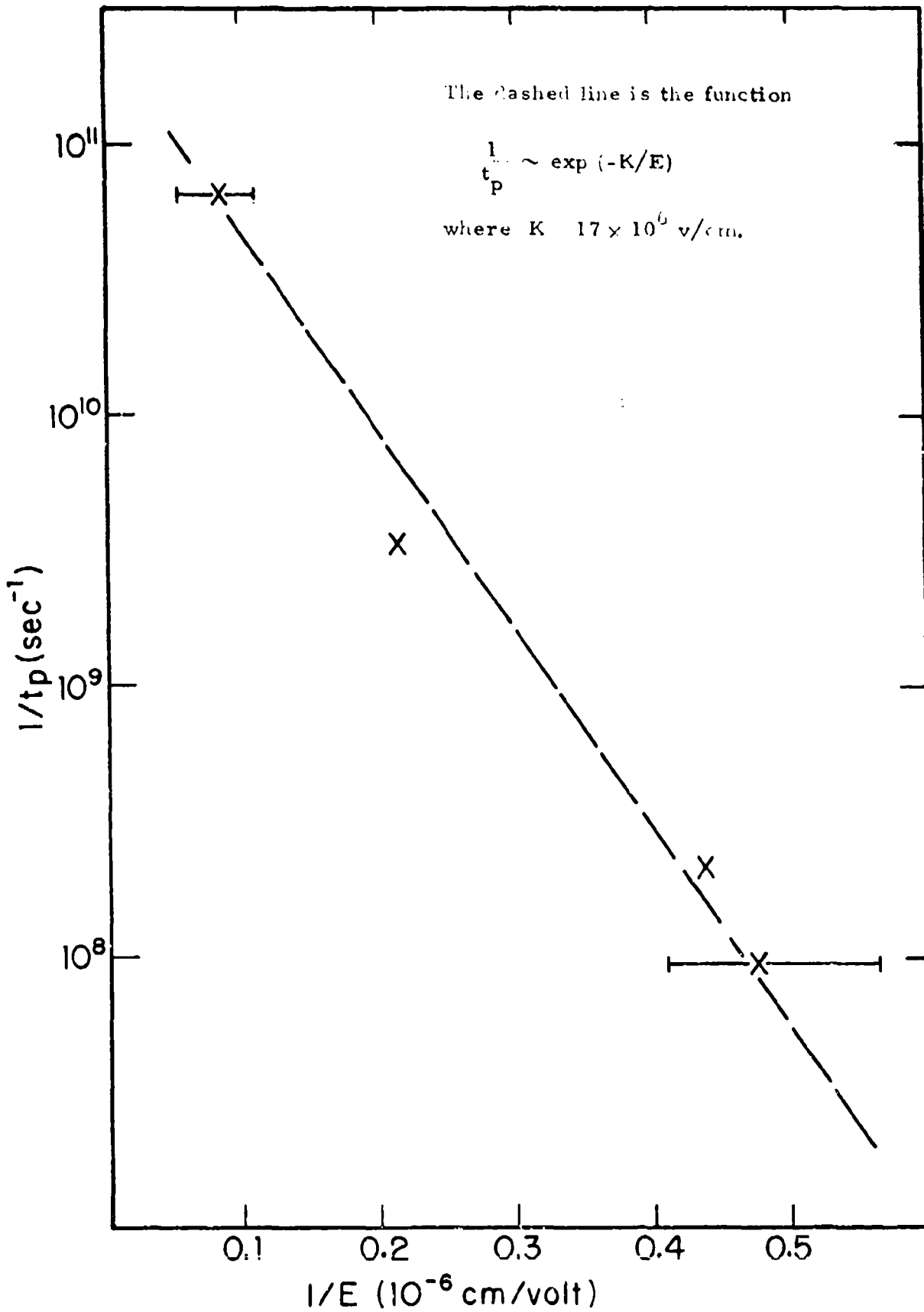


Fig. 32. COMPARISON OF SUBNANOSECOND LASER DATA TO SHOCKLEY MODEL

electron energy uncertainty is comparable to the band-gap energy. If the effective collision frequency  $\nu_i$  is determined by the electron dynamics at energies much larger than  $\hbar\omega_{LO}$ , as Holway has found,<sup>68</sup> then the Fröhlich interaction is not capable of explaining this result. We are left with the suggestion of Seitz that the non-polar or deformation potential interaction may be important in describing avalanche breakdown. In addition, the details of the frequency dispersion summarized in Fig. 19 of Chapt. 5 give evidence that deep-lying exciton levels may play a role in the avalanche at least for wide band-gap insulators such as NaF.

We thus realize that the high frequency limit of the Fröhlich interaction which was used by Zverev *et al.*,<sup>50</sup> Wasserman,<sup>57</sup> and Holway<sup>67, 68</sup> does not describe the energy gain in intense optical fields at least when the frequencies are less than about  $4 \times 10^{14}$  herz in the materials we have studied. It should be noted, incidently, that the laser frequency dependence displayed by Eq. (1-1) is not the true prediction of relaxation-time models of avalanche breakdown.<sup>68</sup> That prediction can only be obtained by averaging Eq. (1-1) over the appropriate electron distribution function.

The dependence of damage field on severe crystalline disorder was considered in Chapt. 5, and the observations of breakdown statistics were summarized in Chapt. 6. Here we merely note that these results further support the conclusion that the intrinsic breakdown mechanism involves ionization from electron heating and not from tunnel ionization or multiphoton

absorption.

Virtually all breakdown theories predict damage fields about an order of magnitude larger than we have observed. An important reason for this discrepancy appears to be that most models have treated avalanche breakdown as an average electron phenomenon. It can be seen very simply, however, that the average electron energy is probably not much greater than about  $\hbar\omega_{LO}$  when damage develops. Consider NaCl, for example. The low-field mobility of about  $10 \text{ cm}^2/\text{volt-sec}$  can be treated as an upper bound for the high-field mobility. If we use the free electron mass, a field of  $2 \times 10^6 \text{ volts/cm}$  produces an average electron energy of less than about 0.2 eV as compared to  $\hbar\omega_{LO} \approx kT = 0.03 \text{ eV}$  and a band-gap energy of about 8 eV. Because the mobility should decrease in high fields,<sup>63</sup> the actual average electron energy may be much less than 0.2 eV. As Baraff and Holway have shown, the diffusion of electrons towards the high energy tail of the energy distribution thus appears to be more important than the average electron energy in determining the avalanche characteristics. Including the diffusion term in the calculation lowers the predicted damage field by about a factor of three or more.<sup>68</sup>

Another source of the discrepancy may be in the choice of modeling for  $\nu_i(\epsilon)$ . Based on Seitz's discussion as summarized in Fig. 31, it appears that a constant  $\nu_i$  may be a more realistic approximation to reality than the perturbation modeling of the Fröhlich interaction. It may also be that the classical relaxation-time approximation normally used to

predict the electron dynamics may not be capable of describing avalanche breakdown.

A complete modeling of avalanche breakdown along the lines of the Thornber-Feynman calculation is probably many years distant. Nonetheless we believe that it is possible to understand many qualitative features of the avalanche by using classical models such as that developed by Holway. In closing this section we will consider possible extensions of Holway's calculations which may be useful in answering a number of theoretical questions raised in the preceding discussion.

The Fokker-Planck equation approach appears to be equivalent to using a first-order nonlinear Boltzmann equation.<sup>96</sup> The advantages it provides over the Boltzmann approach are that the Fokker-Planck equation is simpler from a computational viewpoint as well as easier to interpret physically.

By using Holway's formalism, a number of problems can be treated in a direct manner. It is possible, for example, to determine the importance of the details of the electron-phonon interaction to the development of the avalanche. Seitz's suggestion that the non-polar interaction may be important can be tested within this formalism by choosing different functional forms for  $\nu(\epsilon)$ , including one that takes account of both the polar and the non-polar interactions.

A second problem to be resolved: Is the relaxation time approximation capable of explaining our experimental results in the alkali halides? In particular, can Holway's formalism with a reasonable choice for  $\nu(\epsilon)$  predict the relative damage

fields we have measured in Chapt. 4 and 5, and can it predict  $\alpha(E)$  in NaCl? It may be possible to fit  $\nu(\epsilon)$  to the experimental results.

Seitz's suggestion that deep-lying exciton states may be important to breakdown can be tested by this model, and it may be possible to develop generalized predictions for  $\alpha(E)$  based on material parameters. The role of impurity states can also be investigated.

In conclusion, we see that although the purist may find avalanche theory to be in a dismal state, relatively simple phenomenological models may be capable of explaining many features of avalanche breakdown. In this area of work, however, experiment must lead the theory, and much more experimental data is needed to provide both a basis and a test for theoretical models.

## CHAPTER 9

## SUGGESTIONS FOR FUTURE WORK

The study of laser induced damage that has been presented in the preceding chapters has considered damage from absorbing inclusions, beam distortion from self-focusing, and electron avalanche breakdown. Many of the basic problems concerning laser damage have been resolved by this work and by other recent studies, but a great many problems remain. In this concluding section we will briefly consider some areas for future experimental work. The following list is not intended to be exhaustive.

1. High-Frequency Avalanche Breakdown and Multiphoton

Absorption: The first evidence of frequency dispersion in the damage fields of the alkali halides has been obtained. Because this dispersion does not follow simple predictions, measurements of high frequency avalanche breakdown should be extended to wavelengths shorter than  $0.69 \mu\text{m}$ . It would be of great interest to track the frequency dependence of intrinsic breakdown over a sufficient range of frequencies to show the eventual development of multiphoton absorption as the intrinsic damage mechanism. Except possibly for the recent work of Bass and Barrett,<sup>13</sup> no unambiguous measurements have yet been made of multiphoton absorption and its frequency and pulse-width dependences. As the laser frequency is increased, complications from self-focusing may get more serious and tighter external focusing may be required. The effective limit to external focusing will be determined by spherical aberrations. Laser damage studies at frequencies near the two-photon absorption

Preceding page blank

resonance, therefore, may be more profitably conducted on surfaces rather than in the bulk, provided that essentially imperfection-free surfaces can be produced. Initial work in this area might be conducted in the alkali halides with a nitrogen-laser-pumped dye laser. It would be of interest to compare the frequency dependence of intrinsic damage in crystalline quartz to that of fused quartz.

2. Subnanosecond Damage Measurements: In Chapt. 6 it was shown that an approximate ionization rate can be found from the dependence of the intrinsic damage field on laser pulse width. These techniques can be applied to other materials in order to determine if the ionization rate has a universal form in insulators. The frequency dependence of the ionization rate can also be determined from subnanosecond studies. It should be noted that dc measurements of dielectric breakdown cannot directly duplicate these studies because high voltage quasi-dc impulses of picosecond duration have not been achieved. In addition, dc measurements are difficult to conduct and may be plagued by a number of poorly understood experimental complications--surface and electrode effects, space charges, internal strains, etc.
  
3. Effect of Disorder on Avalanche Breakdown: Measurements were presented in Chapt. 6 which suggest that severe microscopic disorder can increase the breakdown strength

of solids. This work can be extended to other transparent materials which can exist in both crystalline and amorphous forms and to alloys such as YAG (yttrium aluminum garnet)-YGG (yttrium gallium garnet) which can be prepared in arbitrary proportions.

4. Exciton Fluorescence: Evidence has been obtained which shows that excitons can be excited in insulators by high-power laser beams confined to subdamaging intensities.<sup>97</sup> Prof. H. Ehrenreich has suggested to the author that a study of exciton fluorescence during damage may help clarify the role of deep lying exciton states in the avalanche process. Such work is only useful in large band-gap materials such as NaF, because the smaller band-gap alkali halides have exciton states which are lifetime-broadened sufficiently in damaging electric fields to overlap the conduction band. Vacuum ultraviolet techniques would therefore be required for such studies.
  
5. Temperature Dependence of Avalanche Breakdown: A great deal of work has been published on the temperature dependence of dc avalanche breakdown. Much of this work, however, is confused and inconsistent. Lasers provide a useful means for measuring the temperature dependence of intrinsic damage thresholds. A careful study of the temperature dependence of intrinsic breakdown has important implications to avalanche theory.<sup>54</sup>

6. Effects of Impurities on Intrinsic Damage Fields: In Chapt. 1 we discussed the role of impurity absorption and found that unless the impurity electrons can be excited into the conduction band (or impurity holes into the valence band), impurities will have little effect on damage fields. Wide band-gap insulators are thus not particularly attractive for impurity studies. Semiconductors such as GaAs or Ge, however, can be used with a CO<sub>2</sub> laser to study impurity effects in optical damage. One can imagine strongly doping the semiconductor, and measuring the intrinsic damage threshold as a function of impurity concentration. If shallow thermalized states are introduced, the gain coefficient  $M_c$  in Eq. (5-2) can in principle be varied and directly measured as function of field.
  
7. Damage to Thin Film Optics: In the present work there has been no discussion of thin film optical damage. Very little fundamental information about optical damage can be obtained from thin film studies, but thin film coatings are nonetheless quite important to the practical design of laser systems. Because we now understand the role of contaminants and structural imperfections in the damage process and because we now have careful measurements of intrinsic bulk damage fields to serve as standards, the complicated problem of thin film damage can be approached with some confidence. Thin film preparation techniques are needed which minimize structural defects and

contamination, and diagnostic tools must be developed to monitor the quality of optical coatings. As Dr. J. M. Khan has observed,<sup>83</sup> thin film damage is fundamentally a materials problem which probably requires sophisticated vacuum and surface equipment.

8. Gas and Liquid Breakdown: Laser induced gas breakdown can be profitably studied with the techniques of the present work. Because the pressure of gases is an experimental variable, it is relatively easy to study the competition between multiphoton ionization and avalanche breakdown. Work along these lines has been reported in the literature with fixed laser pulse durations,<sup>52</sup> but the pulse-width dependence of intrinsic processes has not yet been carefully determined and interpreted in terms of dc breakdown.<sup>98</sup> Gas breakdown studies are particularly attractive because the breakdown process is much better understood in gases at dc and at optical frequencies than it is in solids. Liquids also offer advantages with respect to laser damage studies. Atomic impurities with short excited state relaxation times can be added to a liquid so that the effects of absorption on laser damage thresholds can be determined.

Optical damage is thus seen to be an area where much fundamental and practical work remains. It is hoped that the present study is not viewed as a closing of another door of experimental physics but rather that it is viewed as the

first series of steps in solving a large and complex set of problems.

## APPENDIX

A practical limit to the degree of focusing that can be achieved with any real lens is set by spherical aberrations. This distortion comes about because the position of the focus for light rays at varying distances above the axis of the lens depends on the value of that distance. A perfectly collimated light beam, then, which would in principle be focused to a point at the geometrical focus, produces instead a blurred image with a finite radius. Spherical aberrations will also be introduced when a light beam is focused through any plane surface.

In this appendix we will show that the spherical aberrations introduced by the focusing lens and plane front surface of the samples under study in the bulk damage studies were negligible compared to diffraction effects. Aberrations of the lens will be characterized by using manufacturer's specifications on the lens along with well-known results available in most standard optics textbooks. A formula describing the aberrations introduced by focusing through a single plane surface will be derived from Snell's law.

When a focusing lens is aligned symmetrically with respect to a diffraction-limited light beam, the intensity distribution at the focus is the far-field diffraction pattern of the beam at the entrance to the lens convoluted with a function describing the lens' spherical aberrations.<sup>99</sup> For any particular lens, the effective focal diameter from spherical

aberrations is approximately proportional to  $R^3$ , where  $R$  is the incident beam radius, and the diffraction-limited focal diameter is  $-(\lambda/2R)f$  where  $f$  is the focal length of the lens. The relative size of the spherical aberrations for a particular lens design as compared to diffraction is thus given by

$$\frac{\text{Spherical Aberrations}}{\text{Diffraction Diameter}} \propto R^4/\lambda \quad (\text{A-1})$$

and it is seen that spherical aberrations become rapidly more important as the incident beam diameter is increased. An optimum value of  $R$  exists which produces a minimum effective focal diameter. For any larger value of  $R$ , the spot size increases and spherical aberrations limit the focal diameter. For smaller values the spot size also increases, but now diffraction limits the focal diameter.

The focusing lens used in the damage studies was designed for minimum spherical aberrations by properly selecting the radii of curvature for the two surfaces. According to the manufacturer's specifications,<sup>100</sup> a  $0.633 \mu\text{m}$  diffraction-limited laser beam incident on this lens will produce the smallest possible focal diameter when the incident beam has a diameter of 3 mm. It can be assumed, therefore, that spherical aberrations and diffraction effects are equal when  $R = 1.5 \text{ mm}$  and  $\lambda = 0.633 \mu\text{m}$ .

In our experiments at  $1.06 \mu\text{m}$ , we used a beam with a diameter of just under 1 mm so that  $R \approx 0.5 \text{ mm}$  and  $\lambda = 1.06 \mu\text{m}$ . The relative size of the spherical aberrations as compared to diffraction can then be calculated from Eq. (A-1) for our

conditions of measurement. It is found to be about 0.01. Because the true beam shape is a convolution of the aberration function and the diffraction pattern, the size of the spherical aberrations and the diffraction-limited diameter do not add to produce the true beam size at the focus. Rather, they combine approximately as the square root of the sum of their respective squares. Spherical aberrations, therefore, introduce a negligible error of about 0.01% into the measured breakdown intensities.

Spherical aberrations introduced by a plane surface can be important for tightly focused laser beams. Fig. 33 illustrates the source of aberrations. An incoming light ray, which intercepts the entrance plane at a height  $h$  and forms an angle  $\theta$  with respect to the horizontal, focuses at a distance  $d_2$  behind the entrance plane. It will be shown that  $d_2$  depends on  $h$  so that different rays will focus at different points in the medium, and the focal area will consequently be blurred.

From Snell's law we can relate  $\theta'$  to  $\theta$ . In particular,

$$\sin \theta = \frac{n'}{n} \sin \theta' = N \sin \theta' \quad (\text{A-2})$$

where

$$\sin \theta = \frac{h}{\sqrt{h^2 + d_1^2}} \quad , \quad \sin \theta' = \frac{h}{\sqrt{h^2 + d_2^2}}$$

Eq. (A-2) can be used to find  $d_2$  in terms of  $d_1$ . With the substitution  $h/d_1 = \tan \theta$ , we find that

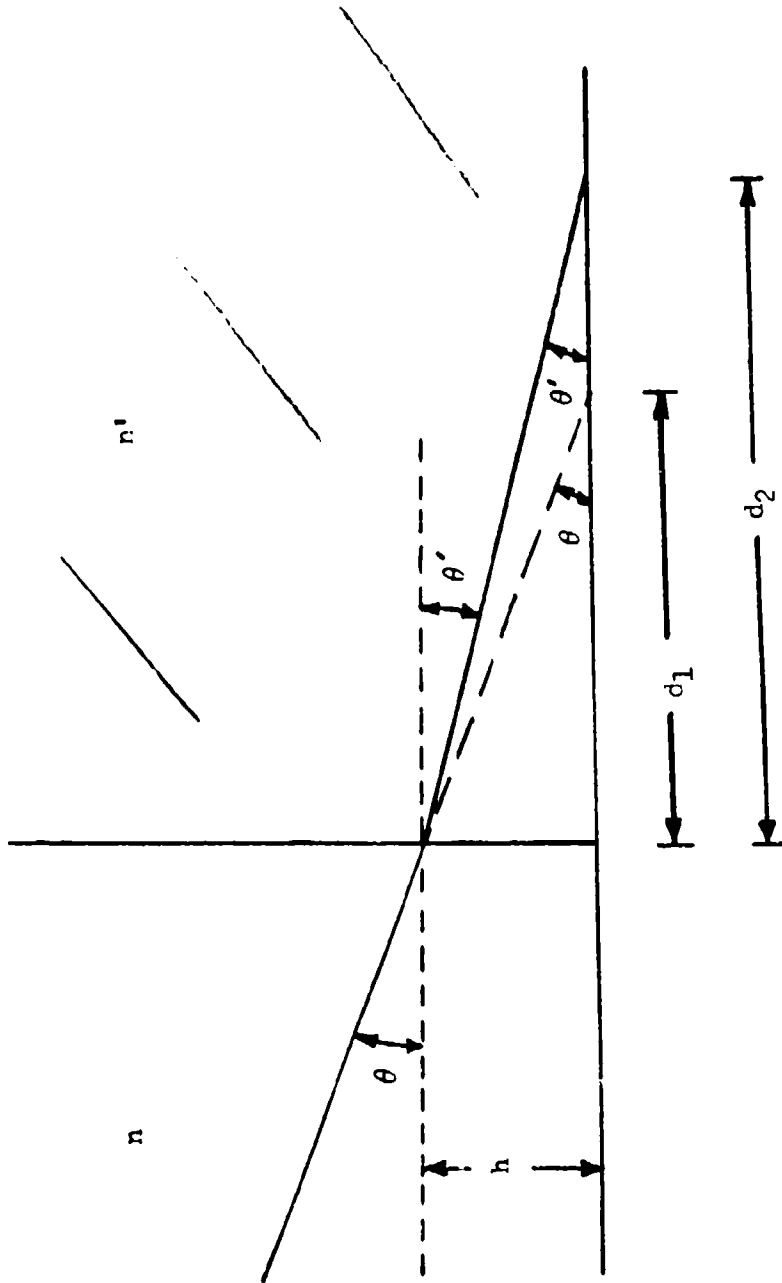


Fig. 33. SPHERICAL ABERRATIONS INTRODUCED BY FOCUSING LIGHT THROUGH A PLANE SURFACE

The direction of light propagation is from left to right. As the light rays enter the medium with index  $n'$ , they are refracted according to Snell's law. Because  $\theta$  varies with  $h$ ,  $d_2$  will depend on  $h$  and the focal region will be blurred.

$$d_2(h) = N d_1 \left[ \left( \frac{N^2 - 1}{N^2} \right) \tan^2 \theta + 1 \right]^{1/2} \quad (A-3)$$

The longitudinal spherical aberration (LSA) is, by definition,  $d_2(h) - d_2(0)$ . According to Eq. (A-3),

$$LSA = N d_1 \left\{ \left[ \left( \frac{N^2 - 1}{N^2} \right) \tan^2 \theta + 1 \right]^{1/2} - 1 \right\} .$$

The quantity of interest is the transverse spherical aberration (TSA) which is equal to the radius of the blurred focal spot. Its value is  $LSA \times \tan \theta'$  or, since

$$\tan \theta' = \frac{\sin \theta'}{\cos \theta'} = \frac{\sin \theta'}{(1 - \sin^2 \theta')^{1/2}} = \frac{\sin \theta}{(N^2 - \sin^2 \theta)^{1/2}} ,$$

the radius of the blurred focal spot is

$$TSA = N d_1 \left\{ \left[ \left( \frac{N^2 - 1}{N^2} \right) \tan^2 \theta + 1 \right]^{1/2} - 1 \right\} \frac{\sin \theta}{(N^2 - \sin^2 \theta)^{1/2}} \quad (A-4)$$

Under the conditions of focusing used in the bulk damage studies,  $\tan \theta \approx \sin \theta \approx \theta$ . Eq. (A-4) then becomes

$$TSA \approx d_1 \left( \frac{N^2 - 1}{N^3} \right) \theta^3 \quad (A-5)$$

If the plane entrance face is in the far field of the focused laser beam, then  $\theta \approx \lambda/2a_0$  where  $a_0$  is the minimum beam radius inside the material. We have focused approximately 2 mm inside the samples, so that  $d_1 \approx 1.3$  mm. From Eq. (A-5)

the calculated value of TSA is less than  $0.1 \mu\text{m}$  as compared to a diffraction-limited beam waist  $a_0$  of about  $10 \mu\text{m}$  for the YAG:Nd Q-switched laser experiments. We thus see that, as was the case with the focusing lens, the distortion introduced by the plane entrance face is negligible for our conditions of measurement.

REFERENCES

1. A. H. Glass, G. E. Peterson, and T. J. Negran, Laser Induced Damage in Optical Materials: 1972, NBS Special Publication 372, p. 15 (1972).
2. C. R. Giuliano, Appl. Phys. Lett. 5, 137 (1964).
3. See, for example, Proceedings of the ASTM-NBS Symposia on Laser Damage 1966-1972 (NBS Special Publications 305, 341, 356, and 372).
4. M. Bass, Laser Induced Damage in Optical Materials: 1970, NBS Special Publication 341, p. 9C (1970).
5. R. W. Hopper and E. R. Uhlman, J. Appl. Phys. 41, 4023 (1970).
6. S. A. Akhmanov, A. P. Sukhorukov, and R. V. Khokhlov, Sov. Phys. Uspekhi 10, 609 (1968).
7. R. M. Zverev and V. A. Pashkov, Sov. Phys. JETP 30, 616 (1968).
8. P. L. Kelley, Phys. Rev. Lett. 15, 1005 (1965).
9. C. R. Giuliano and J. H. Marburger, Phys. Rev. Lett. 27, 905 (1970).
10. Yu. K. Danileiko, A. A. Manenkov, A. M. Prokhorov, and V. Ya. Chirnov-Malikov, Sov. Phys. JETP 31, 18 (1970).
11. B. E. Newnam and L. G. DeShazier, Laser Induced Damage in Optical Materials, NBS Special Publication 372, p. 123 (1972). See also, E. S. Bliss and D. Milam, *ibid.*, p. 108.
12. M. Bass and H. H. Barrett, IEEE J. Quant. Elect. QE-8, 338 (1971).
13. M. Bass and H. H. Barrett, Appl. Optics 12, to be published (April 1973).
14. E. Yablonovitch, Appl. Phys. Lett. 19, 495 (1971).
15. N. Bloembergen, Appl. Optics 12, to be published (April 1973).
16. J. M. Khan, private communication (1972).
17. M. D. Crisp, N. L. Boling, and G. Dabe, Appl. Phys. Lett. 21, 364 (1972).
18. E. Yablonovitch and N. Bloembergen, Phys. Rev. Lett. 29, 907 (1972).
19. M. J. Weber, private communication (1972).
20. Multiphoton absorption in the present work will be understood Zener tunneling unless stated otherwise. See L. V. Keldysh, Sov. Phys.



- JETP 20, 1307 (1965).
21. W. S. Bliss, Damage in Laser Materials, NBS Special Publication 341, p. 105 (1970).
  22. H. Bloembergen, Nonlinear Optics (W. A. Benjamin Inc., New York), 1965.
  23. L. F. Kotova and M. V. Tarentev, Sov. Phys. JETP 25, 481 (1967).
  24. L. Holway, Jr., Phys. Rev. Lett. 28, 280 (1972).
  25. O. Rahn and M. Maier, Phys. Rev. Lett. 29, 558 (1972).
  26. E. L. Lawes and J. H. Marburger, Phys. Rev. 179, 862 (1969).
  27. J. H. Marburger, private communication (1972).
  28. V. I. Talanov, Sov. Phys. JETP Lett. 2, 138 (1965).
  29. C. S. Wang, Phys. Rev. 173, 908 (1968).
  30. W. G. Wagner, H. A. Hans, and J. H. Marburger, Phys. Rev. 175, 256 (1968).
  31. M. Born and E. Wolf, Principles of Optics (Pergamon Press, New York), 1959.
  32. E. L. Kerr, IEEE J. Quant. Elect. QE-6, 616 (1970).
  33. Y. R. Shen, Phys. Lett. 20, 378 (1966).
  34. C. R. Giuliano, J. H. Marburger, and A. Yariv, Appl. Phys. Lett. 20, 58 (1972).
  35. H. Bloembergen, Am. J. Phys. 35, 989 (1967).
  36. C. C. Wang and E. L. Baardsen, Phys. Rev. 185, 1079 (1969).
  37. M. Bass, IEEE J. Quant. Elect. QE-7, 350 (1971).
  38. M. A. Duguay, J. W. Hansen, S. L. Shapiro, IEEE J. Quant. Elect. QE-6, 725 (1970).
  39. J. M. McMahon, Laser Induced Damage in Optical Materials: 1972, NBS Special Publication 372, p. 100 (1972).
  40. B. E. Newman and L. G. DeShazier, Laser Induced Damage in Optical Materials: 1971, NBS Special Publication 356, p. 113 (1971).
  41. In Chapt. 6 it is shown that intrinsic laser-induced damage is an inherently statistical process. For the materials studied in the present work, however, breakdown is virtually threshold-like. A

damage intensity  $I_d$  can be defined as that value of light intensity inside the material which is necessary in order to induce damage on a single shot with a probability of 0.5.

42. The pulse-width dependence to avalanche breakdown is discussed in Ref. 18 and in Chapt. 5. An increase in damage intensity of no more than about 15% is predicted as the laser pulse duration is varied from 20 to 5 nsec. This prediction was confirmed by the results of Chapt. 4. A frequency dependence to the breakdown intensity will, if present, act to compensate this change. Because of possible inaccuracies introduced from the pulse-width and frequency dependence to breakdown, experiments designed to use the technique reported in the text should be conducted at a single frequency with the pulse duration being held reasonably constant.
43. G. D. Boyd and H. Kogelnik, Bell System Tech. J., 41, 1347 (1962).
44. L. G. DeShazer and J. H. Parks, Damage in Laser Materials: 1971, NBS Special Publication 356, p. 124 (1971).
45. C. R. Giuliano, R. W. Hellwarth, L. D. Hess, and G. R. Rickel, Damage Threshold Studies in Laser Crystals, Final Report for ARPA Contract No. F 19628-69-C-0277 (1972) at Hughes Research Laboratories.
46. A. J. DeMaria, A. D. Stetser, and H. Heynau, Appl. Phys. Lett. 8, 174 (1966).
47. J. P. Letellier, Naval Research Laboratory Report 7463 (1972).
48. F. Horrigan, private communication (1972).
49. I. A. Ferman, L. D. Khazov, and G. I. Tikhomirov, Sov. J. of Quant. Elect. 1, 248 (1971).
50. G. M. Zverev, T. N. Mikhailova, V. A. Pashkov, N. M. Solov'eva, Sov. Phys. JETP 26, 1053 (1968).
51. A. Wasserman, Appl. Phys. Lett. 10, 132 (1967).
52. H. T. Buscher, R. G. Tomlinson, and E. K. Damon, Phys. Rev. Lett. 15, 847 (1965).
53. H. Raether, Electron Avalanches and Breakdown in Gases (Butterworths, London), 1964.
54. A. von Hippel, J. Appl. Phys. 8, 815 (1937).
55. E. Yablonovitch, thesis, Harvard University (1972).
56. R. K. Ahrenkiel and F. C. Brown, Phys. Rev. 136, A223 (1964). See also, K. Teegarden and G. Baldiri, Phys. Rev. 155, 896 (1967).
57. K. K. Thornber and R. P. Feynman, Phys. Rev. B1, 4099 (1970).

58. J. J. O'Lwyer, The Theory of Dielectric Breakdown of Solids (Oxford University Press, London), 1964.
59. J. H. Calderwood, R. Cooper, and A. A. Wallace, Proc. IEEE 100 Pt. IIA, 1051 (1963).
60. D. W. Watson, W. Heyes, K. C. Kao, and J. H. Calderwood, IEEE Trans. Elec. Insul. EI-1, 30 (1965).
61. G. A. Vorob'ev, N. I. Lebedeva, and G. S. Naderova, Sov. Phys. Solid State 13, 736 (1971). See also, A. A. Vorob'ev, G. A. Vorob'ev and L. T. Murashko, Sov. Phys. Solid State 4, 1441 (1963).
62. The difference in absolute field strength of NaCl between von Hippel's published dc result, op. cit., and the laser data in Table V is actually larger than indicated. In dc experiments a range of dc values are often found. Von Hippel consistently selected the largest values. It was later shown by Calderwood et al., op. cit., that because lattice strains tend to bias the dc breakdown field upward, the lower values of dc damage fields are more meaningful. The lower value in von Hippel's study is about 1 MV/cm which agrees well with later dc measurements. Whether highest field values or lowest values are chosen, however, makes little difference for the relative damage fields.
63. E. M. Conwell, High Field Transport in Semiconductors, Solid State Physics Supplement 7 (Academic Press, New York and London), 1967.
64. H. Fröhlich, Proc. Roy. Soc. A 160, 230 (1937).
65. F. Seitz, Phys. Rev. 76, 1376 (1949).
66. A pulse-width dependence to optical damage in thin films was observed by E. S. Bliss and D. Milam, Laser Induced Damage in Optical Materials: 1972, NBS Special Publication 372, p. 108 (1972). The mechanism of damage was not identified, however. Since it is known that thin films can have a large residual absorption and significant structural defects, it is not clear that the change in damage fields which were observed by Bliss and Milam reflect a property of an intrinsic bulk damage mechanism. A similar dependence of breakdown field on laser pulse duration was observed in the gas breakdown studies of Ref. 98 in which a full mode-locked laser train was used to induce breakdown.
67. L. Holway, Phys. Rev., 28, 280 (1972).
68. L. Holway, Final Report for ARPA Contract No. F19628-70-C-0223 at Raytheon Research Division (1973).
69. Prof. Y. R. Shen has suggested (private communication, 1972) that local field effects may be important in an electron avalanche and may explain the difference in absolute field strengths between dc and optical frequencies. The damage fields reported in the literature, however, are not corrected for local fields because it is normally assumed that any local field effects are averaged out by the electrons' rapid movement across the unit cell. The validity of this latter assumption has

not been established.

70. V. D. Kuchin, Sov. Phys. Solid State 1, 405 (1959).
71. J. R. Hanscomb, J. Appl. Phys. 41, 3597 (1970).
72. H. Kawamura, H. Ohkura, T. Kikuchi, J. Phys. Soc. Japan 19, 541 (1954).
73. D. B. Watson, W. Heyes, K. C. Kao, and J. H. Calderwood, IEEE Trans. Elect. Insul. EI-5, 58 (1970).
74. R. E. Slusher, W. Giriat, and S. R. J. Brueck, Phys. Rev. 183, 758 (1969).
75. A. von Hippel and R. J. Maner, Phys. Rev. 59, 820 (1941).
76. C. Kittel, Introduction to Solid State Physics, Third Edition (John Wiley and Sons, New York), 1967.
77. D. W. Howe, unpublished measurements.
78. R. A. Wijsman, Phys. Rev. 75, 833 (1949).
79. M. Bass and D. W. Fradin, IEEE J. Quant. Elect., submitted for publication.
80. W. Shockley, Czech. J. Phys. B11, 81 (1961) and Sol. St. Elect. 2, 35 (1961).
81. H. Barrett, private communication (1973).
82. N. Bloembergen, private communication (1972).
83. J. M. Khan, private communication (1972).
84. C. DeMichelis, IEEE J. Quant. Elect. QE-5, 188 (1969).
85. As noted in Ref. 12, the intrinsic damage statistics should become less pronounced as larger focal volumes of the crystal are sampled.
86. In the region of the focus, a diffraction-limited light beam changes its radius by a factor of  $\sqrt{2}$  after propagating the confocal distance  $z_c$ . If  $a_0$  is the minimum radius of the focused beam, then  $z_c = \pi a_0^2 / \lambda$ . We can assume that a focused beam is effectively collimated over a distance of about  $0.1 z_c$  near the focus. For  $1 \mu\text{m}$  light with  $a_0 = 12 \mu\text{m}$ , the collimation distance is therefore about  $50 \mu\text{m}$ .
87. C. R. Giuliano, Appl. Phys. Lett. 21, 39 (1972).
88. H. B. Callen, Phys. Rev. 76, 1394 (1949). See also, H. B. Callen and E. L. Offenbacher, Phys. Rev. 90, 401 (1953).
89. H. Fröhlich, Proc. Roy. Soc. A 188, 532 (1947).

90. H. Fröhlich and B. V. Paranjape, Proc. Phys. Soc. B, 69, 21 (1956).
91. R. Stratton, Proc. Roy. Soc. A 246, 406 (1958).
92. S. C. Brown, Introduction to Electrical Discharges in Gases (John Wiley and Sons, New York and London), 1966.
93. G. A. Baraff, Phys. Rev. 128, 2507 (1962).
94. This choice for  $M_0$  will be referred to as the "20-odd generation" model.
95. W. Franz, Z. Phys. 132, 285 (1952).
96. L. Holway, private communication (1973).
97. T. P. Belikova and F. A. Sviridenkov, JETP Lett. 1, 171 (1965).
98. I. Meyer and H. Timm, Opt. Comm. 6, 339 (1972).
99. W. J. Smith, Modern Optical Engineering (McGraw Hill, New York), 1966.
100. Special Optics Corp., Cedar Grove, New Jersey, 07009.

PUBLICATIONS

Many of the results of this report have been published or submitted for publication in the technical literature. The following list summarizes these publications:

1. D. Bua, D. W. Fradin, and M. Bass, "A Simple Method for Longitudinal Mode Selection," IEEE J. Quant. Elect. QE-8, 916 (1972).
2. D. W. Fradin, E. Yablonovitch, and M. Bass, "Comparison of Laser Induced Bulk Damage in Alkali Halides at 10.6, 1.06, and 0.69 Microns," Laser Induced Damage in Optical Materials, NBS Special Publication 372, p. 27 (1972).
3. D. W. Fradin, E. Yablonovitch, and M. Bass, "Confirmation of an Electron Avalanche Causing Laser Induced Bulk Damage at 1.06 Microns," Appl. Optics, accepted for publication (April 1973).
4. D. W. Fradin and M. Bass, "A Comparison of Laser Induced Surface and Bulk Damage," Appl. Phys. Lett. 22, 157 (1973).
5. D. W. Fradin and M. Bass, "Electron Avalanche Breakdown Induced by Ruby Laser Light," Appl. Phys. Lett. 22 (1 March 1973).
6. M. Bass and D. W. Fradin, "Statistics in Surface and Bulk Breakdown and Identification of Intrinsic Mechanisms," IEEE J. Quant. Elect., submitted for publication.
7. D. W. Fradin, "The Measurement of Self-Focusing Parameters  $n_{\text{eff}}$  ; Intrinsic Optical Damage," IEEE J. Quant. Elect., submitted for publication.
8. D. W. Fradin, M. Bass, N. Bloembergen, and J. P. Letellier, "Electron Avalanche Breakdown at Optical Frequencies," Bull. Am. Phys. Soc. II 18, 7L (1973).
9. D. W. Fradin, N. Bloembergen, and J. P. Letellier, "The Pulsewidth Dependence of Avalanche Breakdown as Studied with Subnanosecond Laser Pulses," Appl. Phys. Lett., submitted for publication.
10. M. Bass, D. W. Fradin, and L. Holway, "Experimentation and Investigation of Optical-Irradiation-Induced Surface Damage in Optically Non-linear Materials," Final Report for Contract No. F19628-70-C-0223 for the Advanced Research Projects Agency of the Department of Defense as monitored by Air Force Cambridge Research Laboratories (Feb. 1973).
11. D. W. Fradin and M. Bass, "Effects of Crystal Disorder on the Intrinsic Optical Breakdown Strength of Solids," manuscript in preparation.